

**Mesostructured Aluminium Phosphates  
Synthesised by Supramolecular  
Structure-Direction**

**DISSERTATION**

zur Erlangung des  
Doktorgrades  
des Fachbereichs  
Chemie  
der Universität  
Hamburg

vorgelegt von

**Michael Tiemann**  
aus Hamburg

August 2001



Universität Hamburg

Die vorliegende Arbeit entstand in der Zeit von November 1997 bis Juli 2001 am Institut für Anorganische und Angewandte Chemie der Universität Hamburg in der Arbeitsgruppe von Prof. Dr. M. Fröba.

Gutachter:

Prof. Dr. M. Fröba

Prof. Dr. R.-D. Fischer

Hiermit versichere ich, die vorliegende Arbeit eigenhändig und ausschließlich unter Verwendung der angegebenen Hilfsmittel und Quellen durchgeführt zu haben. Die Arbeit ist zuvor keiner Prüfungsbehörde in gleicher oder ähnlicher Form vorgelegt worden.

Hamburg, 3. August 2001

Michael Tiemann

*I love deadlines.  
I like the whooshing sound they make as they fly by.*

Douglas Adams (1952 - 2001)

# Contents

<b>1. Introduction</b>	<b>1</b>
1.1. Structure-directed Synthesis of Ordered Mesostructured Materials	1
1.2. Ordered Mesostructured Aluminium Phosphates	9
1.3. Aim of this Work	19
<b>2. Experimental</b>	<b>20</b>
2.1. Synthetic Procedures	20
2.2. Chemical Compounds	22
2.3. Characterisation	22
<b>3. Aqueous Synthesis with <i>n</i>-Dodecyl Phosphate as Structure-director</b>	<b>26</b>
3.1. Basic Characterisation	26
3.2. <i>In-situ</i> SAXS	31
3.3. Structural Models	34
3.4. NMR Spectroscopy	37
3.5. XANES Spectroscopy	42
3.6. Thermal Analysis	46
3.7. Conclusions	51
<b>4. Alcoholic Synthesis with <i>n</i>-Dodecyl Phosphate as Structure-director</b>	<b>53</b>
4.1. Basic Characterisation	53
4.2. Structural Model of the Hexagonal Mesophase	55
4.3. <i>In-situ</i> SAXS	59
4.4. On the Synthesis Mechanism	60
4.5. NMR Spectroscopy	62
4.6. XANES Spectroscopy	64
4.7. Thermal Analysis	65
4.8. Conclusions	67

<b>5.</b>	<b>Alcoholic Synthesis with <i>n</i>-Alkyl Amines as Structure-directors</b>	<b>69</b>
5.1.	Basic Characterisation	69
5.2.	Post-synthetic Treatment and Surfactant Removal	71
5.3.	Nitrogen Physisorption	74
5.4.	<i>In-situ</i> SAXS	76
5.5.	NMR Spectroscopy	77
5.6.	XANES Spectroscopy	81
5.7.	Thermal Analysis	82
5.8.	Conclusions	83
<b>6.</b>	<b>Synthesis from a Single-source Precursor</b>	<b>84</b>
6.1.	Motivation and Scope	84
6.2.	The Single-source Precursor $[\text{Al}(\text{PO}_4)(\text{HCl})(\text{C}_2\text{H}_5\text{OH})_4]_4$	85
6.3.	Basic Characterisation	88
6.4.	Surfactant Removal	91
6.5.	Nitrogen Physisorption	92
6.6.	NMR Spectroscopy	93
6.7.	Conclusions	95
<b>7.</b>	<b>Studies on the Phase Behaviour of the System <i>n</i>-Dodecyl Phosphate / Water</b>	<b>96</b>
7.1.	Motivation and Scope	96
7.2.	Results and Discussion	97
7.3.	Conclusions	102
<b>8.</b>	<b>Summary</b>	<b>104</b>
<b>9.</b>	<b>Zusammenfassung (German Summary)</b>	<b>107</b>
<b>10.</b>	<b>References</b>	<b>110</b>
	<b>Appendix</b>	<b>119</b>
	Thanks	119
	List of Publications	120
	Curriculum Vitae	124
	Hazardous Chemicals	125



# 1. Introduction

## 1.1. Structure-directed Synthesis of Ordered Mesostructured Materials

### 1.1.1. Overview

The utilisation of supramolecular arrays of organic amphiphiles as structure-directing species in the synthesis of mesostructured materials was introduced in 1992 by KRESGE and BECK *et al.* [1,2]. Their work focused on the preparation of mesoporous silica and aluminosilicate materials (referred to as M41S materials), which are obtained in a two-step procedure: The initial synthesis leads to an inorganic/organic composite material, in which the organic component (the amphiphile) is periodically arranged within the amorphous inorganic (silica) matrix. The symmetric order in the composite corresponds to the self-aggregation behaviour of the amphiphilic species in the respective solvent, although this behaviour may be significantly influenced by the presence of the inorganic reactant(s); the phase diagram of a commonly used surfactant (*n*-hexadecyltrimethylammonium bromide, CTABr) is shown in **Figure 1-1** as an example. In a second step the amphiphile is removed from the solid material (*e.g.* by calcination or solvent extraction), which leads to regularly arranged mesopores with uniform size and shape.

According to a IUPAC recommendation [3], 'mesoporous' materials exhibit pores with diameters between 2 and 50 nm. (Pores with a smaller diameter (< 2 nm) are denoted as 'micropores' and those with a larger diameter (> 50 nm) as 'macropores'.) The term 'mesostructured' is regularly used for materials with a structural order in the same region, *i.e.* several nanometers; mesostructured materials are not necessarily mesoporous. In order to create mesopores, the inorganic network must be stable enough and consist of a three-dimensional network in order to maintain its mesostructure after removal of the organic component.

Corresponding to the variable symmetric phases found in lyotropic systems, silica materials with various kinds of mesostructures have been synthesised. These include the two-dimensional hexagonal MCM-41 materials (space group  $p6m$ ), the cubic

MCM-48 materials (space group  $Ia3d$ ), and the lamellar MCM-50 materials reported by KRESGE and BECK *et al.* [1,2]. HUO *et al.* introduced the cubic SBA-1 material (space group  $Pm3n$ ) [4], the three-dimensional hexagonal SBA-2 material (space group  $P6_3/mmc$ ) [5], and the two-dimensional hexagonal SBA-3 material [6]. ZHAO *et al.* reported the synthesis of SBA-8, a material which has a similar structure as MCM-41, but a centred rectangular lattice (space group  $cmr$ ) [7]. Other materials have less well-ordered structures; phases with randomly ordered tubular pores, MSU-1 and HMS-1, were reported by BAGSHAW *et al.* [8] and by TANEV and PINNAVIA [9]. The KIT-1 and LMU-1 phases reported by RYOO *et al.* [10] and BEHRENS *et al.* [11], respectively, have three-dimensionally interconnected pores (sponge-like structures).

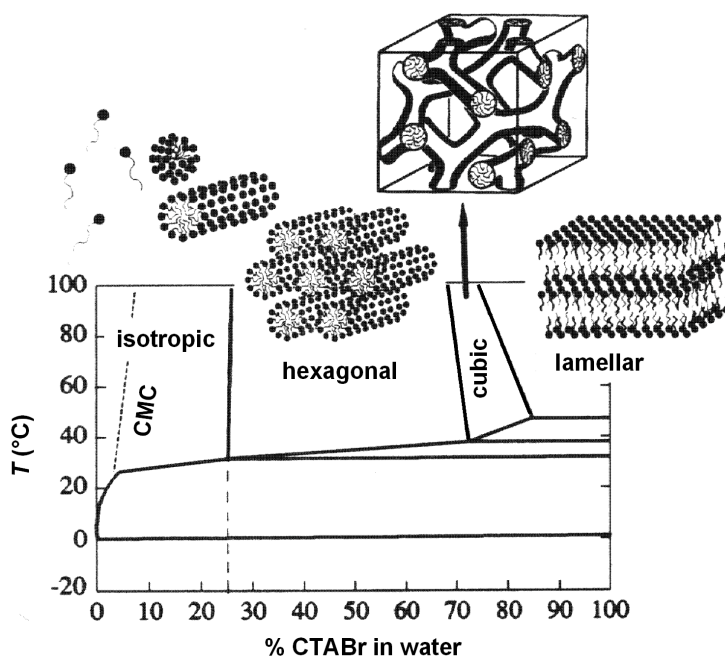


**Figure 1-1.** Phase diagram of *n*-hexadecyltrimethylammonium bromide (CTABr)/water [12,13]. When a surfactant like this is used as a structure-director for the synthesis of mesostructured materials, *i.e.* when the inorganic reactants are added, the phase behaviour may change significantly. (CMC: Critical micelle concentration.)

Apart from the synthesis of mesoporous silica and aluminosilicate materials, the concept of supramolecular structure-direction was applied to the preparation of numerous other mesoporous or mesostructured materials, including metal oxides [4,14-24], chalcogenides [25-32], and aluminium phosphates; the latter shall be

discussed in detail in chapter 1.2. The synthesis and application of mesostructured materials has been subject to several reviews [33-40].

Mesoporous materials are of great interest for numerous potential applications, for example as molecular sieves or size-selective catalysts or catalyst supports. However, all ordered mesostructured materials, including those which are not porous, have in common unique structural properties on the level of several nanometers, which suggest further potential applications such as novel conducting or semiconducting devices, photoactive materials, or host-guest compounds. Regardless of whether or not the organic component can be removed without collapse of the mesostructure, the synthesis of inorganic/organic mesostructured composite materials is always interesting for structural investigations or mechanistic studies.

### 1.1.2. Synthesis Mechanism

In their pioneering work, KRESGE and BECK *et al.* [1,2] suggested two distinct pathways for the structure formation in the synthesis of mesostructured silica with a cationic ammonium surfactant: (i) The "liquid crystal templating" (LCT) pathway assumes that the inorganic walls are formed in the solvent regions between the surfactant micelles in a pre-formed lyotropic liquid crystal. This kind of mechanism was later established by ATTARD and GÖLTNER *et al.* for syntheses in which very high surfactant concentrations are chosen [41,42]. (ii) In an alternative pathway the inorganic species themselves interact with the head groups of the surfactant molecules and mediate their ordering into the mesostructure. This co-operative mechanism is more plausible for "regular" syntheses (with rather low surfactant concentrations) than the LCT mechanism, as it accounts for the fact that the synthesis is often successful even in those cases where the surfactant concentration is below the critical micelle concentration (CMC), *i.e.* when no liquid crystal phase exists in the absence of the inorganic species. A general scheme of the overall synthesis is shown in **Figure 1-2**.

MONNIER *et al.* [43] presented a more detailed picture of the co-operative mechanism, based on the characterisation of mesostructured silica materials synthesised under various conditions (such as synthesis time, temperature, or pH, all of which led to various degrees of silicate polymerisation): For the synthesis of silica mesostructures with cationic surfactants (such as alkyltrimethylammonium salts) they

postulated that the structure formation is governed by (i) multidentate binding of anionic silica oligomers to the cationic head groups, (ii) preferred polymerisation of silicate at the surfactant-silicate interface, and (iii) 'charge density matching' across the interface. This term refers to the fact that the symmetry of the surfactant arrangement is determined by the number of negatively charged silanol groups, *i.e.* by the degree of silicate polymerisation. As the polymerisation proceeds, the charge density is diminished; consequently, the surface area which is exposed by each (cationic) surfactant head group at the interface must increase. The latter depends on the micelle curvature: The surfactant arrangement changes from lamellar to tubular. This model is supported by the observation of an intermediate lamellar mesophase during the early stages of the formation of hexagonal MCM-41 silica.

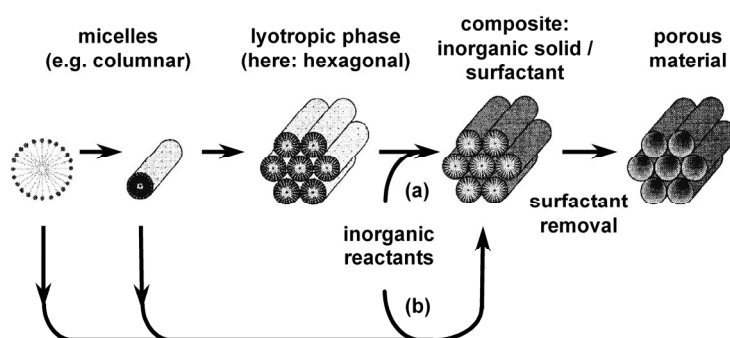


**Figure 1-2.** General scheme of various possible pathways in the synthesis of mesoporous materials by the utilisation of supramolecular arrays of surfactants as structure-directing agents [2]. The self-assembly of the surfactant micelles into periodic arrays may either precede the addition of the inorganic reactants (liquid crystal templating pathway, **a**) or be induced by the interactions with them (co-operative mechanism, **b**).

Further contemplations regarding the reaction mechanism, including syntheses that utilise anionic or neutral surfactants as well as syntheses of non-silica materials, have been made subsequently [4,9,14,16,44,45]. These were basically founded on the properties of the final products from the respective syntheses as well as on theoretical considerations. However, insights into the mechanisms of the structure formation may be gained from *in-situ* investigations on these reactions.

### 1.1.3. *In-situ* Investigations of the Synthesis Mechanism

*In-situ* studies on the mechanism of the structure formation in the synthesis of ordered mesostructured materials have so far been restricted mainly to silica phases prepared in aqueous media.

Extensive investigations in this field were performed by GLINKA and FIROUZI *et al.* [46-48] who employed a variety of characterisation methods, such as small angle X-ray (SAXS) and neutron (SANS) scattering, polarised light optical microscopy (POM), and NMR spectroscopy ( $^2\text{H}$ ,  $^{13}\text{C}$ ,  $^{29}\text{Si}$ ,  $^{81}\text{Br}$ ). They confirmed the co-operative organisation of silicate anions and/or oligomers with *n*-hexadecyltrimethylammonium bromide surfactant into nanostructured assemblies. They also studied the phase behaviour of a "passive" liquid-crystalline model system containing both the surfactant and the silicate species, in which the polymerisation of the silicate is suppressed by highly alkaline conditions. In comparison, RATHOUSKÝ *et al.* [49] have investigated the formation of mesostructured silica from a similar synthesis mixture using X-ray diffraction; their system is not lyotropic in the passive state (at high pH) and the mesostructure evolves only after acidification, *i.e.* after the start of the silicate polymerisation.

Further confirmation of the co-operative synthesis mechanism was subsequently reported by a number of authors: O'BRIEN *et al.* [50,51] studied the synthesis of silica mesostructures by time-resolved synchrotron X-ray diffraction, focusing particularly on the effect of using different silica sources. They also confirmed the existence of an intermediate lamellar silicate/surfactant mesophase, which had formerly been postulated by MONNIER *et al.* [43] (see chapter 1.1.2.). CALABRO *et al.* [52] employed ATR/FTIR spectroscopy to simultaneously study the changes and synergies in both the lyotropic phase in the synthesis mixture and the solid product. REGEV [53] studied the synthesis of hexagonal MCM-41 silica by *in-situ* SAXS and *ex-situ* cryo-transmission electron microscopy. He observed a transition from spherical to elongated micelles after the addition of the silicate source to the surfactant/water mixture, confirming the co-operative synthesis mechanism. PEVZNER and REGEV [54] also used SAXS to investigate the synthesis of cubic MCM-48 silica; the cubic phase seems to evolve by transition from a hexagonal phase. The co-operative mechanism in the synthesis of hexagonal MCM-41 silica was confirmed by ZHANG *et al.* [55] and by

GALARNEAU *et al.* [56] who carried out *in-situ* EPR studies utilising appropriate spin probe species.

High time-resolution kinetic investigations were carried out by LINDÉN and ÅGREN *et al.* [57-61], who used *in-situ* synchrotron X-ray diffraction in a specific tubular reactor and observed the structure formation of MCM-41 type silica phases as early as three minutes after the start of the reaction. They also carried out investigations on hexagonal and/or lamellar  $\text{Zr}(\text{SO}_4)_2/\text{surfactant}$  and  $\text{TiOSO}_4/\text{surfactant}$  mesophases, which were found to form even more rapidly (within less than 1 second). In particular, the influence of the surfactant chain length and of the ionic strength of the solution, as well as that of the addition of co-surfactants or solubilisation agents on the structure formation was studied and interpreted in the light of their impact on the packing parameter.

#### 1.1.4. Single-source Molecular Precursors

Every attempt to improve the structure-directed synthesis of ordered mesostructured materials must deal with a variety of parameters that have strong influence on the quality of the products. Various mutual interactions of the species present in the synthesis mixture may decrease the chance to efficiently control these reactions: Non-silica materials often require more than one reactant; these interact with each other as well as with the surfactant. The surfactant's self-assembly, on the other hand, is strongly influenced by the presence of the inorganic species and the degree of their polymerisation (as was discussed above). Additionally, several oligomeric intermediates with different physical and/or chemical properties (hydrolytic behaviour, diffusion properties, chemical reactivities) may be formed in the course of the condensation reaction. Simple as it may seem at first sight, the concept of utilising organic amphiphiles as structure-directors for the preparation of mesostructured materials regularly confronts the chemist with fairly complex and delicate synthetic procedures.

Single-source molecular precursors provide an elegant means to reduce the complexity of the synthesis system and to improve control over the reaction. The general idea in this concept is to replace the inorganic reactants that serve as separate sources of the elements (of which the final inorganic network is supposed to consist)

by one single soluble molecular unit. This unit contains the respective elements in a pre-defined stoichiometry and short-range structural order; it remains intact during the synthesis and, therefore, serves as a building unit for the inorganic network. This opens new opportunities to create 'tailor-made' materials by modifying the precursors, which are prepared independently before the structure-directed synthesis of the solid.

The utilisation of single-source molecular precursors is a well-established technique in various synthetic fields, such as (non-oxide) amorphous ceramic materials [62-64, and references cited therein] or organic/inorganic hybrid composites (xerogels) prepared from silylated organic compounds by polycondensation [65, and references cited therein]. However, in the field of the synthesis of mesostructured materials with the utilisation of supramolecular arrays of amphiphiles only a few publications involving this concept have been made so far.

The first structure-directed syntheses of ordered mesostructured materials utilising single-source precursors were reported by FYFE and FU *et al.* [66,67], who prepared various mesostructured silica materials from a double four-ring silicate ( $\text{Si}_8\text{O}_{20}^{8-}$ ), as well as mesostructured aluminosilicates from an analogous precursor ( $\text{Si}_4\text{Al}_4(\text{OH})_8\text{O}_{12}^{4-}$ ). The core units of these compounds consist of cube-like arrangements of Si atoms or (alternating) Si and Al atoms, respectively, with bridging oxygen atoms between them. Both Al and Si are additionally coordinated by one OH group, which leads to an overall coordination number of 4 (**Figure 1-3**). The precursors can be prepared as water-soluble crystalline tetramethylammonium salts. Solid-state  $^{29}\text{Si}$  and  $^{27}\text{Al}$  MAS NMR data confirm that the building blocks remain intact within the final mesostructured materials, although calcination of the hexagonal aluminosilicates leads to a partial dealumination.

MACLACHLAN *et al.* [28,29] have employed the adamantanoid  $\text{Ge}_4\text{S}_{10}^{4-}$  cluster to synthesise hexagonal mesostructured transition metal thiogermanates by addition of  $\text{Co}^{2+}$ ,  $\text{Ni}^{2+}$ ,  $\text{Cu}^+$ , or  $\text{Zn}^{2+}$  cations. RAMAN spectroscopic data indicate that the cluster remains intact. However, this approach is not a true single-source precursor synthesis, since two separate reactants (the  $\text{Ge}_4\text{S}_{10}^{4-}$  salt and the respective metal salts) are used. The mesostructured materials are not stable for calcination. About simultaneously, WACHHOLD *et al.* [31,32] published a very similar synthesis of tubular mesostructured

transition metal thiogermanates ( $\text{Co}^{2+}$ ,  $\text{Ni}^{2+}$ ,  $\text{Cd}^{2+}$ ,  $\text{Hg}^{2+}$ ,  $\text{Zn}^{2+}$ ); their materials are partially calcinable.

Finally, HOLLAND *et al.* [68,69] have used polyoxometalate clusters ( $\text{AlO}_4\text{Al}_{12}(\text{OH})_{24}(\text{H}_2\text{O})_{12}^{7+}$ ,  $\text{GaO}_4\text{Al}_{12}(\text{OH})_{24}(\text{H}_2\text{O})_{12}^{7+}$ ) to prepare mesoporous aluminium-phosphate-based materials. Again, an additional species (a phosphate) is added for the synthesis, which means that the reaction is actually not a single-source synthesis. There are indications that the clusters do not remain intact in the course of the reaction. Further discussion on this synthesis will be made in chapter 1.2.4.

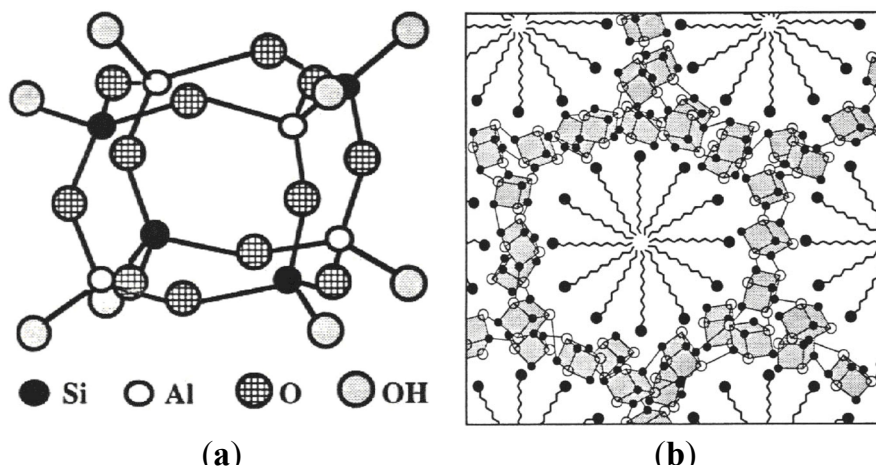


**Figure 1-3.** Schematic representation of a molecular precursor (a) for the preparation of a mesostructured aluminosilicate material (b, hexagonal symmetry, cross section through the  $hk$  plane). The precursor ( $\text{Al}_4\text{Si}_4\text{O}_{12}(\text{OH})_8^{4-}$ ) exhibits a cube-like arrangement of Al and Si connected *via* O bridges; an additional OH ligand is connected to each corner atom. In the final product the intact building units are connected with each other *via* oxygen bridges [67].

## 1.2. Ordered Mesostructured Aluminium Phosphates

### 1.2.1. Important Aspects in the Synthesis of Mesostructured Aluminium Phosphates

Crystalline microporous (zeolite-analogous) aluminium-phosphate- and silicoaluminium-phosphate-based materials ( $\text{AlPO}_4\text{-}n$ ,  $\text{SAPO-}n$ ) [70,71] possess an immense significance in the field of heterogeneous catalysis. For example, aluminium phosphates containing transition metals in their network (*e.g.* V, Cr, Mn, Co) can be used for various oxidation reactions of alkanes, cycloalkanes, or phenols; transition metal substituted silicoaluminium phosphates are efficient catalysts for methanol conversion. A comprehensive review on this topic has been published by HARTMANN and KEVAN [72].

Accordingly, there is an apparent interest in ordered mesoporous aluminium phosphates which combine this catalytic potential with larger pores, giving way to the catalytic conversion of new (larger) substrates. Over the last few years such materials have been synthesised in a variety of mesostructures, including lamellar, hexagonal (*i.e.* analogous to MCM-41 silica [1,2]), or randomly ordered tubular (comparable to MSU-1 [8] or KIT-1 [10] silica materials). However, in the non-lamellar phases the degree of structural order is generally somewhat lower as compared to mesostructured silica materials. No mesostructured aluminium phosphates with cubic symmetries (analogous to MCM-48 [1,2] or SBA-1 [4] silicas) have been reported so far. The reason for the poorer structural order and the lower symmetry may to some degree be attributed to the fact that the syntheses are carried out utilising two inorganic reactants (*i.e.* two separate sources of Al and P) rather than just one, as in case of silica materials. Another remarkable tendency in the synthesis of mesostructured aluminium phosphates is that non-lamellar structures have almost never been obtained from utilising surfactants with neutral or anionic head groups; cationic surfactants are the most favourable ones.

The initial publications on mesostructured aluminium phosphates were dominated by reports on lamellar materials. Porous (*i.e.* non-lamellar) phases, which are the more promising ones with respect to their potential application in catalysis, have turned out to be more difficult to synthesise as compared to silica-based materials. However, many of the reports on lamellar aluminium phosphates offer interesting aspects on the

role of the surfactant and its influence on the mesostructure (as will be shown below). In the following, the literature will be reviewed in two sections, the first one focusing on lamellar materials and the other one on non-lamellar materials.

### 1.2.2. Some General Remarks

#### *'Structure-Director' vs. 'Template'*

The structure-directed synthesis of aluminium phosphate materials started in 1982 with the introduction of the above-mentioned crystalline microporous aluminium phosphates and silicoaluminium phosphates, the preparation of which involves single molecular units serving as templates. The synthesis of the so-called mesostructured aluminium phosphates, on the other hand, which are to be discussed here, uses supramolecular arrays of organic amphiphiles as structure-directing species. These are not adequately denoted as 'templates', since a template, in the original sense, leads to one particular, structurally unique product; there is an indispensable correlation between the choice of the template and the (crystalline) structure of the product. Contrary to that, supramolecular arrays of amphiphiles led to mesostructures which can often be created by a variety of (amphiphilic) species; the resultant mesostructured products are periodically ordered, but usually amorphous with respect to their short-range atomic structure.

#### *Synthesis pH*

The pH is a crucial factor in the synthesis, which is sometimes underestimated. The initial pH values in the reaction mixtures (which are sometimes not explicitly stated in the literature, but can usually be estimated from the compositions of the reaction mixtures) span a broad range from strongly acidic over neutral to slightly alkaline. In this context it must be stressed that phosphoric acid, which usually serves as the P source, brings high acidity to the synthesis system. On the other hand, the choice of the surfactant as well as its relative quantity with respect to the inorganic reactants is another factor that may have strong influence on the pH conditions; for example, the alkaline potential of primary amine surfactants should not be underrated. Apart from that, a drastic shift towards higher pH is often observed (or to be expected) during the synthesis, as phosphoric acid is used up in the course of the reaction.

### *Short-range Order in Mesostructured Aluminium Phosphates*

The short-range order of the inorganic matrix is one of the most important aspects in the synthesis of non-crystalline mesostructured aluminium phosphates. In a regular  $\text{AlPO}_4$  network every Al atom is tetrahedrally surrounded by four O-P units and every P atom by four O-Al units. The relative Al/P ratio in the final product is 1; characterisation of the material (*e.g.* by  $^{27}\text{Al}$  /  $^{31}\text{P}$  solid-state NMR) should reveal that both Al and P are entirely in a tetrahedral co-ordination. However, in reality the situation is usually different, as will be discussed below. The Al/P ratio may be greater or smaller than one and Al is often found to have both four- and six-fold co-ordination within the same sample; both Al and P may turn out be partially co-ordinated by units other than O-P or O-Al, respectively. A variety of reasons must be considered for any deviation from the "ideal"  $\text{AlPO}_4$  network in each individual case. The condensation of the inorganic reactants may be incomplete, resulting in a partial coordination of Al or P with terminal (*i.e.* non-bridging) groups like O, OH, or  $\text{OH}_2$ ; in addition to O-P, Al may be coordinated by a number of OH or  $\text{OH}_2$  groups, leading to a coordination number of up to six. The mesostructured aluminium phosphate sample may contain more or less significant amounts of aluminum oxide and/or oxyhydroxide species; these may either be part of the mesostructured product or be a second (possibly X-ray amorphous) phase. Furthermore, the co-ordination environment of Al and P is different at the boundary between the inorganic domains and the surfactant (or at the pore walls) than "inside" the inorganic walls. Studies of the short-range order in non-crystalline materials will usually lack completeness; modern NMR methods which correlate different nuclei (*e.g.* Al, P, H, C, N) with each other are probably the most promising approach to obtain as much information as possible.

**Table 1-1** (page 18) summarises the reports on mesostructured / mesoporous aluminium phosphates found in the literature; in the following, a detailed discussion of the publications will be made.

#### 1.2.3. Lamellar Mesostructured Aluminium Phosphates

The first periodically ordered mesostructured aluminium phosphate materials that were synthesised using supramolecular arrays of single-head-group surfactants as structure-directing species were reported in 1995 by OLIVER and OZIN *et al.* [73-76],

who employed primary long-chain amine surfactants ( $C_nH_{2n+1}NH_2$ ,  $n = 10, 11$ ) in a medium of tetraethylene glycol (TEG) and low quantities of water; phosphoric acid ( $H_3PO_4$  85%) and pseudo-boehmite (poorly crystallised boehmite,  $\gamma-AlO(OH)$ , with significant amounts of water) served as the inorganic reactants. According to powder X-ray diffraction (powder XRD) the products have lamellar mesostructures with Al/P ratios around 0.5, which suggests that considerable amounts of the phosphate units are not interconnected with Al units. Particular attention was paid to the morphological properties of these materials, which exhibit, among featureless flake-like particles, hollow spherical units and shell-like structures with diameters between 1 and 500  $\mu m$  and regular surface patterns or macropores, as shown by scanning electron microscopy (SEM). These hierarchical structures resemble certain morphologies of siliceous *diatom* or *radiolaria* biominerals.

About simultaneously, two other groups (SAYARI *et al.* and GAO *et al.*) independently reported the synthesis of lamellar mesostructured aluminium phosphates, again utilising neutral long-chain amines; these works were the first to focus on the mesostructural properties and the short-range order of the products rather than merely morphological aspects: SAYARI *et al.* [77,78] carried out their syntheses under aqueous conditions using primary as well as tertiary amine surfactants ( $C_nH_{2n+1}NH_2$ ,  $n = 8, 10, 12$ , and  $C_{12}H_{25}N(CH_3)_2$ ),  $H_3PO_4$ , and aluminium oxide; the initial pH in the reactions was 2.5 - 3.5. The relative amounts of Al and P as well as of the surfactant used in the syntheses were systematically changed; the resultant Al/P ratios in the products varied over a broad range (*ca.* 0.5 - 2). The authors also observed coaxial cylindrical layers by TEM with indications that the growth of these curved layers originates from the centre of the cylinders (CHENITE *et al.*) [79]. This structural feature, which was previously not observed among mesostructured inorganic/surfactant composite materials, suggests that, despite the apparent existence of rod-like surfactant arrangements (as found in the centres of the cylinders), a layered structure growth is favoured in the inorganic/surfactant composite. GAO *et al.* [80,81] carried out a similar synthesis employing primary amine surfactants ( $C_nH_{2n+1}NH_2$ ,  $n = 6, 8, 10, 12$ ), aluminium isopropoxide ( $Al(O^iPr)_3$ ), and  $H_3PO_4$ ; however, they conducted their syntheses under predominantly non-aqueous conditions using a 1:1 mixture of ethylene glycol (EG) and a primary alcohol ( $C_nH_{2n+1}OH$ ,  $n = 4 - 8$ ). The materials have Al/P ratios around 2.

Several more reports were made on syntheses of lamellar mesostructured aluminium phosphates. KHIMYAK and KLINOWSKI [82-84], used a cationic ammonium surfactant (CTACl,  $C_{16}H_{33}N[CH_3]_3^+ Cl^-$ ) under aqueous conditions. The pH was varied by addition of tetramethylammonium hydroxide (TMAOH); the Al/P ratio in the products is less than unity. KIMURA *et al.* [85,86], POPHAL *et al.* [87], and PEREZ O. *et al.* [88] also used cationic hexadecyltrimethylammonium surfactants under aqueous conditions; a short-chain amine surfactant was used by ESWARAMOORTHY *et al.* [89] (see below).

Another synthesis of lamellar aluminium phosphates that deserves to be discussed was published as early as 1993 by KRAUSHAAR-CZARNETZKI *et al.* [90], who employed long-chain alkylene diamine "bolaform" surfactants ( $H_2N-[CH_2]_n-NH_2$ ,  $n = 8, 10, 12$ ),  $H_3PO_4$ , and  $Al(O^iPr)_3$  under aqueous conditions; they also incorporated Co and Si into the network. The inorganic parts of these materials are crystalline, with the empirical formula  $Al_3H_3(PO_4)_4$ , *i.e.* they exhibit a three-dimensional periodicity on the atomic scale, although no crystal data are available in the paper. A very similar synthesis utilising the same kinds of diamine surfactants, but under non-aqueous conditions (ethylene glycol, EG), was more recently reported by FENG *et al.* [91], who also provided crystal data (the inorganic layers have the formula  $Al_{13}(PO_4)_{18}H$ ). The diamines are arranged in monolayers between the crystalline inorganic sheets, as can be deduced from the correlation between chain length and interlayer distance. However, the precise atomic positions could not be determined for all of the C atoms. Materials prepared with different chain lengths turn out to have the same inorganic composition and architecture, but varying interlayer distances. The surfactant arrangement can be adequately termed as 'supramolecular'. This structure-directing process is a special situation at the boundary between "classic" template-directed synthesis and structure-direction via supramolecular amphiphile arrays: The inorganic layers exhibit a crystal structure which is formed only by the utilization of this specific surfactant head group; nevertheless, the relationship between the surfactant and the inorganic crystal structure is not unambiguous, since the latter is not affected by a variation in the surfactant chain length. The fact that the organic layers consist of diamine monolayers rather than of less well-defined bilayers of single-head-group surfactants apparently leads to a better "structural communication" between two

adjacent inorganic layers and, thus, to a higher degree of periodic order on the atomic scale.

CHENG *et al.* [92] used primary amine surfactants with short hydrocarbon chains ( $C_nH_{2n+1}NH_2$ ,  $n = 4, 6, 8$ ) to synthesise layered materials from  $H_3PO_4$  and pseudo-boehmite under aqueous conditions. The inorganic sheets of the products may be assumed to be crystalline (empirical formula  $AlPO_3(OH)_2$ ); based on NMR and IR data, which reveal that both Al and P are entirely in tetrahedral co-ordination, the authors suggest a monolayer structure similar to the silicate layers of the naturally occurring mineral *kanemite*. However, no crystal data are available. The exact arrangement of the alkyl amine molecules in the interlayer region is not clear, but they can be exchanged against Na or K cations as well as hexadecyltrimethylammonium surfactant cations. In the latter case, a restructuring of the inorganic domains is observed, resulting in a mesostructure with presumably disordered tubular surfactant arrangement, which is thermally unstable and collapses upon removal of the surfactant.

#### 1.2.4. Non-Lamellar Mesostructured Aluminium Phosphates

One of the principal goals in the synthesis of mesostructured aluminium phosphates is to remove the organic amphiphile after the synthesis of the initial inorganic/organic composite in order to create a porous material with molecular sieve properties that may serve as, for example, size-selective catalysts or catalyst supports. For this purpose it is necessary that the inorganic network extends in all three dimensions and is stable enough to maintain its mesostructure after the removal of the organic part. Several papers on the first non-lamellar mesostructured aluminium phosphates (some of which contain additional elements in the network) were published independently in 1997 (refs. 68,69,93-103):

FENG *et al.* [93] employed a cationic ammonium surfactant (CTABr,  $C_{16}H_{33}N[CH_3]_3^+ Br^-$ ) with  $Al(O^iPr)_3$ ,  $H_3PO_4$ , and HF as reactants under aqueous conditions (pH adjusted to 8.3 by addition of TMAOH). Their product has an Al/P ratio slightly above 1 and consists of a three-dimensional inorganic network in which the surfactant is arranged in hexagonally packed rod-like (columnar) arrays, comparable to MCM-41 silica. However, the product turned out to be not stable

enough to maintain its mesostructure upon removal of the surfactant; the structure transforms to a lamellar phase at elevated temperatures and collapses when the amphiphile is removed by calcination.

ZHAO and LUAN *et al.* [94,95] used CTACl, H<sub>3</sub>PO<sub>4</sub>, and aluminium hydroxide under aqueous conditions with a pH of 8.5 (or above). They obtained products with Al/P ratios higher than 1, exhibiting mesostructures in which the surfactant arrangement consists of randomly ordered (non-linear) tube-like arrays. Their products are calcinable in flowing oxygen at a temperature of 500 °C, *i.e.* the surfactant can be thermally removed with only a partial network collapse (leading to a small decrease of the specific surface areas), yielding mesoporous materials with high specific surface areas around 700 m<sup>2</sup>/g. They also incorporated Si into the inorganic network, which led to an increase in stability and surface area in the products (*ca.* 900 m<sup>2</sup>/g). Particular attention should be paid to their subsequent reports on mesoporous aluminium phosphates transition metals integrated in the network [96-98]. The incorporation of Mn (Mn/Al up to 0.2) led to a better thermal stability, whereas V (V/Al up to 0.1) caused a decrease in structural order and stability. The preparation of metal-substituted materials is one of the most important goals in the synthesis of mesoporous aluminium phosphates; the generation of acidic sites and/or reactive metal ion valence states in the network is necessary for many catalytic applications, such as oxidation reactions.

Very similar synthesis conditions were employed by KIMURA *et al.* [99] who synthesised mesostructures with hexagonal symmetry under aqueous conditions, utilising CTACl, H<sub>3</sub>PO<sub>4</sub>, and Al(O<sup>*i*</sup>Pr)<sub>3</sub>. By calcination at 600 °C in air they obtained porous materials with surface areas around 450 m<sup>2</sup>/g and comparably low pore diameters with physisorption data indicating micro- rather than mesopores. However, the utilisation of a longer hydrocarbon chain in the surfactant (C<sub>22</sub>H<sub>45</sub>N[CH<sub>3</sub>]<sub>3</sub><sup>+</sup> Cl<sup>-</sup>) as well as the addition of triisopropylbenzene to the synthesis mixture, which presumably causes a "swelling" of the rod-like surfactant arrays, subsequently resulted in a significant increase in pore size from micro- to mesoporous (surface area > 700 m<sup>2</sup>/g) [100,101]. This group demonstrated how the symmetry of the mesostructured products (*i.e.* lamellar or hexagonal) depends on the synthesis conditions [86]. The starting pH was adjusted to 8 - 10; the Al/P ratio is greater than 1 in most of the products. In lamellar materials the condensation of the aluminium phosphate network is relatively

complete, as indicated by NMR data; the hexagonal phases, on the other hand, consist of a less condensed network. This is consistent with the observation that higher synthesis temperatures led to lamellar phases, whereas hexagonal materials are formed only at sufficiently low temperatures ( $< 130\text{ }^{\circ}\text{C}$ ). Their formation seems to proceed by transition of a layered phase which is composed of aluminium phosphate oligomers and surfactant cations into a hexagonal phase with further condensation of the oligomers.

CHAKRABORTY *et al.* [102,103]. reported the aqueous synthesis of hexagonal silicoaluminium phosphate materials with surface areas of *ca.*  $900\text{ m}^2/\text{g}$  after calcination at  $600\text{ }^{\circ}\text{C}$  in nitrogen and air. They used CTACl,  $\text{H}_3\text{PO}_4$ , and  $\text{Al}(\text{O}^i\text{Pr})_3$  under aqueous conditions with a rather low pH of 2.5. Powder XRD data indicate that the degree of structural order in these materials is remarkably high. However, the overall content of Si in the samples is quite low (about 2 - 3 % with respect to either Al or P); the Al/P ratio is about 1.

An interesting synthesis route for the preparation of mesoporous aluminium-phosphate-based materials was introduced by HOLLAND *et al.* [68,69], who utilised polyoxometalate clusters ( $\text{AlO}_4\text{Al}_{12}(\text{OH})_{24}(\text{H}_2\text{O})_{12}^{7+}$ ,  $\text{GaO}_4\text{Al}_{12}(\text{OH})_{24}(\text{H}_2\text{O})_{12}^{7+}$ ) as Al or Al/Ga sources, respectively. These positively charged clusters are precipitated as layered salts of an anionic surfactant (sodium *n*-dodecyl sulfate,  $\text{C}_{12}\text{H}_{25}\text{OSO}_3^- \text{Na}^+$ ) under pH conditions which prevent covalent linking of adjacent cationic units. A mesostructured network is then formed in aqueous solution by addition of phosphate ions as linking species; the pH is adjusted to *ca.* 3. This process is accompanied by a phase transition from a layered to a nearly hexagonal structure. NMR data indicate that during the phosphate linking step the clusters break up leading to a uniform (gallo)aluminium phosphate network with an Al/P ratio of 1.3. The surfactant can be removed by anion exchange extraction yielding specific surface areas up to  $630\text{ m}^2/\text{g}$ ; the products are thermally stable up to  $350\text{ }^{\circ}\text{C}$ . The anion exchange properties were further investigated (KRON *et al.*) [104].

Following these initial publications, several more mesoporous aluminium phosphates with randomly ordered tubular pore arrangement were reported. CABRERA *et al.* [105] used CTABr,  $\text{H}_3\text{PO}_4$ , and  $\text{Al}(\text{O}^s\text{Bu})_3$  under slightly alkaline aqueous conditions (pH adjusted to 8 - 9 by addition of triethylamine) and obtained

products with Al/P ratios between 1.3 and 6.7, the relative amount of Al being correlated with the pore size, which ranged from microporous (low amounts of Al; 480 m<sup>2</sup>/g) to mesoporous (high amounts of Al; 650 m<sup>2</sup>/g). Calcination was achieved at 500 °C under flowing air atmosphere. Similar synthetic conditions were used by KHIMYAK and KLINOWSKI [84], who used CTABr under aqueous conditions to prepare tubular porous materials from H<sub>3</sub>PO<sub>4</sub> and Al(O<sup>i</sup>Pr)<sub>3</sub>; the Al/P ratio in the products is between 0.6 and 1; pore sizes range from micro- to mesoporous with specific surface areas up to 990 m<sup>2</sup>/g (calcination at 500 °C in air). KAPOOR and RAJ [106] used CTABr, H<sub>3</sub>PO<sub>4</sub>, and Al(O<sup>i</sup>Pr)<sub>3</sub> under aqueous conditions to synthesise materials with Al/P ratios of 1.25 and surface areas up to 800 m<sup>2</sup>/g (calcination at 400 °C in air); they also incorporated Ti in the network, which led to an increase in thermal stability. These materials were successfully tested with respect to their catalytic activity for the epoxidation of olefins. ESWARAMOORTHY *et al.* [89] prepared micro- rather than mesoporous materials utilising a short-chain alkyl amine (C<sub>6</sub>H<sub>13</sub>NH<sub>2</sub>), H<sub>3</sub>PO<sub>4</sub>, aluminium hydroxide, and HF under predominantly aqueous conditions at neutral pH; depending on the synthesis conditions the products exhibit Al/P ratios from 0.5 to 1 and limited thermal stability; calcination at 300 °C led to a removal of only 60 % of the amine. CHENG *et al.* [92] obtained tubular mesostructures by surfactant ion exchange in layered materials as mentioned above.

**Table 1-1.** Summary of mesostructured aluminium phosphates synthesised by the utilisation of supramolecular arrays of amphiphiles as structure-directing agents reported in the literature.

Surfactant	Solvent	Structure <sup>a</sup>	Surface area <sup>b</sup>	Al/P <sup>c</sup>	Authors	Remarks
<b>neutral:</b>						
C <sub>n</sub> H <sub>2n+1</sub> NH <sub>2</sub> (n=10,11)	TEG, (H <sub>2</sub> O)	lam	-	0.5	OLIVER <i>et al.</i> [73-76]	
C <sub>n</sub> H <sub>2n+1</sub> NH <sub>2</sub> (n=8,10,12)	H <sub>2</sub> O	lam	-	0.5 - 2	SAYARI <i>et al.</i> ; CHENITE <i>et al.</i> [77-79]	
C <sub>n</sub> H <sub>2n+1</sub> NH <sub>2</sub> (n=6,8,10,12)	EG,ROH, H <sub>2</sub> O	lam	-	~2	GAO <i>et al.</i> [80,81]	
C <sub>n</sub> H <sub>2n+1</sub> NH <sub>2</sub> (n=4,6,8)	H <sub>2</sub> O	lam, tub	-	1 <sup>d</sup>	CHENG <i>et al.</i> [92]	
C <sub>6</sub> H <sub>13</sub> NH <sub>2</sub>	H <sub>2</sub> O, (MeOH)	tub, lam	190 <sup>e</sup>	0.5 - 1	ESWARAMOORTHY <i>et al.</i> [89]	
H <sub>2</sub> N(CH <sub>2</sub> ) <sub>n</sub> NH <sub>2</sub> (n=8,10,12)	H <sub>2</sub> O	lam	-	0.75 <sup>d</sup>	KRAUSHAAR- CZARNETZKI <i>et al.</i> [90]	Co <sup>f</sup>
H <sub>2</sub> N(CH <sub>2</sub> ) <sub>n</sub> NH <sub>2</sub> (n=9 12)	EG	lam	-	0.72 <sup>d</sup>	FENG <i>et al.</i> [91]	
<b>cationic:</b>						
CTABr	H <sub>2</sub> O, (EtOH)	hex	-	1.18	FENG <i>et al.</i> [93]	
CTABr	H <sub>2</sub> O	tub	480-650	1.3 - 6.7	CABRERA <i>et al.</i> [105]	
CTABr	H <sub>2</sub> O, (EtOH)	hex	800	1.25	KAPOOR and RAJ [106]	Ti <sup>f</sup>
CTABr	H <sub>2</sub> O	hex	900	~1	CHAKRABORTY <i>et al.</i> [102,103]	
CTABr	H <sub>2</sub> O	lam, hex	-	1 - 1.35	PEREZ O. <i>et al.</i> [88]	
CTACl	H <sub>2</sub> O	tub	700	>1	ZHAO and LUAN <i>et al.</i> [94-98]	Si, Mn, V <sup>f</sup>
CTACl <sup>g</sup>	H <sub>2</sub> O, (MeOH)	hex, lam	>700	>1	KIMURA <i>et al.</i> [85,86,99-101]	
CTACl	H <sub>2</sub> O	lam, tub	990	0.6 - 1	KHIMYAK and KLINOWSKI [82-84]	
C <sub>16</sub> H <sub>33</sub> (CH <sub>3</sub> ) <sub>3</sub> N <sup>+</sup> OH <sup>-</sup>	H <sub>2</sub> O	lam	-		POPHAL <i>et al.</i> [87]	
<b>anionic:</b>						
C <sub>n</sub> H <sub>2n+1</sub> OPO(OH) <sub>2</sub> (n=6,8,10)	H <sub>2</sub> O	lam	-	~1	TANAKA and CHIKAZAWA [107,108]	
C <sub>12</sub> H <sub>25</sub> OSO <sub>3</sub> <sup>-</sup> Na <sup>+</sup>	H <sub>2</sub> O	hex	630	1.3	HOLLAND <i>et al.</i> ; KRON <i>et al.</i> [68,69,104]	Ga <sup>f</sup>

<sup>a</sup> lam = lamellar, hex = hexagonal, tub = randomly ordered tubular. <sup>b</sup> if porous (g/m<sup>2</sup>). <sup>c</sup> in the products.  
<sup>d</sup> crystalline. <sup>e</sup> microporous. <sup>f</sup> element(s) also incorporated in network. <sup>g</sup> also C<sub>22</sub>H<sub>45</sub>N(CH<sub>3</sub>)<sub>3</sub><sup>+</sup> Cl<sup>-</sup>.

### 1.3. Aim of this Work

As discussed in the preceding chapters, the synthesis of ordered mesostructured aluminium phosphates is governed by a variety of parameters which affect the overall quality of the products. A synthesis system which involves supramolecular arrays of amphiphiles as structure-directors is always rather complex and difficult to control. In contrast to the relatively well-established mesoporous silica materials, which usually require only one single reactant (such as tetraethyl orthosilicate), aluminium phosphates have so far exclusively been prepared from separate sources of aluminium and phosphorous (*e.g.*  $\text{Al}(\text{iOPr})_3$  and  $\text{H}_3\text{PO}_4$ ). Owing to this complexity of the syntheses it is generally difficult to control the reactions in a rational way. This becomes apparent from the fact that the stoichiometric composition of the products often quite dramatically defers from the desired ratio of  $\text{Al/P} = 1$  (cf. Table 1-1).

This work aims at new strategies to decrease the complexity of the synthesis systems in the preparation of mesostructured aluminium phosphates in order to gain a better control over the reactions. For this purpose various distinct concepts are pursued and, where possible, combined with each other: (i) *n*-Dodecyl phosphate is used as a structure-directing amphiphile, which may simultaneously serve as the phosphorous source for the inorganic matrix, *i.e.* as one of the two reactants; thus, the number of chemical compounds employed in the reaction can be reduced by one as no additional P source is required. (ii) Water as a solvent is replaced by alcohols; this drastically decelerates the reaction kinetics, thus providing a better control over the syntheses. In addition, non-aqueous reaction conditions give way to (iii) the utilisation of a single-source molecular precursor with a pre-defined Al-O-P arrangement and short-range order, providing the most powerful means to attain control over the stoichiometry of the mesostructured products.

Apart from this purpose (to establish improved synthesis strategies), particular attention is paid to a better understanding of the synthesis reactions by *in-situ* X-ray diffraction studies. In particular, time-resolved investigations benefit from the slow reaction kinetics in alcoholic (instead of aqueous) syntheses.

## 2. Experimental

### 2.1. Synthetic Procedures

#### 2.1.1. Aqueous Synthesis of Mesostructured Aluminium Phosphates with *n*-Dodecyl phosphate as Structure-director

In a typical synthesis 5.11 g  $\text{Al}(\text{O}^i\text{Pr})_3$  and 2.89 g  $\text{H}_3\text{PO}_4$  (85 %) were added to a solution of 1.66 g *n*-dodecyl phosphate ( $\text{C}_{12}\text{H}_{25}\text{OPO}(\text{OH})_2$ ) in 15 g water, corresponding to an approximate molar ratio in the synthesis mixture of  $\text{Al} / \text{P} / \text{surfactant} / \text{water} = 1 / 1 / 0.25 / 35$ . The relative amounts of  $\text{Al}(\text{O}^i\text{Pr})_3$ ,  $\text{H}_3\text{PO}_4$ , and surfactant were varied as discussed in chapter 3. The mixture was stirred at room temperature for 1 hour, transferred into a teflon-lined steel autoclave and kept at 393 K for 24 hours without agitation. The product was filtered off, washed with ethanol and dried in vacuum.

#### 2.1.2. Alcoholic Synthesis of Mesostructured Aluminium Phosphates with *n*-Dodecyl phosphate as Structure-director

In a typical synthesis 5.11 g  $\text{Al}(\text{O}^i\text{Pr})_3$  and 2.89 g  $\text{H}_3\text{PO}_4$  (85 %) were added to a solution of 6.66 g *n*-dodecyl phosphate ( $\text{C}_{12}\text{H}_{25}\text{OPO}(\text{OH})_2$ ) in 58 g ethanol (99.8 %) and 1.0 g water, corresponding to an approximate molar ratio in the synthesis mixture of  $\text{Al} / \text{P} / \text{surfactant} / \text{ethanol} / \text{water} = 1 / 1 / 1 / 50 / 3$ . The relative amount of the surfactant was varied as discussed in chapter 4. The mixture was stirred at room temperature for 30 minutes, transferred into a teflon-lined steel autoclave and kept at 363 K for 48 hours without agitation. The synthesis temperature was varied as discussed below. The product was filtered off, washed with ethanol and dried in vacuum.

### 2.1.3. Alcoholic Synthesis of Mesoporous Aluminium Phosphates with *n*-Alkyl Amines as Structure-directors

#### *Synthesis from Al(O<sup>i</sup>Pr)<sub>3</sub> and H<sub>3</sub>PO<sub>4</sub>*

In a typical synthesis 8.2 g Al(O<sup>i</sup>Pr)<sub>3</sub> was added to a solution of 4.6 g H<sub>3</sub>PO<sub>4</sub> (85 %) in 50 g ethanol (99.8 %) and 1.4 g water. The mixture is stirred vigorously for 30 minutes at room temperature. A solution of 4.8 g *n*-hexadecylamine (C<sub>16</sub>H<sub>33</sub>NH<sub>2</sub>) in 10 g ethanol (99.8 %) was then added, corresponding to an approximate molar ratio in the synthesis mixture of Al / P / surfactant / ethanol / water = 1 / 1 / 0.5 / 32 / 3. *n*-Tetradecylamine (C<sub>14</sub>H<sub>29</sub>NH<sub>2</sub>) or *n*-dodecylamine (C<sub>12</sub>H<sub>25</sub>NH<sub>2</sub>) were also used. After stirring at room temperature for another 30 minutes the slurry was transferred into a teflon-lined autoclave and kept at 363 K for 48 hours without agitation. The product was filtered off, washed with ethanol and dried. In a post-synthetic treatment 5 g of the dry sample was stored in a closed container over 10 g of water. The container was sealed and stored at 363 K in for 12 hours without agitation. By this procedure the sample was exposed to water vapour, but was not in contact with liquid water. For the extraction of the surfactant 5 g of the sample (after the post-synthetic treatment) was dispersed in a solution of 20 g methanol and 5 g aqueous hydrochloric acid (1 mol/l). The mixture was stirred at room temperature for 15 minutes, filtered off, and washed with methanol. The process was repeated three times.

#### *Synthesis from [Al(PO<sub>4</sub>)(HCl)(C<sub>2</sub>H<sub>5</sub>OH)<sub>4</sub>]<sub>4</sub>*

In a typical synthesis a solution of 4.8 g *n*-hexadecylamine (C<sub>16</sub>H<sub>33</sub>NH<sub>2</sub>) in 10 g ethanol (99.8 %) was added to a solution of 13.8 g [Al(PO<sub>4</sub>)(HCl)(C<sub>2</sub>H<sub>5</sub>OH)<sub>4</sub>]<sub>4</sub> in 50 g ethanol (99.8 %), corresponding to an approximate molar ratio in the synthesis mixture of Al / P / surfactant / ethanol = 1 / 1 / 0.5 / 32. The synthesis was otherwise carried out as described for the synthesis from Al(O<sup>i</sup>Pr)<sub>3</sub> and H<sub>3</sub>PO<sub>4</sub>.

### 2.1.4. Synthesis of [Al(PO<sub>4</sub>)(HCl)(C<sub>2</sub>H<sub>5</sub>OH)<sub>4</sub>]<sub>4</sub>

The synthesis was carried out in a variation of the procedure described by CASSIDY *et al.* [109]: A solution of 8.65 g H<sub>3</sub>PO<sub>4</sub> (85 %) in 50 ml ethanol (99.8 %) was slowly added (over a time interval of *ca.* 2 minutes) to a solution of 10 g AlCl<sub>3</sub> in 100 ml ethanol (99.8 %) under light stirring at 0 °C under nitrogen atmosphere. The

solution was then immediately transferred to a refrigerator. The product crystallised in the course of 12 – 24 hours after which it was filtered off, washed with small quantities of dry ethanol, and stored under nitrogen atmosphere. Further information on the synthesis procedure is given in chapter 6.2.

## 2.2. Chemical Compounds

Aluminium triisopropylate ( $\text{Al}(\text{O}^i\text{Pr})_3$ , Merck), aluminium chloride ( $\text{AlCl}_3$ , anhydrous, sublimed, Merck), phosphoric acid ( $\text{H}_3\text{PO}_4$ , 85 %, Merck), tetramethylammonium hydroxide ( $(\text{CH}_3)_4\text{NOH}$ , pentahydrate, Fluka), *n*-dodecyl phosphate ( $\text{C}_{12}\text{H}_{25}\text{OPO}(\text{OH})_2$ , (Lancaster, Alfa), *n*-dodecylamine ( $\text{C}_{12}\text{H}_{25}\text{NH}_2$ , Merck), *n*-hexadecylamine ( $\text{C}_{16}\text{H}_{33}\text{NH}_2$ , Merck), and *n*-tetradecylamine ( $\text{C}_{14}\text{H}_{29}\text{NH}_2$ , Aldrich) were used as received. For small-angle X-ray scattering (SAXS) studies, *n*-dodecyl phosphate was purified by recrystallisation from ethanol/water.

## 2.3. Characterisation

### 2.3.1. Powder X-ray Diffraction

Powder X-ray diffraction (powder XRD) was performed on a Philips PW 1050/25 diffractometer using filtered  $\text{Cu-K}\alpha$  radiation (samples from aqueous syntheses) and on a Bruker AXS D8 Advance diffractometer, equipped with a secondary monochromator, using filtered  $\text{Cu-K}\alpha$  radiation (samples from non-aqueous syntheses).

*In-situ* temperature-resolved powder X-ray diffraction was carried out using a Philips low temperature chamber mounted on a PW 3020 goniometer.

### 2.3.2. Transmission Electron Microscopy

Transmission electron microscopy (TEM) was carried out with a Philips STEM 400 electron microscope. Samples were prepared from an ethanolic dispersion on a carbon foil supported on a copper grid.

### 2.3.3. Thermal Analysis

Simultaneous thermogravimetry (TG), differential thermal analysis (DTA) and mass spectrometry (MS) was performed on a Netzsch STA 409 thermobalance and a Baltzer QMG 421 quadrupole mass spectrometer coupled by a Baltzer 403/4 capillary coupling system (multiple ion detection method); samples were heated by 5 K per minute in an open alumina crucible at normal pressure under dynamic air atmosphere.

Differential scanning calorimetry (DSC) was carried out with a Mettler DSC 27 HP calorimeter. Samples were heated at 5 K/min in open crucibles under air atmosphere.

### 2.3.4. IR Spectroscopy

Infrared (IR) spectroscopic measurements were performed in a KBr matrix on a Perkin Elmer FT-IR 1720 spectrometer.

### 2.3.5. Polarised Light Optical Microscopy

Polarised light optical microscopy (POM) was carried out with an Olympus BX50 microscope and a Mettler Toledo FP82HT heating stage. Samples were homogenised by vortexing at 70 °C in sealed Eppendorf tubes, kept at room temperature for several days, and investigated in flame-sealed glass capillaries.

### 2.3.6. Physisorption

Nitrogen physisorption analysis was carried out on a Quantachrome Autosorb 1 apparatus; the samples were dried at 90 °C in high vacuum for 24 hours. Specific surface areas were calculated by the BET equation [110] for relative pressures between 0.05 and 0.2; pore size distributions were calculated by the BJH formula [111] from the desorption isotherm.

### 2.3.7. Elemental Analysis

Elemental analysis was carried out at the *Department of Analytical Chemistry, University of Hamburg*. Carbon, hydrogen, and nitrogen were analysed by combustion spectrometry. For phosphorous and aluminium analysis, samples were decomposed

with sulfuric acid ( $\text{H}_2\text{SO}_4$ ) and perchloric acid ( $\text{HClO}_4$ ). Phosphorous was analysed by photometry ('molybdenum blue' method); aluminium was analysed by induced coupled plasma (ICP) spectroscopy. All analyses were carried out twice with separate sampling.

### 2.3.8. X-ray Absorption Spectroscopy

X-ray absorption (XANES) spectra at the Al K-edge of samples from aqueous syntheses were recorded at beamline 3-3 at *Stanford Synchrotron Radiation Laboratory* (SSRL) at *Stanford Linear Accelerator Center* (SLAC), USA, at room temperature in total electron yield mode. The SPEAR electron storage ring was running at 3 GeV with a current of *ca.* 60 - 95 mA. The beamline was equipped with a  $\text{YB}_{66}$  (400) double-crystal monochromator [112,113].

X-ray absorption (XANES) spectra at the Al K-edge of samples from alcoholic syntheses were recorded at beamline SA32 at *Laboratoire pour l'Utilisation du Rayonnement Électromagnétique* (LURE), *Centre Universitaire Paris-Sud*, Orsay Cedex, France, at room temperature in total electron yield mode, using a quartz double-crystal monochromator. The electron storage ring was running at 0.8 GeV with currents of *ca.* 220 - 420 mA.

All spectra were calibrated against the edge position of pure aluminium (1559 eV), pre-edge fitted and normalised with WINXAS software [114].

### 2.3.9. *In-situ* Small Angle X-ray Scattering

Temperature- and time-resolved small angle X-ray scattering (SAXS) investigations were carried out at beamline X 13 at *European Molecular Biology Laboratory* (EMBL) and beamline A2 at *Hamburger Synchrotronstrahlungslabor* (HASYLAB) at *Deutsches Elektronensynchrotron* (DESY), Hamburg. The samples were placed in the X-ray beam in flame-sealed glass capillaries of 1 mm diameter. Samples of pure surfactant/water mixtures were homogenised by vortexing at 70 °C in sealed Eppendorf tubes and kept at room temperature for several days. Investigations on samples containing the inorganic species were carried out within 5 - 10 minutes after the addition of  $\text{Al}(\text{O}^i\text{Pr})_3$  and  $\text{H}_3\text{PO}_4$  to the surfactant/solvent mixture. The temperature

was controlled by a circulating water bath at a heating rate of 5 °C per minute; the samples were kept at the desired temperature for three minutes before the data were taken. For temperature-resolved measurements the following procedure was used: 4 minutes heating (by 20 K at 5 K/min) – 3 minutes temperature equilibration – 4 minutes data collection. Diffraction patterns were recorded with a 1024 channel linear detector [115]. Data processing was carried out with OTOKO software [116]; diffraction peak positions were calibrated against silver behenate ( $d_{001} = 5.8380(3)$  nm) [117] and transformed for clarity into a  $2\theta$  scaling based on the wavelength of Cu-K $\alpha$  radiation (0.15405 nm).

### 2.3.10. Solid-state NMR Spectroscopy

Solid-state NMR spectroscopic investigations were carried out at the *Institute of Optics and Quantum Electronics, Friedrich-Schiller-Universität, Jena*, on a BRUKER AXS 400 spectrometer operating at a magnetic field  $B_0 = 9.4$  T. NMR frequencies were 102 MHz for  $^{27}\text{Al}$  and 161 MHz for  $^{31}\text{P}$  NMR, respectively. Two double resonant BRUKER MAS probes were used with a 4 mm rotor system for MAS frequencies up to 14 kHz and a 2.5 mm rotor system for very fast MAS up to 35 kHz.  $^{27}\text{Al}$  MAS NMR spectra were recorded using a spinning frequency of 10 kHz with proton decoupling acquiring typically 512 scans. These spectra were referenced against YAG as secondary standard using the narrow signal of the six-fold coordinated Al site at 0.6 ppm. For  $^{31}\text{P}$  NMR measurements the repetition time was 20 sec with 16 ... 32 scans. The MAS frequencies were varied between 10 and 28 kHz and proton high power dipolar decoupling was required. Chemical shifts were referenced against a solution of 85% phosphoric acid.

The  $^{27}\text{Al}$  multiple quantum MAS experiments (MQMAS) [118-120] were carried out using the  $z$ -filter sequence with three r. f. pulses. The rotation frequency in these experiments was 10 kHz with a sweep width of the  $f_1$  triple quantum dimension of 66.7 kHz. The repetition time was 0.1 s and pulse widths of 3.5  $\mu\text{s}$  and 1.6  $\mu\text{s}$  for the first two pulses were used at the  $B_1$  field strength that corresponds to 100 kHz. The third weak pulse was 8  $\mu\text{s}$  long using a field strength of 20 kHz. A total of 256  $t_1$  increments (15  $\mu\text{s}$  incrementation time, hypercomplex data acquisition) was measured with 1k scans for each increment. The total measuring time was approximately 4 hours.

### 3. Aqueous Synthesis with *n*-Dodecyl Phosphate as Structure-director

#### 3.1. Basic Characterisation

Mesostructured aluminium phosphates were synthesised from equal amounts of aluminium triisopropylate ( $Al(O^iPr)_3$ ), phosphoric acid ( $H_3PO_4$ ) and *n*-dodecyl phosphate ( $C_{12}H_{25}OPO(OH)_2$ , in the following:  $C_{12}$ - $PO_4$ ) (synthesis method A). Different amounts of water were used to vary the surfactant concentration over the range 1 - 23 % w/w (0.05 - 1.11 mol/l). The powder XRD patterns (**Figure 3-1**) of these products are similar to each other and consist of one set of equidistant reflections which may be explained as  $00l$  reflections of a single lamellar phase with a  $d$  spacing of *ca.* 3.55 nm; in some cases an additional set of equidistant reflections of low intensity, corresponding to a second lamellar phase ( $d$  spacing *ca.* 2.69 nm), is observed (**Table 3-1**). **Figure 3-2** shows a transmission electron micrograph of the sample **A3** prepared with a surfactant concentration of 5 % w/w; the striped pattern is consistent with the lamellar structure.

**Table 3-1.** Synthesis parameters and  $d$  spacings (minor phases in parentheses) of lamellar mesostructured aluminium phosphates prepared from equal amounts of  $Al(O^iPr)_3$ ,  $H_3PO_4$  (where noted), and  $C_{12}$ - $PO_4$  under aqueous conditions (methods A or B).

surfactant concentration		synthesis with $H_3PO_4$ (method A)		synthesis without $H_3PO_4$ (method B)		
% w/w	mol/l	No.	$d$ (nm)		No.	$d$ (nm)
1	0.05	<b>A1</b>	3.55	(2.68)	<b>B1</b>	2.71
2	0.09	<b>A2</b>	3.54	(2.69)	<b>B2</b>	2.71
5	0.18	<b>A3</b>	3.52		<b>B3</b>	2.69
7	0.28	<b>A4</b>	3.52		<b>B4</b>	2.71
9	0.37	<b>A5</b>	3.56		<b>B5</b>	(3.58) 2.70
13	0.55	<b>A6</b>	3.52		<b>B6</b>	3.55 (2.70)
16	0.74	<b>A7</b>	3.52		<b>B7</b>	3.54 (2.69)
23	1.11	<b>A8</b>	3.55		<b>B8</b>	3.55 (2.69)

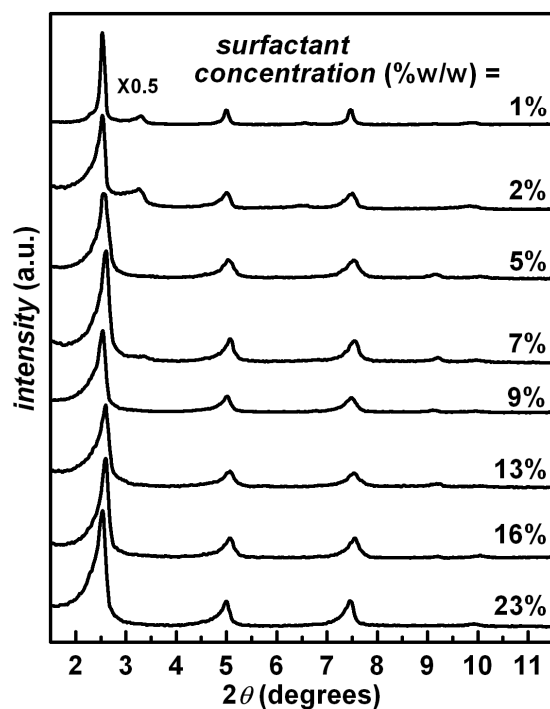


**Figure 3-1.** Powder XRD patterns of mesostructured aluminium phosphates prepared with equal amounts of  $\text{Al}(\text{O}^i\text{Pr})_3$ ,  $\text{H}_3\text{PO}_4$ , and  $\text{C}_{12}\text{-PO}_4$  under aqueous conditions (method A). A lamellar phase with a  $d$  spacing of *ca.* 3.5 nm is observed for all surfactant concentrations; for low concentrations (1-2 % w/w) a second lamellar phase with a smaller  $d$  spacing of *ca.* 2.7 nm is found (cf. Table 3-1).

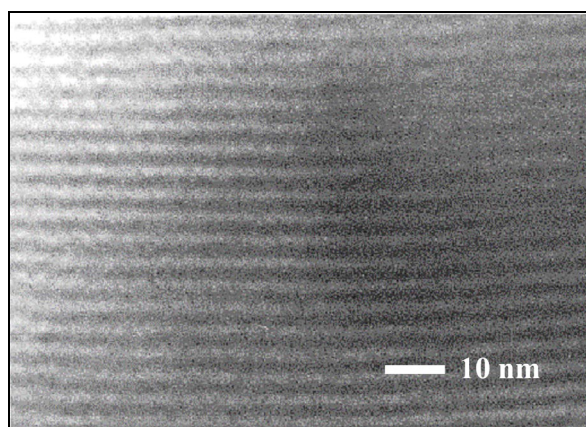


**Figure 3-2.** Transmission electron micrograph of a representative lamellar mesostructured aluminium phosphate prepared with equal amounts of  $\text{Al}(\text{O}^i\text{Pr})_3$ ,  $\text{H}_3\text{PO}_4$ , and  $\text{C}_{12}\text{-PO}_4$  under aqueous conditions (method A, sample A3).

The same synthesis procedures were carried out without  $\text{H}_3\text{PO}_4$  as a phosphorous source (synthesis method B). In these cases the only phosphate groups available in the

reaction mixture are those from the surfactant. In the following, the synthetic method in which  $H_3PO_4$  is used will be referred to as method A and the synthesis without  $H_3PO_4$  will be denoted as method B. For low surfactant concentrations the powder XRD patterns of these method B products (**Figure 3-3**) indicate a single lamellar phase with a  $d$  spacing of *ca.* 2.70 nm; a second lamellar phase with a  $d$  spacing of *ca.* 3.55 nm occurs and becomes predominant when the surfactant concentration is increased (see Table 3-1).

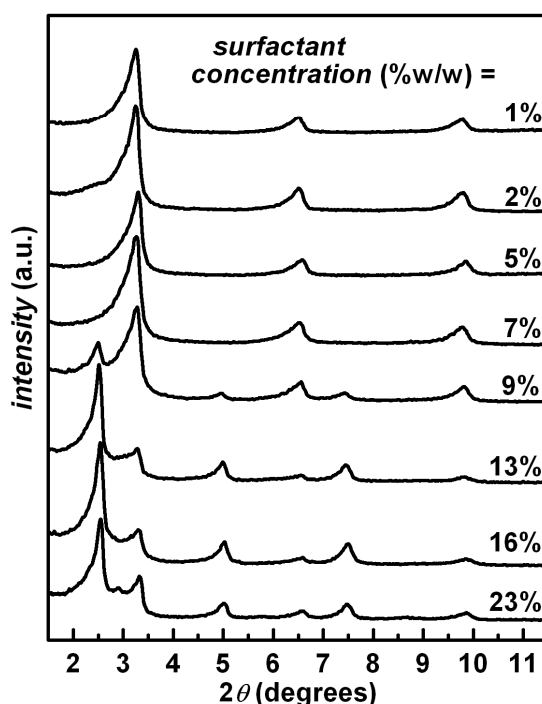


**Figure 3-3.** Powder XRD patterns of lamellar mesostructured aluminium phosphates prepared with equal amounts of  $Al(O^iPr)_3$  and  $C_{12}$ - $PO_4$  under aqueous conditions (method B). A lamellar phase with a small  $d$  spacing of *ca.* 2.70 nm is observed for all surfactant concentrations in the synthesis; for high concentrations (9-23 % w/w) a second lamellar phase with a larger  $d$  spacing of *ca.* 3.55 nm is found (cf. Table 3-1).

Finally, syntheses with a constant surfactant concentration of 13 % w/w and variable amounts of  $Al(O^iPr)_3$  and  $H_3PO_4$  were carried out. Again, the same syntheses were repeated without  $H_3PO_4$ . Information on the molar compositions of the samples is obtained from C, Al and P elemental analysis. The relative ratios of the elements in the samples have to be compared to the relative ratios of the reactants used for the preparations. Particular interest lies in the amount of P and its origin, since in those

products that are synthesised by method A two different P sources contribute to the final overall P content.

**Table 3-2** shows the relative Al/P and C/P ratios in the products as found by elemental analysis compared to the relative amounts of Al(O<sup>*i*</sup>Pr)<sub>3</sub>, H<sub>3</sub>PO<sub>4</sub>, and C<sub>12</sub>-PO<sub>4</sub> originally used for the syntheses. The Al/P ratios found by analysis are greater than expected when the theoretical value is low, and smaller than expected when the theoretical values are high, the latter being the case especially for samples prepared with H<sub>3</sub>PO<sub>4</sub> (method A). For the samples prepared without H<sub>3</sub>PO<sub>4</sub> (method B) the C/P ratio fits in with the expected one, C/P = 12 (with a deviation averaging *ca.* 2.5 %). Accordingly, for those samples which were prepared with H<sub>3</sub>PO<sub>4</sub> (method A), the relative contributions of P from H<sub>3</sub>PO<sub>4</sub> and P from the surfactant to the overall amount of P can be calculated by  $P_{\text{H}_3\text{PO}_4}/P_{\text{surfactant}} = (12 \cdot P/C) - 1$ . The powder XRD patterns of the products prepared with - (**Figure 3-4**) and without H<sub>3</sub>PO<sub>4</sub> (**Figure 3-5**) show two sets of equidistant reflections, corresponding to two lamellar phases with *d* spacings of *ca.* 2.70 nm and 3.55 nm, respectively, with variable relative intensities in dependence on the Al/P ratio (see below).

**Table 3-2.** Synthesis parameters, elemental analysis and *d* spacings (minor phases in parentheses) of samples prepared with different relative amounts of Al(O<sup>*i*</sup>Pr)<sub>3</sub>, H<sub>3</sub>PO<sub>4</sub>, and C<sub>12</sub>-PO<sub>4</sub> (13 % w/w) under aqueous conditions.

No.	input ratio <sup>a</sup>	analytical molar ratios		ratio <sup>b</sup> calcd. from anal.	<i>d</i> (nm) 1st and 2nd phase	
		C/P	Al/P			
<b>A9</b>	0.5/1/1	10.70	0.45	0.51/0.12/1		3.53
<b>A10</b>	1/1/1	4.86	0.79	1.95/1.47/1		3.52
<b>A11</b>	1.5/1/1	4.40	0.83	2.26/1.73/1		3.49
<b>A12</b>	2/1/1	5.77	0.88	1.83/1.08/1	2.68	(3.44)
<b>A13</b>	3/1/1	5.29	1.24	2.83/1.27/1	2.71	(3.65)
<b>A14</b>	8/1/1	5.06	3.36	7.97/1.37/1	2.69	
<b>B9</b>	0.25/0/1	11.84	0.46	0.46/0/1	(2.67)	3.56
<b>B10</b>	0.5/0/1	12.70	0.55	0.55/0/1		3.56
<b>B11</b>	1/0/1	11.50	1.11	1.11/0/1	(2.70)	3.55
<b>B12</b>	1.25/0/1	11.65	1.30	1.30/0/1	(2.71)	3.56
<b>B13</b>	1.5/0/1	12.23	1.51	1.51/0/1	2.73	
<b>B14</b>	2/0/1	12.05	1.78	1.78/0/1	2.72	(3.51)
<b>B15</b>	4/0/1	12.02	3.93	3.93/0/1	2.73	

<sup>a</sup> Al(O<sup>*i*</sup>Pr)<sub>3</sub>/H<sub>3</sub>PO<sub>4</sub>/C<sub>12</sub>-PO<sub>4</sub> ratio. <sup>b</sup> Al/P<sub>H<sub>3</sub>PO<sub>4</sub></sub>/P<sub>C<sub>12</sub>-PO<sub>4</sub></sub> ratio.

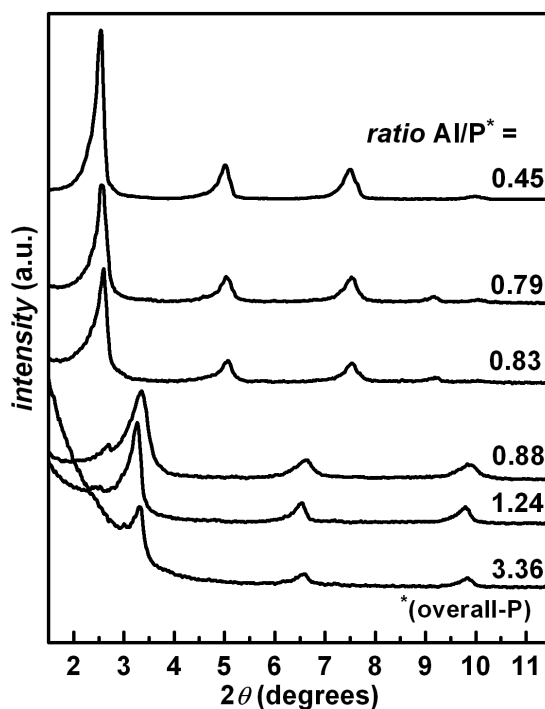


**Figure 3-4.** Powder XRD patterns of mesostructured aluminium phosphates prepared with variable relative amounts of  $Al(O^iPr)_3$ ,  $H_3PO_4$ , and  $C_{12}$ - $PO_4$  (13%wt) under aqueous conditions (method A). The relative ratios Al to overall-P as found by elemental analysis are indicated. A lamellar phase with a large  $d$  spacing of *ca.* 3.52 nm is observed for low Al/P ratios (up to 0.83); for higher values (from 0.88) a lamellar phase with a smaller  $d$  spacing of *ca.* 2.70 nm is found (cf. Table 3-2).

Both types of syntheses (methods A and B) led to X-ray amorphous materials when no surfactant or no  $Al(O^iPr)_3$  was used; when both  $H_3PO_4$  and the surfactant were absent in the reaction mixture, the product could be identified by powder XRD as  $\gamma$ - $AlO(OH)$  (*boehmite*). The acidity of the surfactant is approximately the same as that of  $H_3PO_4$ ; accordingly, the pH conditions of the syntheses with and without  $H_3PO_4$  are quite similar (pH  $\approx$  2).

In conclusion, mesostructured materials prepared with  $H_3PO_4$  consist almost exclusively of one lamellar phase with a large  $d$  spacing (3.55 nm) as long as Al and P are used in approximately the same relative amounts; no systematic dependence of the surfactant concentration is observed. Phases with smaller  $d$  spacings (2.69 nm) occur only when the Al/P ratio is increased. Even when no free phosphate ions from  $H_3PO_4$  are available in the reaction mixture, lamellar mesostructured materials are obtained. For equal amounts of Al and P, these phases have smaller  $d$  spacings than samples

prepared with  $H_3PO_4$ , unless the surfactant concentration is very high; in that case, an additional phase with a large  $d$  spacing, equal to that of samples prepared with  $H_3PO_4$ , becomes predominant. The same trend is observed when the Al/P ratio is decreased.

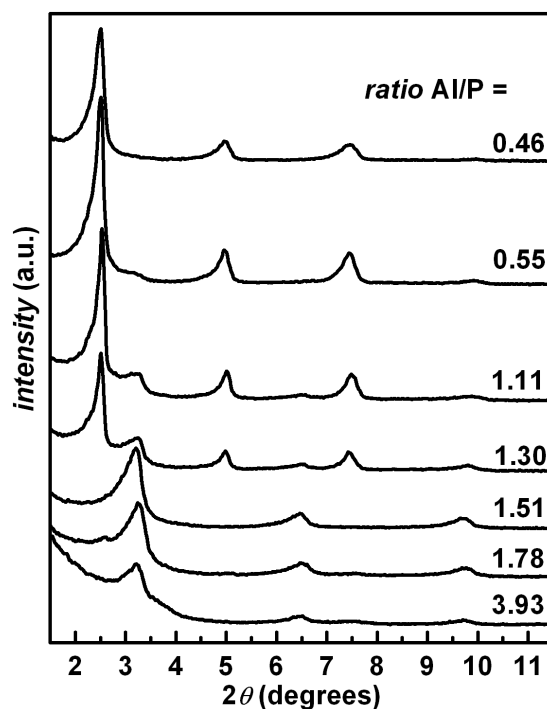


**Figure 3-5.** Powder XRD patterns of mesostructured aluminium phosphates prepared with variable relative amounts of  $Al(O^iPr)_3$  and  $C_{12}$ - $PO_4$  (13%wt) under aqueous conditions (method B). The relative ratios Al/P as found by elemental analysis are indicated. A lamellar phase with a large  $d$  spacing of *ca.* 3.55 nm is observed for low Al/P ratios (up to 1.30); for higher values (from 1.51) a lamellar phase with a smaller  $d$  spacing of *ca.* 2.72 nm is found; for moderate values both phases coexist (cf. Table 3-2).

### 3.2. *In-situ* SAXS

The standard temperature and reaction time for the aqueous synthesis was 120 °C and 24 hours, respectively. However, a variation of the temperature within the region 20 - 120 °C and/or of the duration of the reaction within the range 12 - 72 hours leads to similar results, although a better quality of the powder XRD patterns, *i.e.* an increase of the degree of order in the products is observed upon increase of either temperature or duration. The interlamellar distances of the products are not affected by these synthesis parameters.

The effect of the reaction temperature is evident from *in-situ* small angle X-ray scattering (SAXS) studies; **Figure 3-6** shows the thermal evolution of a synthesis mixture containing equal amounts of  $C_{12}\text{-PO}_4$ ,  $\text{Al}(\text{O}^i\text{Pr})_3$ , and  $\text{H}_3\text{PO}_4$  in water with a surfactant concentration of 30 % w/w (corresponding to a synthesis by method A). The intensities of the  $00l$  peaks grow with increasing temperature without any notable peak narrowing (the full widths at half maximum remain basically constant), which suggests that a more condensed structure develops as the reaction temperature is raised. However, the peak positions ( $d_{001} = 3.61$  nm) remain constant. In comparison, a sample which is kept constantly at 20 °C over the same time period as for the temperature-dependent measurements (*ca.* 45 minutes) exhibits no such change in the peak intensities. Hence, it may be concluded that an increase of temperature leads to a more complete reaction extent and, thus, to a higher density in the structure, but does not affect the interlamellar distances; this is consistent with the above-mentioned effect of the synthesis temperature on the final solid products as evidenced by powder XRD.

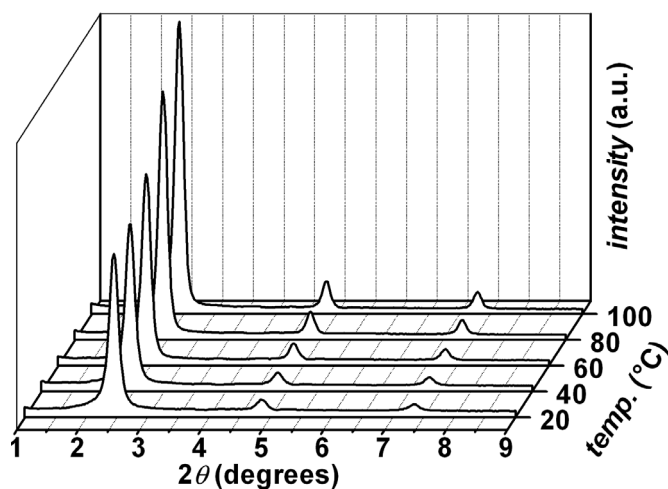


**Figure 3-6.** Thermal evolution of the SAXS diagrams of the aqueous synthesis mixture:  $C_{12}\text{-PO}_4$  / water (30/70 w/w),  $\text{Al}(\text{O}^i\text{Pr})_3$ ,  $\text{H}_3\text{PO}_4$ . (Equimolar amounts of  $C_{12}\text{-PO}_4$ ,  $\text{Al}(\text{O}^i\text{Pr})_3$ , and  $\text{H}_3\text{PO}_4$ .) The reflections correspond to a lamellar mesophase;  $d_{001} = 3.61$  nm.

Temperature-resolved SAXS studies on the lyotropic surfactant/water system (*i.e.* without the inorganic species) are presented below (chapter 7). At the same surfactant concentration of 30 % w/w the pure  $C_{12}\text{-PO}_4$ /water system has a considerably larger interlamellar distance than the system containing the inorganic

reactants, which is explained by the presence of high amounts of water between the adjacent surfactant bilayers (cf. Figure 7-2). The  $d_{001}$  value is 9.83 nm at 20 °C and reduces to 9.02 nm at 100 °C; this is caused by a shrinkage of the surfactant bilayers due to stronger Brownian lateral oscillation of the hydrophobic surfactant chains. The reflections are much broader and weaker than in case of the mesostructure containing the inorganic species, which is explained by fluctuations of the interlayer distance, which, in turn, is less well-defined.

It must be pointed out that the SAXS data of the synthesis mixture were collected immediately after the addition of the inorganic reactants ( $\text{Al}(\text{O}^i\text{Pr})_3$  and  $\text{H}_3\text{PO}_4$ ) to the surfactant / water system (5 - 10 minutes, see experimental section). Therefore, two significant features must be stressed in terms of the time scale of these investigations: (i) Once the inorganic reactants are added, the lamellar structure with the small interlamellar distance ( $d_{100} = 3.61$  nm), which is comparable to that of the final solid products obtained from the synthesis ( $d_{100} = 3.47$  nm), forms within these first few minutes of the reaction without any further changes, apart from the quality of order. The  $d_{001}$  value is drastically diminished, which means that most of the water is immediately removed from the regions between the surfactant bilayers. (ii) The interlamellar distance is virtually independent of the temperature. Thus, it may be concluded that, from the beginning on, the inorganic building units are already interconnected with each other to some degree; otherwise a swelling of the lamellae at higher temperatures would be expected, caused by an increased thermal movement of the individual (non-interconnected) inorganic units. Any temperature-induced swelling is only to be expected in the inorganic part rather than in the organic, *i.e.* hydrophobic part. (The thickness of the hydrophobic part will rather decrease when the temperature is raised, cf. chapter 7.2) Also, a swelling between one organic layer and the adjacent inorganic layer (at the organic/inorganic boundary) can only be expected as long as the inorganic units are not yet interconnected with each other. In this context it should also be mentioned that the interaction between the inorganic layer and the surfactant head groups is of a covalent nature. Such a temperature-dependent shift in the SAXS reflections is observed in the non-aqueous syntheses as will be discussed below.

On the other hand, it is important to note that at this early stage of the reaction no structured solid material can be isolated from the synthesis mixture yet; the complete

condensation of the reactants, *i.e.* the formation of a fully-developed solid network, requires several hours, depending on the temperature. Accordingly, the mutual interactions between the inorganic building units, the surfactant head groups, and the remaining water molecules are strong enough to provide a certain rigidity in the mesostructure, but the formation of the final aluminium phosphate layers with exclusively covalent Al-O-P bonds has by far not been completed yet.

### 3.3. Structural Models

There are two possible explanations for the occurrence of mesostructured materials from the syntheses free of  $H_3PO_4$  (method B). The first is that the aluminium building units react with the phosphate groups of the surfactant molecules; the surfactant head groups become part of the inorganic networks in the products. This explanation is strongly supported by the fact that smaller  $d$  spacings are observed in samples prepared without  $H_3PO_4$  than in those prepared with  $H_3PO_4$  (as long as the Al/P ratio is approximately 1 and the surfactant concentration is not too high): The double layer of the surfactant molecules between the inorganic lamellae is thinner, because the phosphate head groups do not contribute, since they are inside and part of the layers themselves.

The possible formation of free phosphate ions by decomposition of the surfactant molecules can be excluded, since the latter is stable under hydrothermal conditions at a temperature of 393 K. After treating an aqueous solution of *n*-dodecyl phosphate under the same experimental conditions the intact surfactant was recovered as evidenced by powder XRD.

The other possible explanation for the formation of mesostructures in the method B syntheses is that no phosphate takes part in the condensation process at all and that the networks in the products consist of aluminium oxide or aluminium oxyhydroxide species, presumably  $\gamma$ -AlO(OH) (*boehmite*), which (as noted above) is formed in a synthesis free of both  $H_3PO_4$  and the surfactant. (*Boehmite* is the thermodynamically favoured aluminium oxide species under the conditions present during the syntheses.) However, this situation cannot be presumed for the products of the reactions with  $H_3PO_4$  (method A); at least here, free phosphate ions definitely do react with the aluminium units, since more P is found by elemental analysis than may be accounted

for by the surfactant head groups. (The formation of an insoluble amorphous phosphorous species under these reaction conditions, which would lead to the same analytical result, is highly unlikely.) This indicates that aluminium oxide or oxyhydroxide species are not the generally favoured product of these syntheses; instead, Al definitely reacts with phosphate, leading to the formation of Al coordinated with P over O-bridges, including P belonging to the surfactant. Accordingly, the  $C_{12}\text{-PO}_4$  serves both as a structure-director and as a reactant. In the following, this will be founded by further evidence (NMR, XANES, thermal analysis).

Finally, the possible formation of pure aluminium oxide or oxyhydroxide outside the lamellae must be taken into consideration; the products could be mixtures of the mesostructured aluminium phosphate phases and, additionally, aluminium oxide phases, either crystalline or amorphous. However the powder XRD patterns do not show the typical indications (broad reflections in the region  $2\theta > 10^\circ$ ) of significant amounts of amorphous material and no reflections of any crystalline material are found. Therefore, any oxide species, if present in the samples, may be considered to be part of the mesostructures.

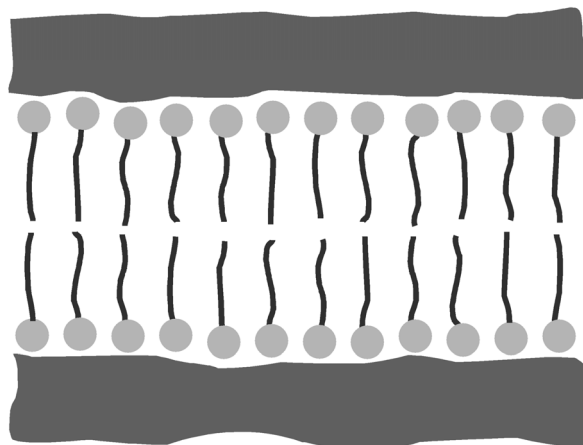


**Figure 3-7.** Schematic representation of a lamellar mesostructured aluminium phosphate prepared with equal amounts of Al and P under aqueous conditions by method A (with  $\text{H}_3\text{PO}_4$ ). Bilayers of  $C_{12}\text{-PO}_4$  surfactant molecules are located between the inorganic layers.

These considerations allow for structural models of the products from method A and B syntheses as depicted schematically in **Figure 3-7** and **Figure 3-8**: In the first case the surfactant molecules serve as a "classic" structure-director in that they form

bilayers which separate the inorganic aluminium phosphate sheets without their head groups being incorporated in the inorganic matrix. In the other case the head groups are incorporated in the inorganic layers, which means that the surfactant plays a role of both structure-director and reactant.

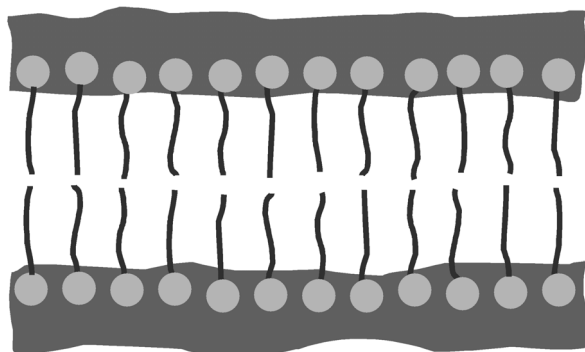


**Figure 3-8.** Schematic representation of a lamellar mesostructured aluminium phosphate prepared with low  $C_{12}\text{-PO}_4$  surfactant concentrations under aqueous conditions by method B (without  $\text{H}_3\text{PO}_4$ ). The surfactant phosphate head groups are part of the inorganic layers, which leads to a shorter distance between them, *i.e.* to a smaller  $d$  spacing.

This model may be extended in order to explain why two lamellar phases are formed when large amounts of surfactant (more than *ca.* 9 % w/w) are used in syntheses without  $\text{H}_3\text{PO}_4$  (method B). In addition to the expected phase with a small  $d$  spacing, a second phase with a large  $d$  spacing is formed (cf. Figure 3-3): Due to the large excess of the surfactant, not all of the head groups can become incorporated in the inorganic layers; this leads to the situation that some surfactant molecules can only act as structure-directors, as demonstrated schematically in **Figure 3-9**. The phase with the smaller  $d$  spacing is analogous to the single-phase product obtained from the synthesis without  $\text{H}_3\text{PO}_4$  (method B); here, the phosphate groups of the surfactant molecules are part of the inorganic layers and therefore do not contribute to the interlayer distance. The other phase with the larger  $d$  spacing corresponds to the situation where the surfactant head groups are not part of the inorganic structure, as in all products prepared by method A; accordingly, the interlayer distance is greater.

The validity of these three different structural models is supported by solid-state NMR, XANES, and thermal analysis, as will be demonstrated in the following sections.

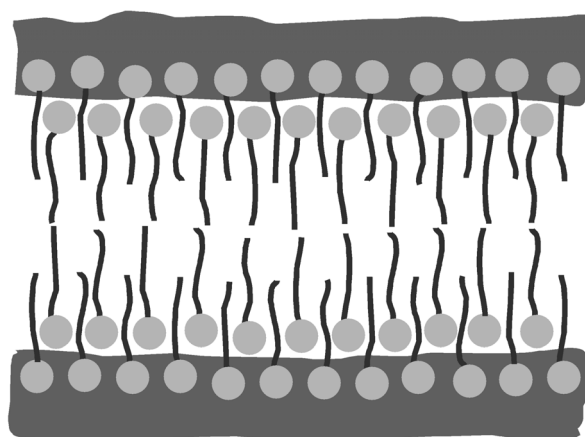


**Figure 3-9.** Schematic representation of a lamellar mesostructured aluminium phosphate prepared under aqueous conditions. This situation corresponds to the second phase found in the products of syntheses with high  $C_{12}\text{-PO}_4$  surfactant concentrations by method B (without  $\text{H}_3\text{PO}_4$ ). Some of the surfactant molecules are part of the inorganic layers (as in **Figure 3-8**), the others form bilayers between them, which leads to a large  $d$  spacing (as in Figure 3-7).

### 3.4. NMR Spectroscopy

The short-range order in the lamellar mesostructured aluminium phosphates was investigated by solid-state  $^{27}\text{Al}$  and  $^{31}\text{P}$  magic-angle spinning (MAS) NMR studies. Apart from verifying that Al is coordinated by O-P groups and P by O-Al groups, one particular purpose of these investigations was to discriminate between various kinds of P sites in the samples. In the light of the structural models introduced in the previous section, three different scenarios for the P environment are possible: (i) P originates from free phosphate employed in the synthesis and is part of the inorganic ( $\text{AlPO}_4$ ) matrix (method A syntheses only); (ii) P of the surfactant head group is incorporated in the inorganic matrix (method B); (iii) P of the surfactant head group is not incorporated in the inorganic matrix, corresponding to the "classic" situation of the surfactant acting as structure-director only (method A and method B, when high amounts of surfactant have been used in the synthesis).

**Figure 3-10** shows the  $^{27}\text{Al}$  MAS NMR spectra of three samples prepared by method A and by method B, as well as by method B with high amounts of surfactants, respectively (samples **A10**, **B13**, and **B7**, cf. Table 3-1 and Table 3-2). Sample **A10** shows a narrow resonance at 40.4 ppm (Al-1a), which corresponds to tetrahedral

$\text{Al(OP)}_4$  groups [121,122]; this resonance is not found in the spectra of the other two samples. All three spectra show numerous lines in the region from 6.0 ppm to -20.3 ppm, which are attributable to six-fold coordinated Al with P in the second coordination shell and, presumably, additional  $\text{H}_2\text{O}$  or OH groups, *i.e.*  $\text{Al(OP)}_x(\text{H}_2\text{O})_{6-x}$  ( $x \leq 4$ ). Among these, a relatively narrow resonance at -16.7 ppm (Al-2) is found in the samples **A10** and **B7**.

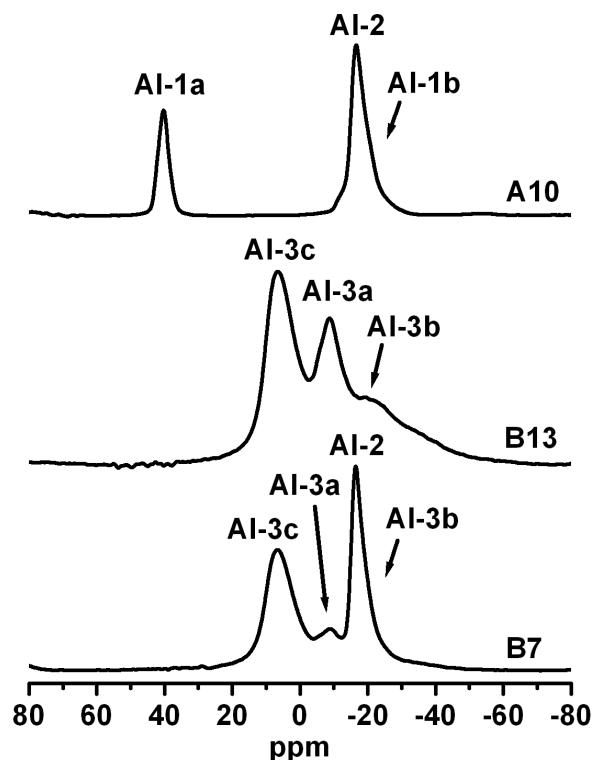


**Figure 3-10.**  $^{27}\text{Al}$  MAS NMR spectra of lamellar mesostructured aluminium phosphates prepared with  $C_{12}\text{-PO}_4$  under aqueous conditions (cf. Table 3-1 and Table 3-2). Resonances are discussed in the text and summarised in Table 3-3.

Three other lines occur in sample **A10** (Al-1b) or in the samples **B13** and **B7** (Al-3a and Al-3b), respectively; they are rather broad and asymmetric, which is typical of second order quadrupolar broadening effects including distributions of the quadrupole and chemical shift parameters. This means that in the corresponding Al-O polyhedra the Al-O distances and O-Al-O bonding angles have certain distribution widths. Finally, samples **B13** and **B7** also show a broad resonance at 6.0 ppm (Al-3c), which may possibly be assigned to  $\gamma\text{-AlO(OH)}$  (*boehmite*) [123]. This is consistent with the fact, that, contrary to sample **A10**, in these samples more Al than P is found by

elemental analysis, which makes it plausible that some of the Al has formed an oxide or oxyhydroxide species.

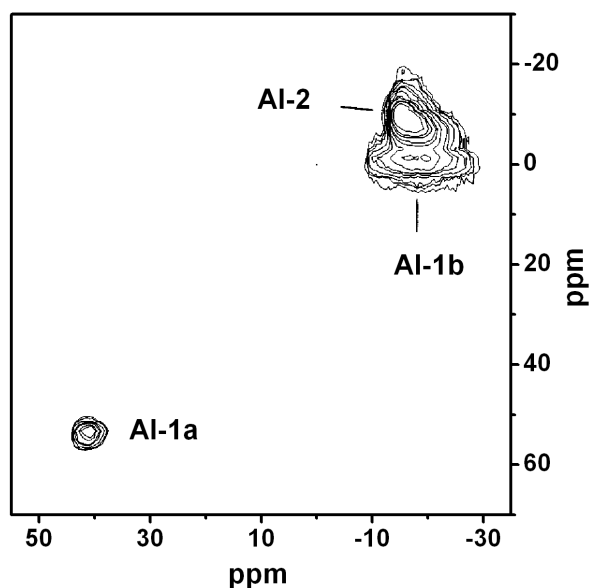


**Figure 3-11.** Sheared  $^{27}\text{Al}$  MQMAS spectrum of the mesostructured aluminium phosphate sample **A10**; the spectrum reveals a third resonance (Al-1b), which cannot be identified unambiguously in the  $^{27}\text{Al}$  MAS spectrum (cf. Figure 3-10).

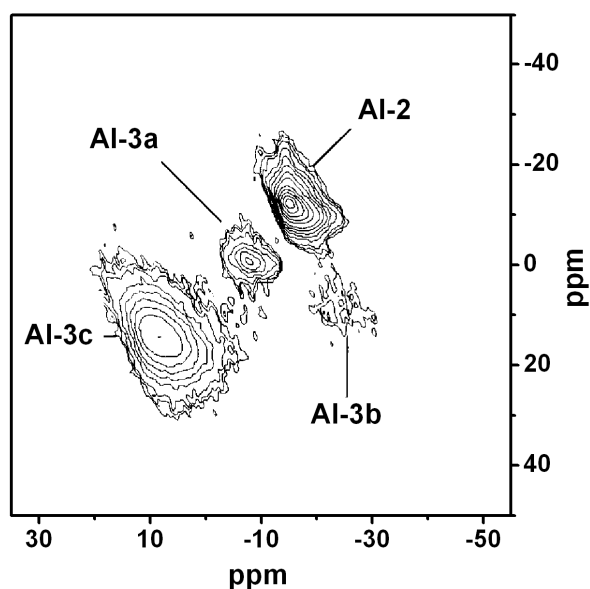


**Figure 3-12.** Sheared  $^{27}\text{Al}$  MQMAS spectrum of the mesostructured aluminium phosphate sample **B7**; the spectrum provides an enhanced resolution of the four resonances (including Al-3b, cf. Figure 3-10).

Some of the  $^{27}\text{Al}$  resonances are difficult to identify in the MAS spectra and can only be resolved by  $^{27}\text{Al}$  multiple quantum MAS (MQMAS), which is a convenient technique to decrease NMR signal broadening which is caused by electric quadrupole interaction in nuclei with  $I > 1/2$ . The MQMAS spectra of the samples **A10** and **B7** are shown in **Figure 3-11** and **Figure 3-12**, respectively. The  $^{27}\text{Al}$  NMR spectra will be further discussed below in combination with the respective  $^{31}\text{P}$  NMR spectra.

The  $^{31}\text{P}$  spectra of the same samples are shown in **Figure 3-13**. All resonances can be subdivided into three groups, the first from -23.5 to -28.3 ppm (P-1), the second from -12.4 to -24.4 ppm (P-2), and the third from -8.5 to -14.8 ppm (P-3). All these spectra are representative of other samples synthesised under the same conditions (methods A/B with low/high amounts of surfactant). Resonances of the P-1 group are only found in the spectrum of sample **A10**, those of the P-2 group occur in the spectra of **A10** as well as **B7**, and those of the P-3 group are found in the spectra of both **B13** and **B7**. This makes it possible to assign these resonances to the three above-mentioned P sites: P-1 resonances correspond to P in the inorganic network, originating from free phosphate units, which is consistent with data found in the literature [121,122]. These resonances occur in all samples prepared by method A, but not in any other samples. P-2 resonances are caused by P in the surfactant head groups which are not incorporated in the inorganic network; the resonances occur in all samples synthesised by method A and also in those synthesised with a large amount of surfactant by method B. Finally, P-3 resonances also correspond to P in the surfactant head groups, but here the head groups are part of the inorganic matrix; these resonances occur in all samples prepared by method B, but not in any other samples. These assignments of the P resonances are in complete agreement with the three structural models.

When the  $^{27}\text{Al}$  spectra are compared to the  $^{31}\text{P}$  spectra, a clear correlation between the occurrence of single  $^{27}\text{Al}$  resonances with that of  $^{31}\text{P}$  resonances becomes apparent. Al-1a/b lines are always paired with P-1 lines; the same is true for Al-2 and P-2 and for Al-3a/b/c and P-3. Thus, a more accurate assignment of the  $^{27}\text{Al}$  resonances may be undertaken: The tetrahedral  $\text{Al}(\text{OP})_4$  coordination (corresponding to the Al-1a resonance) occurs only when  $\text{H}_3\text{PO}_4$  was used in the synthesis. (The same is true for the octahedral  $\text{Al}(\text{OP})_x(\text{H}_2\text{O})_{6-x}$  ( $x \leq 4$ ) coordination which corresponds to the Al-1b

resonance.) The octahedral  $\text{Al(OP)}_x(\text{H}_2\text{O})_{6-x}$  coordination corresponding to the Al-2 resonance, on the other hand, occurs always and only in those samples, in which the surfactant molecules are not or not completely incorporated into the inorganic network. Finally, the octahedral  $\text{Al(OP)}_x(\text{H}_2\text{O})_{6-x}$  coordination corresponding to the Al-3a/b resonances as well as the octahedral coordination which is assignable to *boehmite* (Al-3c), is found always and only in those samples that were prepared without  $\text{H}_3\text{PO}_4$ , *i.e.* in samples with surfactant head groups being (at least partially) incorporated into the inorganic layers. A summary of the  $^{27}\text{Al}$  and  $^{31}\text{P}$  resonance assignments is given in **Table 3-3**.

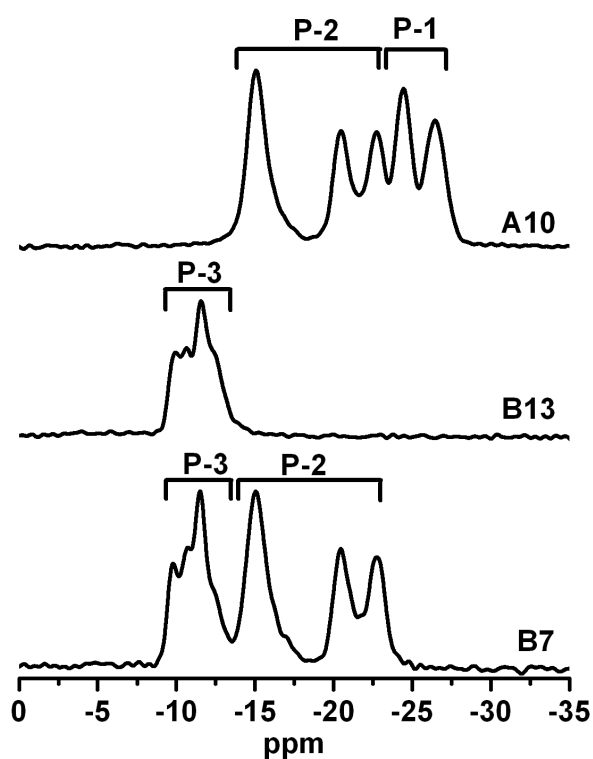


**Figure 3-13.**  $^{31}\text{P}$  MAS NMR spectra lamellar mesostructured aluminium phosphates prepared with  $C_{12}\text{-PO}_4$  under aqueous conditions (cf. Table 3-1 and Table 3-2). Resonances are discussed in the text and summarised in Table 3-3.

**Table 3-3.** Summary of the solid-state  $^{27}\text{Al}$  and  $^{31}\text{P}$  MAS NMR resonances of lamellar mesostructured aluminium phosphates prepared under aqueous conditions.

NMR lines		Al is coordinated with...	P originates from...	P resides...	found in samples		
$^{27}\text{Al}$	$^{31}\text{P}$				A10	B13	B7
Al-1 (a/b)	P-1	O-P (tetr.) <sup>a</sup> , O-P/OH <sub>2</sub> (oct.) <sup>b</sup>	H <sub>3</sub> PO <sub>4</sub>	within the inorg. layers	x		
Al-2	P-2	O-P/OH <sub>2</sub> (oct.)	C <sub>12</sub> -PO <sub>4</sub>	outside the inorg. layers	x		x
Al-3 (a/b/c)	P-3	O-P/OH <sub>2</sub> (oct.) <sup>c</sup> , O/OH (oct.) <sup>d</sup>	C <sub>12</sub> -PO <sub>4</sub>	within the inorg. layers		x	x

<sup>a</sup> (Al-1a); <sup>b</sup> (Al-1b); <sup>c</sup> (Al-1a/b); <sup>d</sup> in *boehmite*-like phase (Al-3c)

### 3.5. XANES Spectroscopy

X-ray absorption spectroscopy provides, among other things, a convenient method to determine coordination number(s) in solids. From XANES spectra at the Al K-edge it is possible to distinguish between tetrahedrally and octahedrally coordinated Al. The exact energy position of the absorption maximum at the K absorption edge, corresponding to the 1s to 3p electron transition, depends on the coordination number of the coordination sphere around the Al atom and differs by approx. 2 eV for the tetrahedral and octahedral coordination, respectively [124]. **Figure 3-14** shows the XANES spectra of four samples with well-defined Al coordination: **(a)** crystalline *berlinite* ( $\text{AlPO}_4$  with a quartz-analogous structure, *i.e.* tetrahedral Al coordination), **(b)** crystalline microporous  $\text{AlPO}_4$ -11 (tetrahedral Al coordination [125]), **(c)** *corundum* ( $\alpha$ - $\text{Al}_2\text{O}_3$ , octahedral Al coordination), and **(d)** *boehmite* ( $\gamma$ - $\text{AlO}(\text{OH})$ , octahedral Al coordination). The *boehmite* sample was prepared by hydrothermal treatment of  $\text{Al}(\text{O}^i\text{Pr})_3$  under the same conditions as for the syntheses of the mesostructured samples. The energy positions of the absorption maxima are located at 1.5667 keV for four-fold coordination and at 1.5686 keV for six-fold coordination. In the following, these spectra will serve as references for the determination of coordination numbers from the absorption energies.

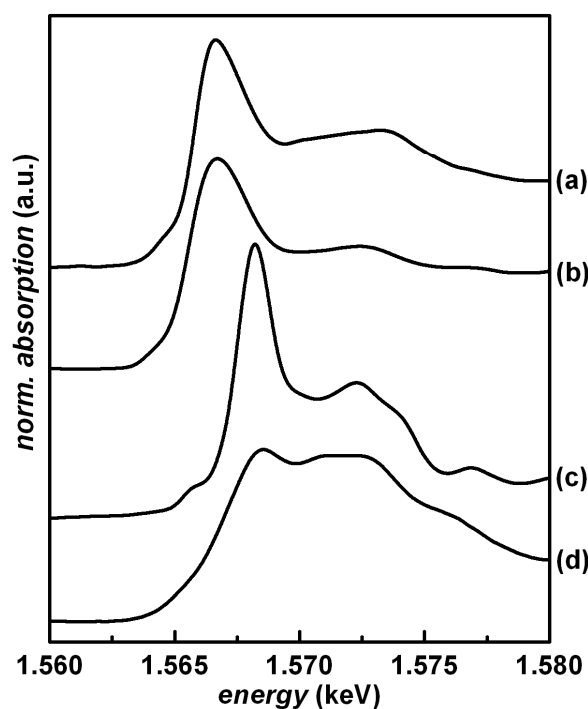


**Figure 3-14.** Al K-edge XANES spectra of **(a)** crystalline *berlinite* ( $\text{AlPO}_4$  with a quartz-analogous structure, *i.e.* tetrahedral Al coordination), **(b)** crystalline microporous  $\text{AlPO}_4\text{-11}$  (tetrahedral Al [125]), **(c)** corundum ( $\alpha\text{-Al}_2\text{O}_3$ , octahedral Al), and **(d)** boehmite ( $\gamma\text{-AlO(OH)}$ , octahedral Al). The energy of the absorption maximum differs by *ca.* 2 eV for the tetrahedral and octahedral coordination, respectively.

**Figure 3-15** and **Figure 3-16** show the XANES spectra of the samples listed in Table 3-2. All samples turn out to contain both tetrahedrally and octahedrally coordinated Al. The spectra also allow for a quantitative determination of the relative amounts of tetrahedrally and octahedrally coordinated Al. This is demonstrated in **Figure 3-17** sample **B10** as an example: The spectrum contains two strongly overlapping peaks corresponding to tetrahedral and octahedral coordination, respectively. This becomes apparent from the second derivative of the smoothed data (smoothing by the method of SAVITZKY and GOLAY [126]), which features two peaks with minima at 1.5669 and 1.5689 keV, respectively. Integration of the second derivative between the roots at each peak's right and left flanks provides the areas under these peaks, the relative ratio of which (here: 0.87/0.13) corresponds to the relative ratio of tetrahedrally and octahedrally coordinated Al in the sample.

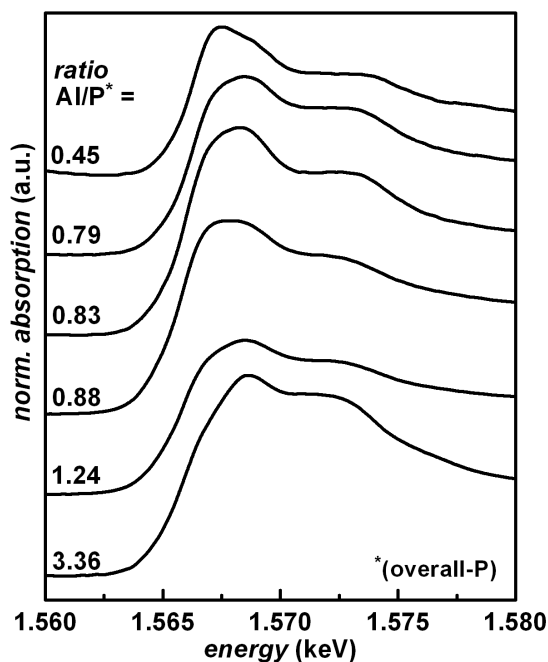


**Figure 3-15.** Al K-edge XANES spectra of lamellar mesostructured aluminium phosphates prepared under aqueous conditions by method A) with variable relative amounts of  $\text{Al}(\text{O}^i\text{Pr})_3$ ,  $\text{H}_3\text{PO}_4$ , and  $\text{C}_{12}\text{-PO}_4$ . The relative Al/P ratios are those found by elemental analysis (cf. Table 3-2).

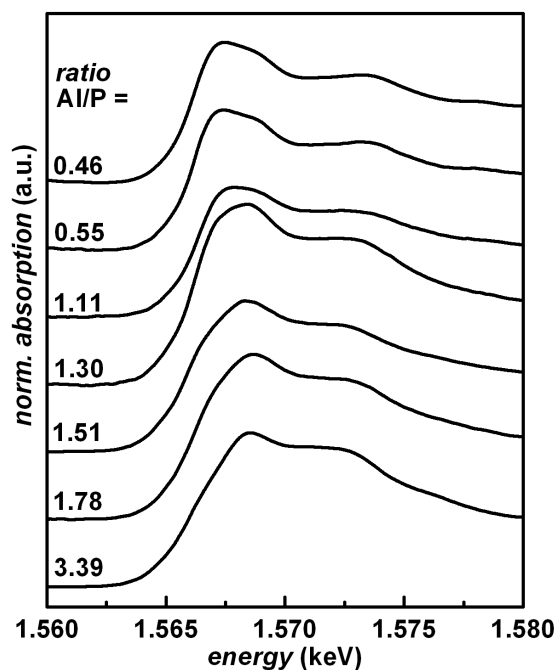


**Figure 3-16.** Al K-edge XANES spectra of lamellar mesostructured aluminium phosphates prepared under aqueous conditions by method B) with variable relative amounts of  $\text{Al}(\text{O}^i\text{Pr})_3$  and  $\text{C}_{12}\text{-PO}_4$ . The relative Al/P ratios are those found by elemental analysis (cf. Table 3-2).

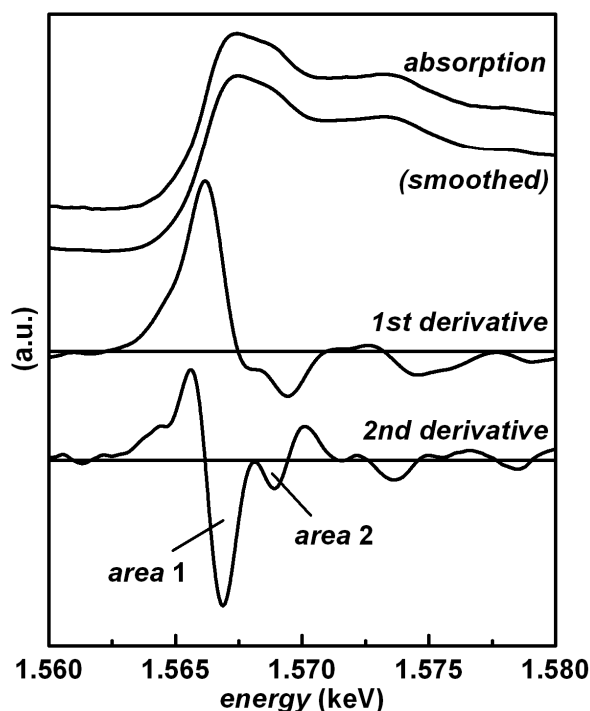


**Figure 3-17.** Example for the procedure of determining the relative amounts of tetrahedral and octahedral Al from the areas 1 and 2 under the spectrum's second derivative. Derivatives were made from the smoothed spectrum. (Sample **B10**)

**Figure 3-18** shows the relative amounts of tetrahedral Al in the mesostructured samples as a function of the Al/P ratio found by elemental analysis. For all samples (prepared both with and without  $\text{H}_3\text{PO}_4$ ) a correlation of the relative amount of tetrahedral Al with the Al/P ratio is observed. The tetrahedral coordination is favoured if the amount of Al is about equal to or lower than that of P. The more Al is present in the samples, the greater is the relative amount of octahedral Al. For small amounts of Al relative to P the presence of octahedrally coordinated Al may be explained by the coordination of water molecules in addition to phosphate groups, *i.e.*  $\text{Al}(\text{OP})_x(\text{H}_2\text{O})_{6-x}$  ( $x \leq 4$ ). However, for samples with Al in a great excess relative to P the great amounts of six-coordinated Al can hardly be attributed to coordination of water alone; thus, more or less significant amounts of an aluminium oxide or oxyhydroxide species, presumably *boehmite*, seem to be present in these samples. This is consistent with the observation of  $^{27}\text{Al}$  NMR resonances attributable to *boehmite*.

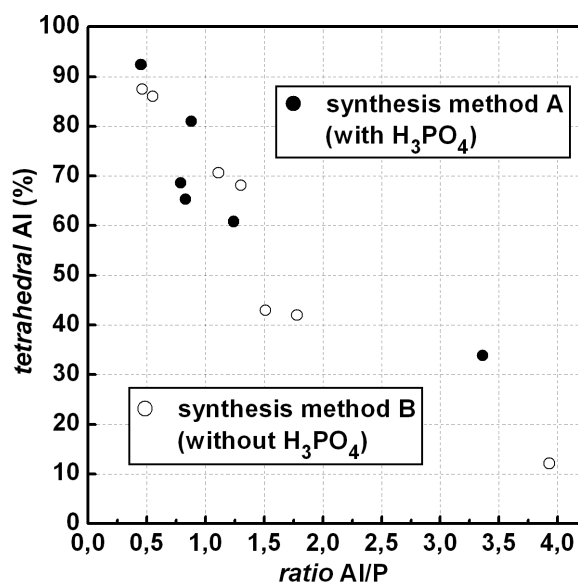


**Figure 3-18.** Relative amounts of tetrahedral Al in the samples listed in Table 3-2. The Al/P ratios are those found by elemental analysis.

### 3.6. Thermal Analysis

The TG/DTA/MS diagram of a representative sample prepared by method A (with equal amounts of  $\text{Al}(\text{O}^i\text{Pr})_3$ ,  $\text{H}_3\text{PO}_4$ , and surfactant) is shown in **Figure 3-19**. A mass loss of 43 % is observed which occurs in two relatively sharp steps, both of which are endothermic. The first one (12 % loss, 120 - 160 °C) is attributable to the removal of water, which is intercalated between the inorganic layers; only water fragments are detected by MS. (This process occurs in two consecutive overlapping steps.) This loss of water molecules from the interlayer regions results in a slightly closer distance between the layers, as can be monitored by *in-situ* temperature-resolved powder XRD (**Figure 3-20**), which shows a very slight shift in the  $00l$  reflections in this temperature region: The intensity of the original reflections becomes weaker with increasing temperature. Simultaneously a new lamellar phase with smaller  $d$  spacing emerges, which, over a temperature interval of *ca.* 120 - 160 °C, coexists with the original one and gradually replaces it. In a second, endothermic step of mass decrease (31 % loss, 240 - 270 °C) water, ethyl, and carbon dioxide fragments are detected, corresponding to the decomposition of the surfactant molecules in the interlayer region. At higher temperatures no further mass change occurs; the final decomposition residue is X-ray amorphous.

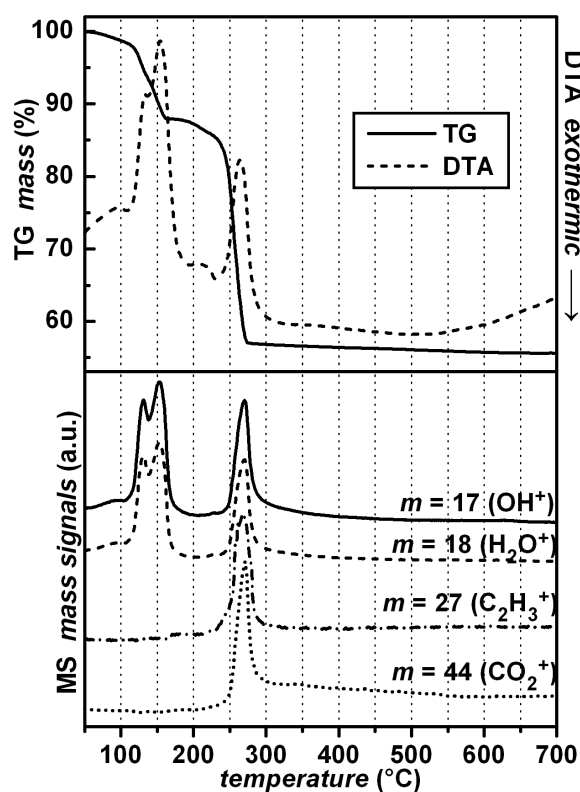


**Figure 3-19.** TG/DTA/MS diagram of a lamellar mesostructured aluminium phosphate prepared under aqueous conditions by method A (sample **A3**). The endothermic decomposition of the surfactant which resides between the inorganic layers is completed at *ca.* 300 °C.

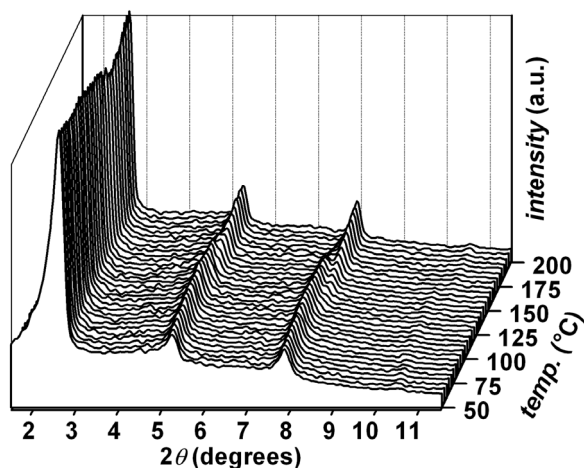


**Figure 3-20.** Thermal evolution of the powder XRD diagram of a lamellar mesostructured aluminium phosphate prepared under aqueous conditions by method A (sample **A3**). Above *ca.* 100 °C the lamellar structure is gradually replaced by a new one which has a slightly lower  $d$  spacing; this is attributable to the loss of interlayer water.

This thermal behaviour is similar to that of the pure  $C_{12}\text{-PO}_4$  surfactant (**Figure 3-21**), where a sharp endothermic mass loss of 62 %, accompanied by the detection of water, ethyl and carbon dioxide fragments, is observed at 180 - 220 °C. Another decrease of mass occurs at a higher temperature (19 % loss, 550-620 °C), but significant amounts of the monitored mass fragments are not detected. (A mass loss of less than 3 % at 90 - 100 °C corresponds to the removal of adsorbed water.) The surfactant molecules in the aluminium phosphate sample seem to be stabilised by their regular arrangement between the inorganic layers, since their decomposition emerges at a temperature *ca.* 50 °C higher than in the pure (molten) state ( $mp = 39 - 45$  °C).

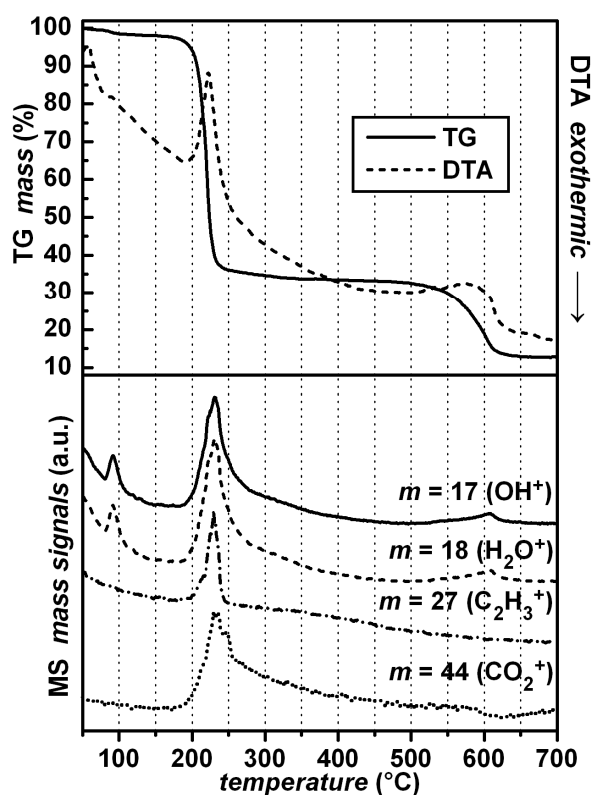


**Figure 3-21.** TG/DTA/MS diagram of *n*-dodecyl phosphate ( $C_{12}\text{-PO}_4$ ). The decomposition of the hydrocarbon chain is endothermic and completed below 300 °C. This thermal behaviour is very similar to that of the surfactant residing in the interlamellar region of the mesostructured aluminium phosphate sample **A3** (cf. Figure 3-19).

The TG/DTA/MS diagram of a representative single-phase sample prepared without  $\text{H}_3\text{PO}_4$  (method B, 5 % w/w surfactant, **Figure 3-22**) reveals a clearly different picture. The overall mass decrease of 61 % extends over a broad temperature region from

ca. 100 to 600 °C and may be divided up into three steps. Again the first one (6 % loss, 100 - 170 °C) corresponds to the endothermic removal of intercalated water. The remaining two steps (42 % loss at 210 - 330 °C and 13 % loss at 330 - 600 °C, respectively) are accompanied by a DTA curve and mass signals of a more complex shape. Three relatively broad exothermic DTA peaks without clear association to the TG curve, and the detection of water, ethyl and carbon dioxide fragments are observed. Thus, in the sample which was prepared without  $\text{H}_3\text{PO}_4$  the surfactant molecules are decomposed less easily than in the sample prepared with  $\text{H}_3\text{PO}_4$ ; their removal requires higher temperatures and is exothermic instead of strictly endothermic. Again, the residue of the thermal analysis is X-ray amorphous.

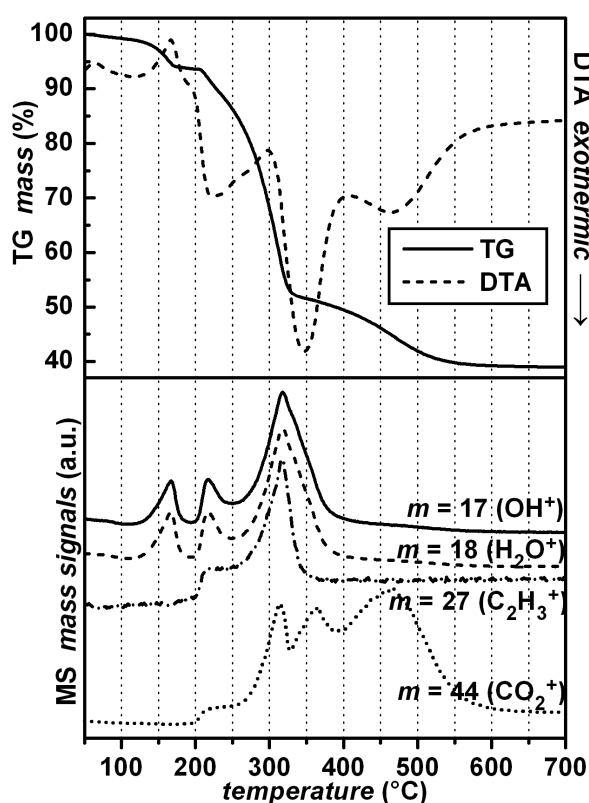


**Figure 3-22.** TG/DTA/MS diagram of a lamellar mesostructured aluminium phosphate prepared under aqueous conditions by method B (sample **B3**). For the complete (partially exothermic) decomposition of the surfactant, which is incorporated in the inorganic layers, a higher temperature is needed than in case of the sample prepared by method A (see Figure 3-19).

These significant differences in the thermal analyses of the samples prepared with and without  $\text{H}_3\text{PO}_4$ , respectively, are a strong indication that in the absence of  $\text{H}_3\text{PO}_4$

the phosphate ions of the surfactant molecules are indeed incorporated into the inorganic network. On the other hand, as long as free phosphate ions are present during the synthesis, they are favoured for the inorganic structure and the surfactant molecules are not covalently bonded to aluminium, but form a rather liquid-crystal-like state between the inorganic layers. This is consistent with the respective structural models formulated above.

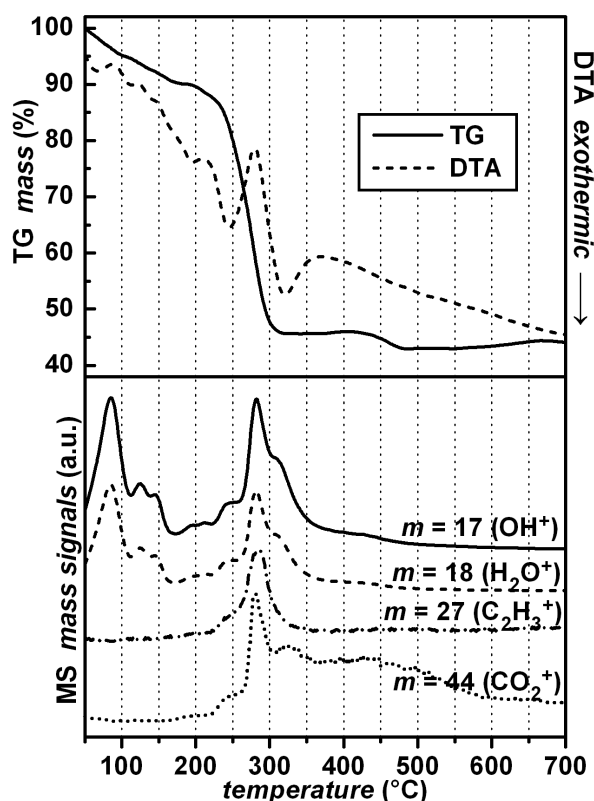


**Figure 3-23.** TG/DTA/MS diagram of a mesostructured aluminium phosphate sample (with two lamellar phases) prepared under aqueous conditions by method B with large quantities of  $C_{12}\text{-PO}_4$  surfactant (sample **B6**.) The thermal behaviour reflects the existence of both phases, corresponding to the samples in Figure 3-19 and Figure 3-22.

The thermal behaviour of a (representative) sample prepared without  $\text{H}_3\text{PO}_4$  (method B), but with high amounts of surfactant (13 % w/w) is shown in **Figure 3-23**. This sample consists of two phases; the dominant phase has a larger  $d$  spacing (see Figure 3-3). The TG/DTA/MS diagram resembles both that of the sample prepared with  $\text{H}_3\text{PO}_4$  (and, accordingly, of the pure surfactant) and that of the single-phase sample prepared without  $\text{H}_3\text{PO}_4$ . The total mass decrease of 57 % is almost complete

at *ca.* 310 °C (52 % loss), but occurs within a broader temperature region than in the sample prepared with  $\text{H}_3\text{PO}_4$ . Also, the DTA shows both endothermic and exothermic peaks rather than merely endothermic peaks. The loss of another 5 % takes place between *ca.* 310 and 600 °C, accompanied by the detection of carbon dioxide.

The thermal similarities of the mixture of the two phases in this sample with both other samples discussed above suggests that the two different phases originate from the two different possible roles of the surfactant phosphate groups: The phase with the smaller  $d$  spacing is analogous to the single-phase product obtained from the synthesis without  $\text{H}_3\text{PO}_4$  (method B); here, the phosphate groups of the surfactant molecules are part of the inorganic layers and therefore do not contribute to the interlayer distance. The other phase with the larger  $d$  spacing corresponds to the situation where the surfactant head groups are not part of the inorganic structure, as in all products prepared by method A; accordingly, the interlayer distance is greater. These results are consistent with the structural models formulated above.

### 3.7. Conclusions

For the first time an anionic surfactant,  $n$ -dodecyl phosphate, was used as a structure-directing agent for the synthesis of mesostructured aluminium phosphates. The hydrothermal synthesis leads to lamellar products, the inorganic parts of which consist primarily of Al-O-P networks, although aluminium oxide or oxyhydroxide species (particularly  $\gamma\text{-AlO(OH)}$ , *boehmite*) also seem to be present, especially when Al was used in excess with respect to P in the synthesis. As long as no free phosphate ions are offered for the condensation process, the phosphate head groups of the surfactant become incorporated into the inorganic layers; thus, the surfactant serves both as structure-director and as reactant. This could be confirmed by significant differences between samples prepared with and without  $\text{H}_3\text{PO}_4$ ; these differences include  $d$  spacing (powder XRD), NMR data, and thermal behaviour.

A surfactant with a head group that can be incorporated into the inorganic network has the potential to give way to mesostructured model compounds that might be of great value for further investigations. The use of  $n$ -dodecyl phosphate makes free phosphate ions redundant in the synthesis of mesostructured aluminium phosphates; by decreasing the number of interacting species by this one reactant, the complexity of the

synthesis is reduced. Thus, new opportunities in the study of the formation processes of mesostructured materials and in their control arise.

## 4. Alcoholic Synthesis with *n*-Dodecyl Phosphate as Structure-director

### 4.1. Basic Characterisation

The synthesis of mesostructured aluminium phosphates from  $Al(O^iPr)_3$  and  $H_3PO_4$  with the utilisation of *n*-dodecyl phosphate as a structure-director under alcoholic conditions leads to results dependent on the synthesis temperature. Lamellar mesostructures are obtained when the synthesis is carried out at temperatures of *ca.* 70 – 90 °C (solvothermal conditions, *i.e.* at temperatures near or above the boiling point of the respective solvent). However, these products exhibit considerably less well-ordered mesostructures than those from the aqueous syntheses (cf. chapter 3); the powder XRD reflections are much broader and of lower intensity. **Figure 4-1a** shows the powder XRD pattern of a representative sample prepared in ethanol at 90 °C ( $d_{001} = 3.50$  nm).

Different products are obtained when the same alcoholic synthesis is carried out at lower temperatures (10 - 70 °C); the powder XRD diagrams of two examples prepared in ethanol at 10 °C and methanol at 25 °C are shown in **Figure 4-1b** and **c**, respectively. In both cases the reflections are attributable to two distinct nanostructured phases, one of which has a clearly hexagonal structure with a remarkably low  $d_{100}$  value of 1.88 nm (corresponding to a lattice parameter of  $a = 2 \cdot d_{100} / \sqrt{3} = 2.17$  nm), which will be discussed in detail below (chapter 4.2). The structure of the other phase cannot be identified from these diffraction patterns, but SAXS investigations (see below) suggest a lamellar phase. (Given the fact that the second and third order reflections of the lamellar product synthesised from the same system at a higher temperature are relatively weak (see **Figure 4-1a**), it is likely that this phase has the same lamellar structure and that the  $00l$  reflections with  $l > 1$  are too weak to be detected.)

The two mesophases evolve competitively; their relative amounts in the products systematically depend on the synthesis temperature as well as on the reaction time. The lamellar phase is relatively favoured at higher temperatures (and is exclusively

formed above *ca.* 70 °C, as shown above). This is seen in **Figure 4-2** for products prepared in ethanol (20 % w/w surfactant) at various temperatures (syntheses duration 12 hours); these samples will be further characterised in the following chapters. A similar evolution is found for products synthesised at a constant temperature but with variable duration of the reaction; the powder XRD reflection (not shown) of the lamellar phase becomes more dominant while those of the hexagonal phase get weaker when the reaction is allowed to take place over a longer time period. Elemental analysis of the samples is discussed in chapter 4.2 (page 55).

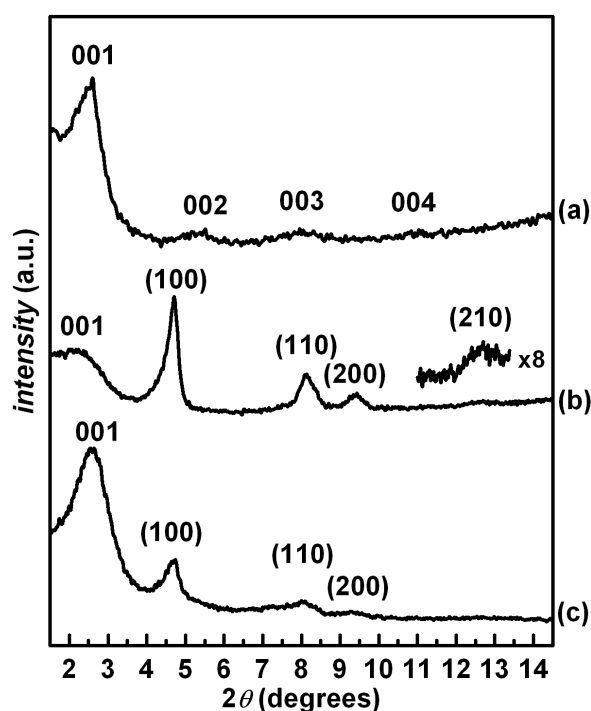


**Figure 4-1.** Powder XRD diagrams of mesostructured aluminium phosphates prepared with *n*-dodecyl phosphate (20 % w/w) under various conditions from  $Al(O^iPr)_3$  and  $H_3PO_4$ : **(a)** ethanol, 90 °C; **(b)** ethanol, 10 °C; **(c)** methanol, 25 °C. Lamellar phases and hexagonal phases (in parenthesis) are indexed.

The conditions of these syntheses are not completely non-aqueous. Low quantities of water are always present in the reaction mixtures; the approximate molar ratio Al/water is 1/3. This turns out to be necessary for the products to exhibit sufficiently well-ordered mesostructures. When lower amounts of water are used, the quality of the products becomes somewhat poorer, *i.e.* the samples display much weaker powder XRD reflections. Apparently water is essential for the hydrolysis of  $Al(O^iPr)_3$ ; in the complete absence of water, the condensation of the reactants into an inorganic network

seems to be insufficient. Larger quantities of water, on the other hand, led to the formation of an increasingly high relative amount of the lamellar phase, comparable to those obtained from syntheses carried out entirely in water (cf. chapter 3). This is an indication that a higher degree of condensation of  $Al(O^iPr)_3$  and  $H_3PO_4$  into a solid network leads to a preferred generation of the lamellar (rather than the hexagonal) phase; this will be further discussed in the context of *in-situ* SAXS investigations (chapter 4.3).

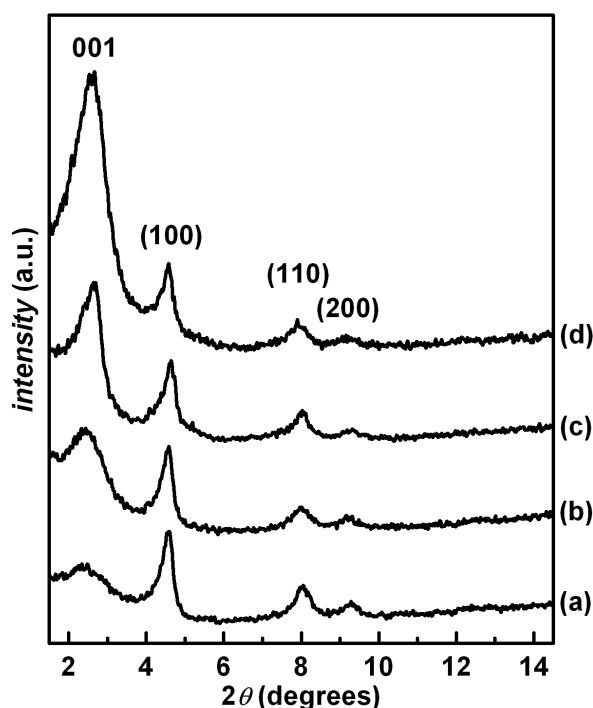


**Figure 4-2.** Powder XRD diagrams of mesostructured aluminium phosphates prepared from  $Al(O^iPr)_3$  and  $H_3PO_4$  in ethanol with  $C_{12}$ - $PO_4$  (20 % w/w) at various temperatures: **(a)** 10 °C; **(b)** 25 °C; **(c)** 40 °C; **(d)** 60 °C; The lamellar phase and the hexagonal phase (in parenthesis) are indexed.

#### 4.2. Structural Model of the Hexagonal Mesophase

The investigation of the hexagonal phase obtained from the non-aqueous low-temperature synthesis reveals some significant properties that are not typical of the usual hexagonal inorganic mesostructures prepared by this kind of synthesis. In the latter the surfactant molecules are arranged in rod-like assemblies with the polar head groups facing outwards; the inorganic solid is structured around these micelles

forming a three-dimensional network\* (**Figure 4-3a**). In mesostructured inorganic / surfactant composite materials with this kind of hexagonal structure the  $d_{100}$  values are usually in the region between 3 and 4 nm (for  $C_{12}$ -surfactants) [19,22,24,127-129].

Contrary to that, the hexagonal structure in the system studied here has a  $d_{100}$  value which is surprisingly low (1.88 nm), even if the possibility is taken into account that the phosphate head groups from the surfactant may be considered as being part of the inorganic matrix, which would diminish the  $d_{100}$  value, as was shown above (cf. chapter 3.3). Therefore, a different hexagonal surfactant arrangement is suggested here as an alternative structure model, in which the surfactant molecules are assembled in an inverted arrangement, *i.e.* the polar head groups are located inside of the rods and the hydrophobic chains are turned outwards (**Figure 4-3b**). In this case the inorganic part is encapsulated in the centres of these assemblies forming individual domains that are not interconnected with each other and extend in one direction only.

Such an inverted hexagonal structure is very rarely observed in pure binary single-chain surfactant / solvent systems. Due to the geometry of these surfactant molecules (one thin hydrophobic chain and a spacious head group) and because of repulsion forces between the surfactant head groups the inverted curvature is usually avoided; micelles, lamellae or structures with non-inverted curvatures are favoured. (However, if two or three hydrophobic chains are attached to each head group, as in biologically relevant phospholipids, inverted hexagonal phases are observed quite frequently.) In the system studied here, the emergence of the inverted structure may be explained by the presence of the inorganic reactants ( $Al(O^iPr)_3$  and  $H_3PO_4$ ). Owing to the interactions of the surfactant head groups with the polar inorganic units the head group repulsion is reduced, which gives way to the inverted curvature. A similar effect, *i.e.* the formation of an inverted phase due to interactions of polar additives with the head groups, was observed by FUNARI [130] in the ternary system phospholipid / alkyl-polyoxyethylene / water. It should again be stressed that in the system  $C_{12}$ - $PO_4$  / alcohol no lyotropic behaviour is observed in the absence of the inorganic

\* The term 'three-dimensional' must be used with care; a lyotropic liquid crystal with a hexagonal symmetry has a two-dimensional structure, as no crystallographic information is obtained regarding the direction along the surfactant rods. However, a solid-state mesostructured network with this symmetry is here referred to as three-dimensional in the sense that the building units are interconnected with each other in all three room directions. With the same reasoning a lamellar solid mesostructure may be denoted as 'two-dimensional', although its crystallographic periodicity is one-dimensional.

components, which proves that the inorganic species definitely play a significant role in the formation of the mesostructure.

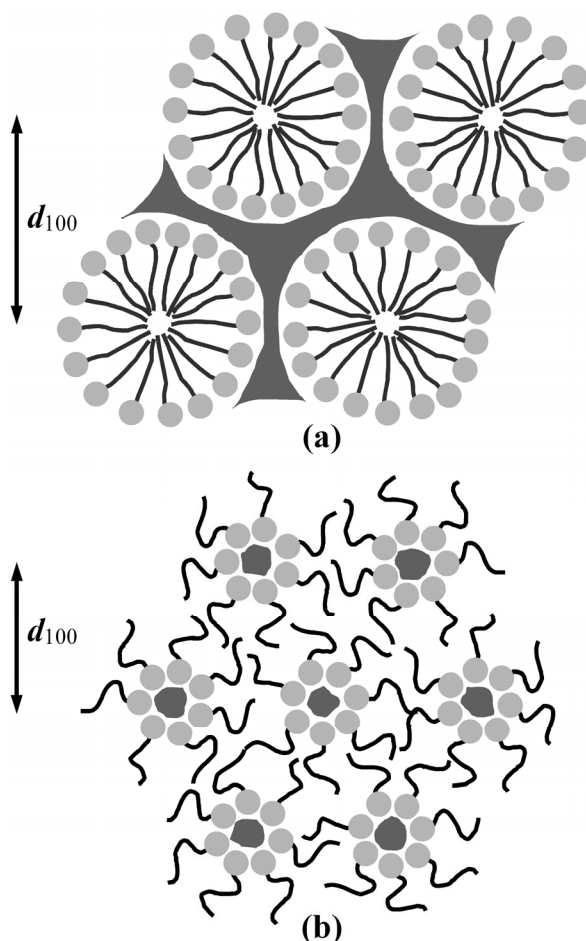


**Figure 4-3.** Schematic representation of two different hexagonal mesostructured aluminium phosphate / surfactant composites (cross section through the  $hk$  plane): **(a)** The "normal" structure with a fully-connected inorganic network (drawn as dark area). **(b)** Inverted surfactant assemblies with single inorganic domains (dark areas) in the centres. In the latter case the diameters of the assemblies (and thus the  $d_{100}$  value) are smaller, since each hydrophobic surfactant chain is allowed more space for its distribution leading to a smaller radial extension; also, some degree of interpenetration of the chains from adjacent surfactant assemblies is possible.

This inverted structure provides a plausible explanation to the remarkably small  $d_{100}$  value, which can be accounted for by the fact that in such a structure there is more space available to each individual hydrophobic surfactant chain than in the non-inverted structure, leading to a reduced radial extension (see Figure 4-3). Also, the micelles may be interpenetrating each other. It must be mentioned, however, that even

in non-inverted micelles the arrangement of the hydrophobic chains is not necessarily rigidly linear, *i.e.* in an all-trans configuration, as may be implied by the schematic representation in **Figure 4-3a**. Bearing in mind, however, that all previously reported (non-inverted) hexagonal mesostructured inorganic / surfactant composite materials (with  $C_{12}$ -surfactants) had much larger  $d_{100}$  values than the structure studied here, the low value of the latter may be considered as a strong indication for the inverted structure.

Elemental analysis shows that a sample in which the inverted hexagonal phase is predominant (as in the sample prepared at 10 °C in Figure 4-2a) contains a slightly higher relative amount of the surfactant than a sample which consists mainly of the lamellar phase (like the sample prepared at 60 °C in Figure 4-2d). The relative contributions of P from  $H_3PO_4$  and P from the surfactant to the overall amount of P is calculated by  $P_{H_3PO_4}/P_{\text{surfactant}} = (12 \cdot P/C) - 1$  (cf. chapter 3.1).

**Table 4-1.** Relative molar ratios of Al, P, C, and N in two representative samples of mesostructured aluminium phosphates with different relative amounts of the inverted hexagonal phase as synthesised under alcoholic conditions from  $Al(i\text{OPr})_3$  and  $H_3PO_4$  with *n*-dodecyl phosphate according to elemental analysis.

predominant phase	elemental analysis (relative molar amounts)					calculated from analysis
	Al	P	C	C/P	Al/P	Al / $P_{H_3PO_4}$ / $P_{C_{12}-PO_4}$
inv. hex.	0.115	0.169	0.976	5.77	0.68	1.31 / 1 / 0.93
lamellar	0.119	0.171	0.928	5.43	0.70	1.28 / 1 / 0.83

Attempts to remove the surfactant without collapse of the structure (*e.g.* by solvent extraction) in order to obtain a porous aluminium phosphate have failed. The structure is thermally extremely unstable; at temperatures above *ca.* 35 °C the solid products will irreversibly transform into single lamellar phases as is found by powder XRD (not shown). This phase transformation will be discussed below. The poor thermal stability fits in with the inverted structure model, as it is consistent with an inorganic network that does not extend in all directions.

Due to its instability the inverted hexagonal phase could not be investigated by transmission electron microscopy (TEM); the impact of the electron beam will

immediately lead to either a phase transformation into the lamellar phase or to the decomposition of the sample. Accordingly not mesostructured phases other than the lamellar phase were observed.

### 4.3. *In-situ* SAXS

The influence of both the temperature and the reaction time on the relative amounts of the two phases can be monitored systematically by *in-situ* small angle X-ray scattering (SAXS) studies. **Figure 4-4** shows the SAXS patterns of a synthesis mixture in ethanol (20 % w/w surfactant) at variable temperatures; upon heating the 001 reflection of the lamellar phase grows in intensity relative to those of the (inverted) hexagonal phase. In this series a thermally induced shift of all reflections is observed. The  $d$  values of both the hexagonal and the lamellar phase slightly increase with higher temperatures ( $d_{100}$  from 1.93 to 2.08 nm for the hexagonal phase,  $d_{001}$  from 3.76 to 4.67 nm for the lamellar phase), which may be explained by an increased thermal oscillation of the inorganic building units that are at this point not yet interconnected with each other to a significant degree. This was not observed for the respective aqueous system (see Figure 3-6). The degree of condensation of the inorganic reactants into a rigid solid network at this early stage of the reaction is obviously much lower in alcohols than in water, which is to be expected in the light of a much slower hydrolysis of  $Al(O^iPr)_3$ .

The temporal evolution of the SAXS patterns of a synthesis mixture with the same composition (20 % w/w surfactant) at constantly 25 °C is shown in **Figure 4-5**; the lamellar phase becomes more and more dominant in the course of time. This progressive formation of the lamellar structure takes place on approximately the same time scale as the condensation of the inorganic reactants into a solid network. As a possible explanation of this correlation it may be assumed that the inverted hexagonal arrangement is progressively disfavoured with an increasing degree of condensation of the reactants; the successive formation of larger inorganic fragments in the course of the reaction seems to lead to a preferred mesostructured arrangement without curvature. The  $d$  values of both phases do not change significantly in the course of the reaction.

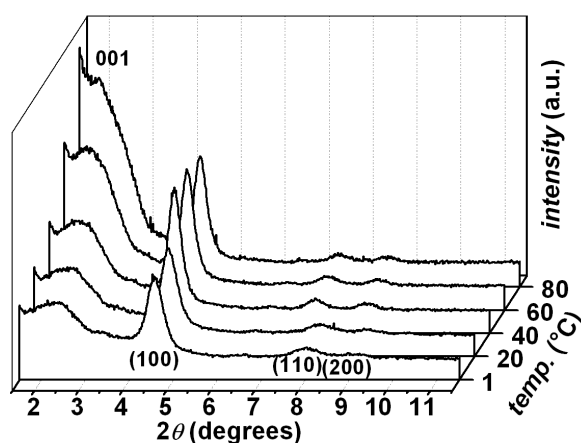


**Figure 4-4.** Thermal evolution of the SAXS diagrams of the alcoholic synthesis mixture:  $C_{12}\text{-PO}_4$  / ethanol (20/80 w/w),  $\text{Al}(\text{O}^i\text{Pr})_3$ ,  $\text{H}_3\text{PO}_4$ . (Equimolar amounts of  $C_{12}\text{-PO}_4$ ,  $\text{Al}(\text{O}^i\text{Pr})_3$ , and  $\text{H}_3\text{PO}_4$ .) The lamellar phase and the hexagonal phase (in parenthesis) are indexed.

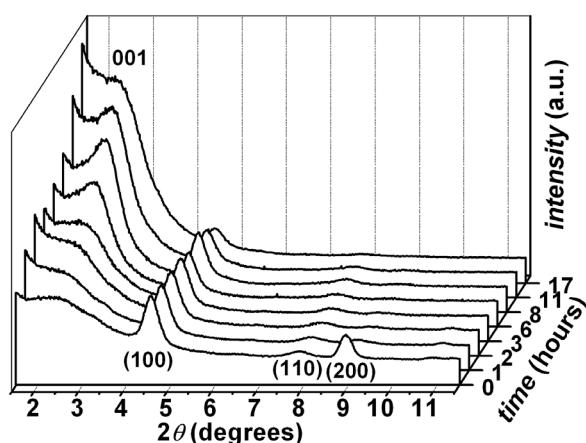


**Figure 4-5.** Temporal evolution of the SAXS diagrams of the alcoholic synthesis mixture:  $C_{12}\text{-PO}_4$  / ethanol (20/80 w/w),  $\text{Al}(\text{O}^i\text{Pr})_3$ ,  $\text{H}_3\text{PO}_4$ . (Equimolar amounts of  $C_{12}\text{-PO}_4$ ,  $\text{Al}(\text{O}^i\text{Pr})_3$ , and  $\text{H}_3\text{PO}_4$ .) The lamellar phase and the hexagonal phase (in parenthesis) are indexed.

#### 4.4. On the Synthesis Mechanism

*n*-Dodecyl phosphate is completely soluble in ethanol under the conditions used in the syntheses. The pure surfactant solutions are optically isotropic, *i.e.* non-birefringent under polarised light as was verified by polarised-light optical microscopy (POM); they do not show any SAXS reflections over the entire temperature range (20 - 90 °C) and concentration region (5 - 50 % w/w) that was studied. Hence, the

evolution of a mesostructure during the synthesis is obviously induced by the presence of the inorganic reactants; the formation of the mesostructure is a highly co-operative process. Both the relatively poor order of the products and the lack of any mesoscopic structure in the absence of the inorganic components are consistent with the fact that the alcohols have a considerably lower polarity than water (*i.e.* lower dielectric constants; at 25 °C:  $\epsilon_{\text{water}} = 78$ ,  $\epsilon_{\text{methanol}} = 33$ ,  $\epsilon_{\text{ethanol}} = 24$ ); thus, the self-aggregation of the surfactant molecules into micelles is relatively disfavoured in these alcohols as compared to water.

The *in-situ* studies (see previous chapter) have shown that the synthesis eventually leads to a single lamellar phase. The inverted hexagonal structure is an intermediate phase which co-exists with the lamellar phase over a certain time interval at the beginning of the reaction, particularly at low temperatures; it finally transforms into the lamellar phase. It is interesting to discuss these findings in the light of the mechanistic considerations mentioned in chapter 1.1.2., which focused on the synthesis of hexagonal mesostructured MCM-41 silica with cationic ammonium surfactants. The concept of 'charge density matching' [43] provided an explanation for a transformation of an intermediate lamellar phase to the final (non-inverted) hexagonal silica material: The surface area which each cationic surfactant head group exposes to the anionic silicate oligomers (at the surfactant/silicate interface) depends on the charge density of these silica oligomers. As the condensation of the silicate species proceeds, the charge density is diminished, which leads to an increase of the surfactant head group's interface area; thus, a curvature of the surfactant arrangement is induced, resulting in columnar micelles (with the head groups turned outwards).

In the system studied here, the transformation of the inverted hexagonal aluminium phosphate mesostructure into the lamellar phase corresponds to a similar increase of each surfactant head group's surface area at the surfactant/inorganic interface. The charges are different as compared to the silica synthesis: The surfactant phosphate head group is clearly anionic. For the inorganic species involved during the generation of the final aluminium phosphate network the charge situation is more complex; both cationic ( $\text{Al}^{3+}$ ) and anionic species ( $\text{H}_x\text{PO}_4^{(3-x)-}$ ,  $x < 3$ ) are present at the initial stages of the reaction; in aqueous solution they are assumed to form soluble "aggregation oligomers" containing Al-O-P linkages [131, and references cited therein], which will

carry both positive and negative charges, corresponding to incompletely connected Al and phosphate units at the "loose ends" of the oligomers. A similar situation may be assumed for the ethanolic solution. At any rate, the density of positive charges within the oligomers, which 'match' the negatively charged surfactant head groups, will decrease in the course of the reaction. Thus, the observation of an inverted hexagonal intermediate which transforms into a lamellar phase is consistent with the 'charge density matching' concept.

#### 4.5. NMR Spectroscopy

In order to obtain information on the short-range coordination environment of aluminium, the samples were investigated by  $^{27}\text{Al}$  MAS NMR spectroscopy; **Figure 4-6a** shows the  $^{27}\text{Al}$  spectrum of a sample which contains relatively high amounts of the inverted hexagonal phase (similar to the sample prepared at 10 °C in Figure 4-2a); the two resonances at *ca.* 43 ppm and -11 ppm are attributable to tetrahedral  $\text{Al}(\text{OP})_4$  and octahedral  $\text{Al}(\text{OP})_x(\text{H}_2\text{O})_{6-x}$  ( $x \leq 4$ ). The same picture is found for a sample with a relatively high amount of the lamellar phase (similar to the sample prepared at 60 °C in Figure 4-2d), which is shown in **Figure 4-6b**. In the latter case the relative intensity of the resonance corresponding to six-fold coordinated Al is slightly higher; the coordination of water molecules to Al within the  $\text{AlPO}_4$  matrix seems to be relatively favoured in the lamellar phase as compared to the inverted hexagonal phase. The NMR spectra do not indicate the presence of any significant amounts of aluminium oxide and/or oxyhydroxide species in the samples.

**Figure 4-7** shows the  $^{31}\text{P}$  spectra of the same samples, which exhibit relatively broad signals between 0 and -30 ppm, attributable to four-fold coordinated P with O-Al (tetrahedral and/or octahedral Al) and various amounts of  $\text{H}_2\text{O}$  or OH groups, *i.e.*  $\text{P}(\text{OAl})_x(\text{H}_2\text{O})_{4-x}$ . The signals seem to consist of several overlapping resonances; this observation is more apparent for the sample with relatively high amounts of the inverted hexagonal phase (**a**) as compared to the sample which mainly consists of the lamellar phase (**b**).

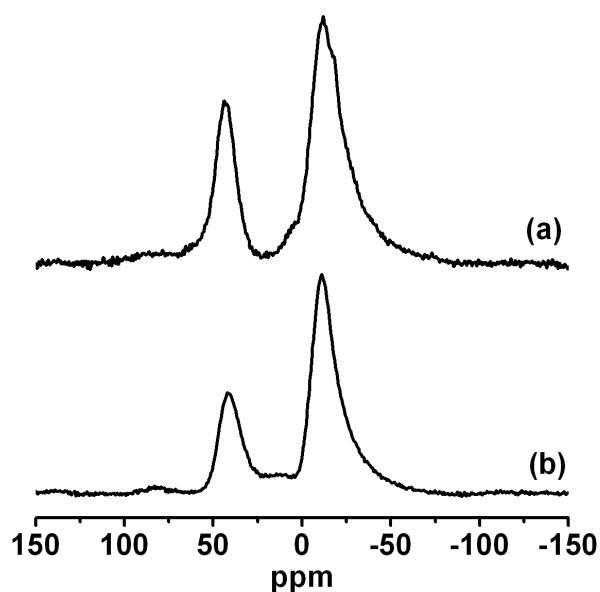


**Figure 4-6.** Solid-state  $^{27}\text{Al}$  MAS NMR spectra of mesostructured aluminium phosphates prepared under alcoholic conditions with  $C_{12}\text{-PO}_4$ ; in sample **(a)** the inverted hexagonal phase is predominant, sample **(b)** consists mainly of the lamellar phase. The two resonances at *ca.* 43 and -11 ppm correspond to  $\text{Al(OP)}_4$  and  $\text{Al(OP)}_x(\text{H}_2\text{O})_{6-x}$ , respectively.

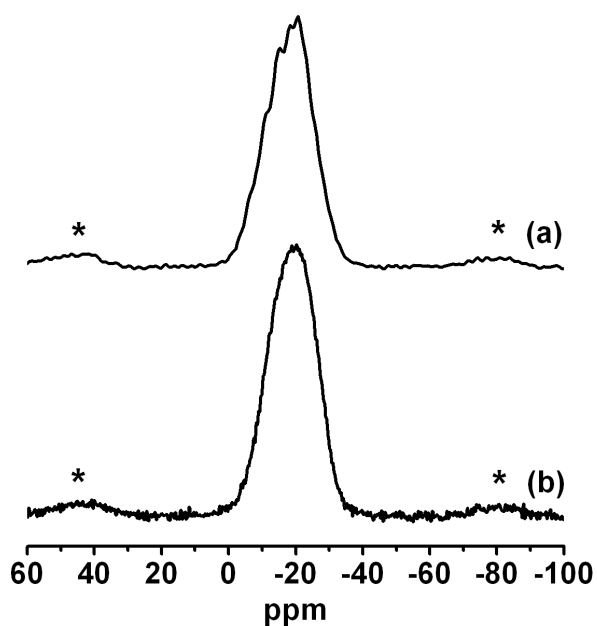


**Figure 4-7.** Solid-state  $^{31}\text{P}$  MAS NMR spectra of mesostructured aluminium phosphates prepared under alcoholic conditions with  $C_{12}\text{-PO}_4$ ; in sample **(a)** the inverted hexagonal phase is predominant, sample **(b)** consists mainly of the lamellar phase. The broad signals, which may be the superposition of several overlapping resonances, correspond to  $\text{P(OAl)}_x(\text{H}_2\text{O})_{4-x}$ . (\*: spinning side bands)

#### 4.6. XANES Spectroscopy

As discussed in chapter 3.5, another convenient method to distinguish between tetrahedrally and octahedrally coordinated Al is provided by XANES spectroscopy at the Al K-edge; the exact energy position of the absorption maximum (corresponding to the 1s to 3p electronic transition) differs by approximately 2 eV for four-fold (1.5666 keV) and six-fold coordination (1.5680 keV), respectively. When both coordination numbers are present in the same sample, the two absorption maxima usually strongly overlap and may therefore be more conveniently distinguished in the second derivative of the spectrum, which shows two well-resolved minima at the respective energies.

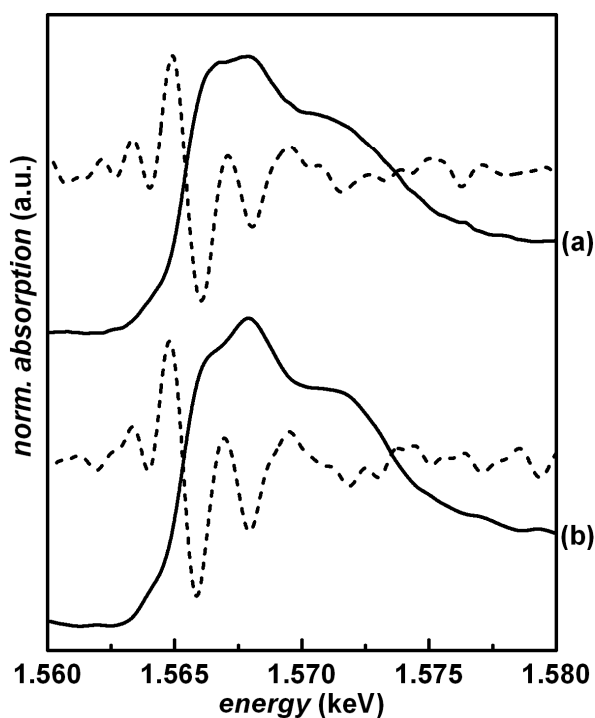


**Figure 4-8.** Al K-edge XANES spectra of mesostructured aluminium phosphates prepared under alcoholic conditions with  $C_{12}\text{-PO}_4$ ; in sample **(a)** the inverted hexagonal phase is predominant, sample **(b)** consists mainly of the lamellar phase. Solid lines: original spectra; dashed lines: second derivatives.

The Al K-edge XANES spectra (**Figure 4-8**) of the same samples as have been investigated by solid-state NMR spectroscopy (see **Figure 4-6**) confirm that the relative amount of six-fold coordinated Al is lower in the sample which predominantly consists of the inverted hexagonal phase **(a)** as compared to the sample with high

amounts of the lamellar phase **(b)**. As discussed in chapter 3.5, the relative intensities of the absorption maxima in the spectra at 1.566 and 1.568 keV correspond to the approximate relative amount of four-fold and six-fold coordinated Al, respectively (cf. Figure 3-14).

#### 4.7. Thermal Analysis

The samples prepared in ethanol at various temperatures (see Figure 4-2, page 55), consisting of the two phases, were investigated by thermal analysis. **Figure 4-9** shows the thermogravimetry / differential thermal analysis / mass spectrometry (TG/DTA/MS) diagram of the sample prepared at 10 °C (cf. Figure 4-2a) as an example.

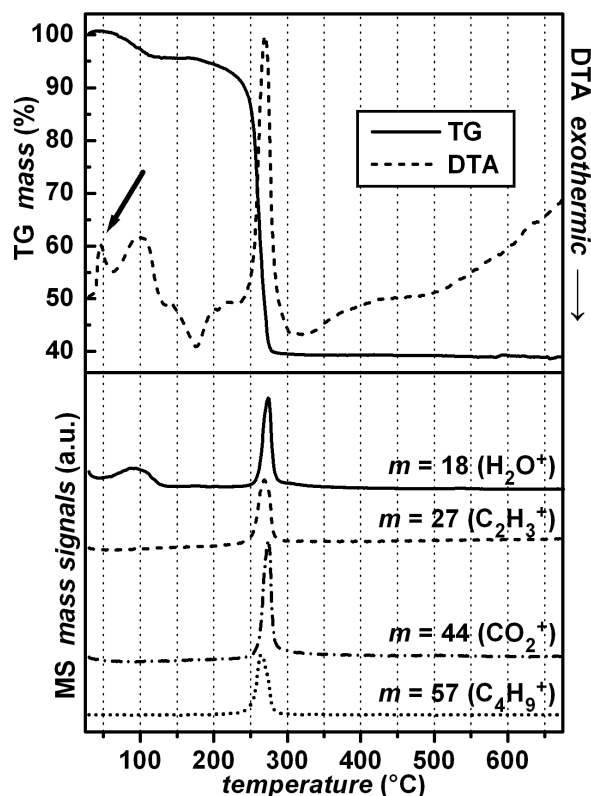


**Figure 4-9.** Thermal analysis (TG/DTA/MS) diagram of a mesostructured aluminium phosphate prepared in from  $Al(O^iPr)_3$  and  $H_3PO_4$  with  $C_{12}$ - $PO_4$  in ethanol at 10 °C (cf. Figure 4-2a). The arrow indicates the phase transition of the hexagonal phase to the lamellar phase.

The decomposition of the surfactant starts at *ca.* 150 °C with an exothermic DTA peak followed by one large endothermic step at *ca.* 230 - 280 °C;  $H_2O^+$ ,  $CO_2^+$ , and several organic mass fragments are detected ( $C_2H_3^+$  and  $C_4H_9^+$  shown exemplarily). The decomposition of the surfactant within such a narrow temperature interval indicates that the phosphate head groups are not incorporated in the aluminium phosphate matrix (cf. chapter 3.6). Prior to that (*ca.* 50 - 120 °C) the removal of water is observed (5 % endothermic mass loss). Below 50 °C an endothermic peak is found in the DTA which is not accompanied by any mass loss; this corresponds to the phase transition of the inverted hexagonal into the lamellar phase (see below).

The TG/DTA/MS diagrams of the other three samples (prepared at higher temperatures) are very similar. The relative mass loss caused by the decomposition of the surfactant varies systematically with the relative amount of the hexagonal phase in the respective sample: The higher the relative intensities of the powder XRD reflections from the hexagonal phase are (cf. Figure 4-2), the greater is the mass loss detected by TG. This is shown in **Table 4-2**; the mass losses are calculated relative to the masses of the samples at 150 °C, *i.e.* after the initial removal of water. This correlation confirms that the amount of surfactant relative to the amount of inorganic material is larger for the inverted hexagonal than for the lamellar phase (cf. elemental analysis, chapter 4.2).

**Table 4-2.** Thermogravimetric data of the surfactant decomposition and calorimetric data of the phase transition (hexagonal-lamellar) in the samples shown in Figure 4-2.

sample		phase transition: calorimetric data		
prepared at	mass loss <sup>a</sup> (%)	$\theta_{onset}$ (°C)	$\theta_{offset}$ (°C)	enthalpy <sup>b</sup> (J/g)
10 °C (a)	58.1	35.8	42.6	58.0
25 °C (b)	50.4	35.2	40.9	37.4
40 °C (c)	47.8	35.5	40.4	24.0
60 °C (d)	44.2	34.8	39.6	11.3

<sup>a</sup> during surfactant decomposition. <sup>b</sup> peak integration

For all samples prepared at various temperatures (see Figure 4-2), the phase transition from inverted hexagonal to lamellar, as detected by DTA, was monitored quantitatively by differential scanning calorimetry (DSC). As expected, the enthalpy of this transition with respect to the overall sample weight systematically depends on the

relative amount of the hexagonal phase in the respective sample. **Figure 4-10** shows the DSC diagrams of the four samples. The plots are normalised with respect to the overall sample weights. It is noticeable that for higher relative amounts of the inverted hexagonal phase the temperature interval in which the phase transition occurs is wider and slightly shifted towards higher temperatures. The calorimetric data are given in **Table 4-2**.

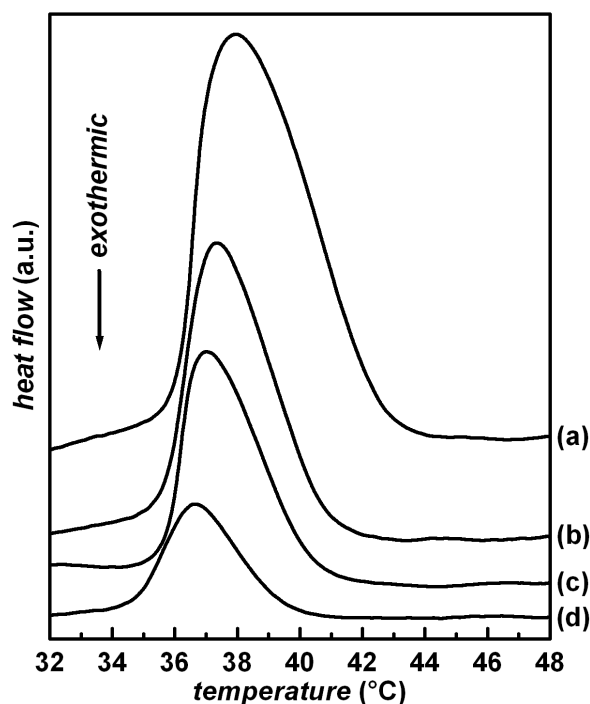


**Figure 4-10.** Differential scanning calorimetry (DSC) diagrams of the transition of the hexagonal phase to the lamellar phase in the samples shown in Figure 4-2, prepared at variable temperatures: **(a)** 10 °C; **(2)** 25 °C; **(c)** 40 °C; **(d)** 60 °C. The analytical data are given in Table 4-2.

#### 4.8. Conclusions

Mesostructured aluminium phosphate materials were successfully prepared in alcoholic media with the utilisation of *n*-dodecyl phosphate as structure-director. This synthesis follows a highly co-operative mechanism, since any mesostructures in the reaction mixtures are formed only after the addition of the inorganic reactant to the surfactant / alcohol solution; the pure surfactant / alcohol systems are not lyotropic. As long as the reaction temperature is kept low, the products consist of two phases, one of which is lamellar. The other phase has an inverted hexagonal structure, which is

thermally unstable; at *ca.* 35 - 43 °C it transforms into the lamellar structure. The lamellar structure is formed exclusively if the synthesis is carried out at higher temperatures, although it has a less well-ordered structure than a lamellar phase prepared under aqueous conditions. *In-situ* SAXS investigations demonstrate that the reaction proceeds slower in alcoholic media than in water and that the product composition systematically changes in dependence of both the synthesis temperature and the reaction time.

## 5. Alcoholic Synthesis with $n$ -Alkyl Amines as Structure-directors

### 5.1. Basic Characterisation

The utilisation of long-chain primary alkyl amines ( $C_nH_{2n+1}NH_2$ , in the following:  $C_n\text{-NH}_2$ ,  $n = 12, 14, 16$ ) as structure-directing agents under alcoholic conditions leads to aluminium phosphates with disordered mesostructures. **Figure 5-1a** shows the powder X-ray diffraction patterns of the *as-synthesised* products. Each pattern consists of one relatively broad reflection at low diffraction angle. This is a typical indication of a randomly ordered arrangement of tubular surfactant arrays within the inorganic matrix; similar structures have often been observed among various mesostructured materials [9,45], including aluminium phosphates [94-96,105]. Depending on the chain lengths of the surfactants, the three products exhibit different  $d$ -spacings corresponding to different powder XRD diffraction angles; the  $d$  spacings are given in **Table 5-1**.

**Figure 5-2** shows a representative transmission electron micrograph (TEM) of an *as-synthesised* sample prepared with  $C_{16}\text{-NH}_2$ ; the disordered mesostructure is evident.

**Table 5-2** shows the elemental analysis of the three *as-synthesised* samples described above. The Al/P ratios in the products are between 1.12 and 1.14, which indicates that the samples may basically be regarded as aluminium phosphates rather than consisting to a significant degree of aluminium oxide species; the latter would certainly lead to a lower relative amount of phosphorous. This is confirmed by NMR data (see below). Elemental analysis also shows that the molar  $C_n\text{-NH}_2$ /P ratio is between 0.42 and 0.51 (corresponding to a  $C_n\text{-NH}_2$ /Al ratio between 0.37 and 0.45), which means that not all of the surfactant used for the synthesis (0.5 moles  $C_n\text{-NH}_2$  per  $H_3PO_4$ ) is found in the products.

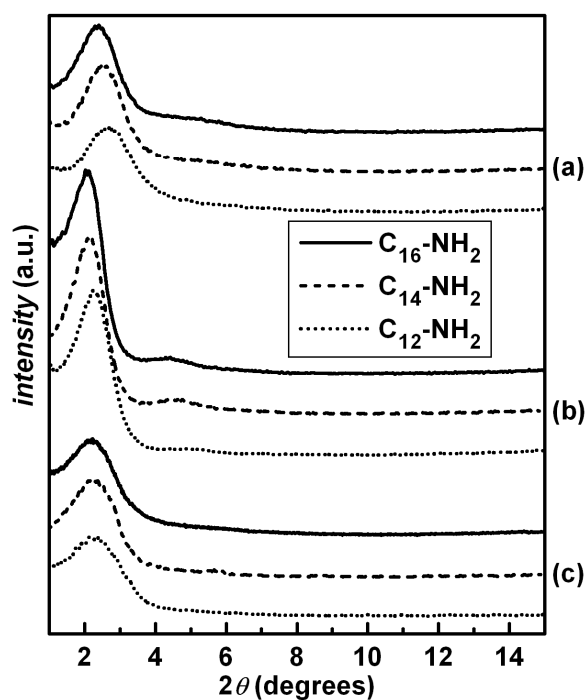


**Figure 5-1.** Powder XRD patterns of mesostructured aluminium phosphates prepared under alcoholic conditions from  $\text{Al}(i\text{OPr})_3$  and  $\text{H}_3\text{PO}_4$  with  $\text{C}_{12}\text{-NH}_2$ ,  $\text{C}_{14}\text{-NH}_2$ , and  $\text{C}_{16}\text{-NH}_2$  (*ca.* 15 % w/w); **(a)** as synthesised, **(b)** after thermal treatment, **(c)** after extraction of the surfactant. The patterns are typical of disordered tubular mesostructures. The structural order increases after thermal treatment and remains intact after surfactant removal. For  $d$  spacings see Table 5-1.

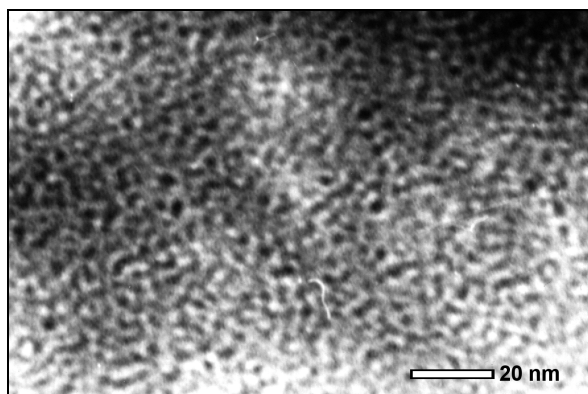


**Figure 5-2.** Representative transmission electron micrograph (TEM) of a mesostructured aluminium phosphate prepared under alcoholic conditions with  $\text{C}_{16}\text{-NH}_2$  showing a disordered mesostructure on the scale of several nanometers.

**Table 5-1.**  $d$  Spacings and pore diameters of mesostructured aluminium phosphates prepared under alcoholic conditions from Al(O<sup>*i*</sup>Pr)<sub>3</sub> and H<sub>3</sub>PO<sub>4</sub> with C<sub>12</sub>-NH<sub>2</sub>, C<sub>14</sub>-NH<sub>2</sub>, and C<sub>16</sub>-NH<sub>2</sub>.

surfactant	$d$ spacing (nm)			pore diameter (nm)
	as synthesised	after thermal treatment	after surfactant extraction	
C <sub>12</sub> -NH <sub>2</sub>	3.31	3.94	3.87	3.2
C <sub>14</sub> -NH <sub>2</sub>	3.50	4.20	3.91	3.4
C <sub>16</sub> -NH <sub>2</sub>	3.71	4.24	4.05	3.5

**Table 5-2.** Relative molar ratios of Al, P, C, and N in three representative mesostructured aluminium phosphates as synthesised under alcoholic conditions from Al(O<sup>*i*</sup>Pr)<sub>3</sub> and H<sub>3</sub>PO<sub>4</sub> according to elemental analysis.

surfactant	elemental analysis (relative molar amounts)				Al/P	C <sub><i>n</i></sub> -NH <sub>2</sub> /P
	Al	P	C	N		
C <sub>12</sub> -NH <sub>2</sub>	0.140	0.125	0.682	0.053	1.12	0.45
C <sub>14</sub> -NH <sub>2</sub>	0.117	0.102	0.730	0.050	1.14	0.51
C <sub>16</sub> -NH <sub>2</sub>	0.122	0.108	0.723	0.044	1.14	0.42

As in case of *n*-dodecyl phosphate surfactant (cf. chapter 4), the reaction mixtures are not completely free of water during the syntheses; the approximate molar ratio Al/water is 1/3. Water turns out to be essential for the successful preparation of well-ordered samples. When lower amounts of water are used, the quality of the products becomes somewhat poorer, *i.e.* the samples display weaker powder X-ray reflections and are thermally less stable. Higher amounts of water, on the other hand, led to the formation of a second mesophase with a lamellar structure, comparable to those obtained from syntheses with the same surfactants carried out entirely in water [77-79]. The influence of water on the quality of the products will be further discussed in the context of post-synthetic thermal treatment of the samples (see below).

## 5.2. Post-synthetic Treatment and Surfactant Removal

Attempts to remove the surfactant from the *as-synthesised* products prepared with Al(O<sup>*i*</sup>Pr)<sub>3</sub> and H<sub>3</sub>PO<sub>4</sub> without collapse of the mesostructure were not successful. Before the post-synthetic thermal treatment (see below), calcination of the samples results in

the complete disappearance of the powder X-ray reflections and no significant specific surface area is found by physisorption measurements. Similarly, solvent extraction under the conditions necessary for a quantitative removal of the surfactant (*i.e.* acidic methanol extraction at room temperature, see below) leads to a significant decrease in structural order and to specific surface areas as low as 100 – 300 m<sup>2</sup>/g.

It is possible to improve the stability of these samples as well as the degree of structural order by post-synthetic thermal treatment in an atmosphere of water vapour. In this procedure the samples are exposed to water vapour at 90 °C, but are not in contact with liquid water. In contrast, thermal treatment of the samples dispersed in liquid water leads to a phase transition into lamellar mesostructures. On the other hand, storage of the dry samples at 90 °C without water vapour does not result in any improvement of the stability or structural order; hence, the presence water plays an essential role in the thermal treatment. **Figure 5-1b** shows the powder XRD patterns of the thermally treated samples. The intensities of the reflections have increased and are shifted to a lower diffraction angle corresponding to larger *d*-spacings as compared to the *as-synthesised* products (see Table 5-1, page 71). According to elemental analysis the relative Al/P/ $C_n$ -NH<sub>2</sub> ratios do not change significantly in the course of the thermal treatment (cf. Table 5-2).

The relatively poor stability of the *as-synthesised* products indicates an incomplete condensation of PO<sub>4</sub> units with aluminium atoms, which, in turn, are most likely coordinated by additional water and/or hydroxyl groups to give the tetrahedral and octahedral aluminium environment observed (see below). Such an incompletely condensed network with Al(OP)<sub>4-x</sub>(H<sub>2</sub>O)<sub>x</sub> has been reported before [86,100,101]. In the light of this assumption, the post-synthetic thermal treatment obviously leads to an additional, *i.e.* more complete, network condensation, by which the stability as well as the structural order are improved.

Another possible interpretation of the effects of the thermal treatment is that the hydrolysis of the aluminium precursor, Al(O<sup>i</sup>Pr)<sub>3</sub>, which proceeds slower in alcohols than in water, is not completed after the initial synthesis and that a further hydrolysis takes place during the post-synthetic treatment. However, according to elemental analysis, the N/C ratios in the *as-synthesised* products correspond to those of the respective surfactants (*i.e.* 1/12 for C<sub>12</sub>-NH<sub>2</sub>, 1/14 for C<sub>14</sub>-NH<sub>2</sub>, and 1/16 for C<sub>16</sub>-NH<sub>2</sub>).

This indicates that the quantitative hydrolysis of the aluminium precursor,  $Al(O^iPr)_3$ , is already completed before the post-synthetic thermal treatment; otherwise additional amounts of carbon would be found due to remaining isopropoxide ligands attached to aluminium. The C/N ratio does not change significantly after the thermal treatment. Thus, the role of the water in the post-synthetic treatment is not to be attributed to a further, *i.e.* more complete, hydrolysis of the aluminium reactant.

The increase in the  $d$ -spacing in the course of the thermal treatment can therefore not be explained by a growth of the inorganic walls due to the additional condensation of the inorganic units. Instead, the rod-like domains between the inorganic walls, where the surfactant molecules reside, may expand. As pointed out above, water is essential in the post-synthetic thermal process; in order to reach all parts of the inorganic domains, the water molecules may well be envisioned to be transported through the rod-like channel system by diffusion (most likely along the boundary regions between the surfactant head groups and the inorganic part), by which they could cause a swelling of the channel diameter.

After the post-synthetic thermal treatment the materials are stable enough to preserve their mesostructure upon removal of the surfactant by acidic extraction with methanol. For a quantitative extraction it has turned out necessary to use at least equimolar amounts of HCl with respect to the approximate amount of surfactant to be extracted. This indicates a cation exchange mechanism for the extraction, in which the surfactant molecules, with their head groups protonated (*i.e.*  $R-NH_3^+$ ), are replaced by protons. After extraction the samples still exhibit the characteristic, though broader and slightly less intense, low-angle powder XRD reflection (**Figure 5-1c**); the  $d$ -spacing is slightly lower (see Table 5-1, page 71), as frequently observed upon removal of the surfactant from a mesoporous material. The complete removal of the surfactant is confirmed by the fact that no carbon is found by elemental analysis in the samples after extraction. Also, infrared (IR) spectroscopy shows that the characteristic C-H valence bands at  $2930-2850\text{ cm}^{-1}$  as well as C-H deformation bands around  $1460\text{ cm}^{-1}$  and  $720\text{ cm}^{-1}$  are absent after extraction (**Figure 5-3**). The surfactant can be isolated from the neutralised solution of the extract. After the removal of the surfactant the samples are thermally stable at temperatures up to *ca.*  $500\text{ }^\circ\text{C}$ .

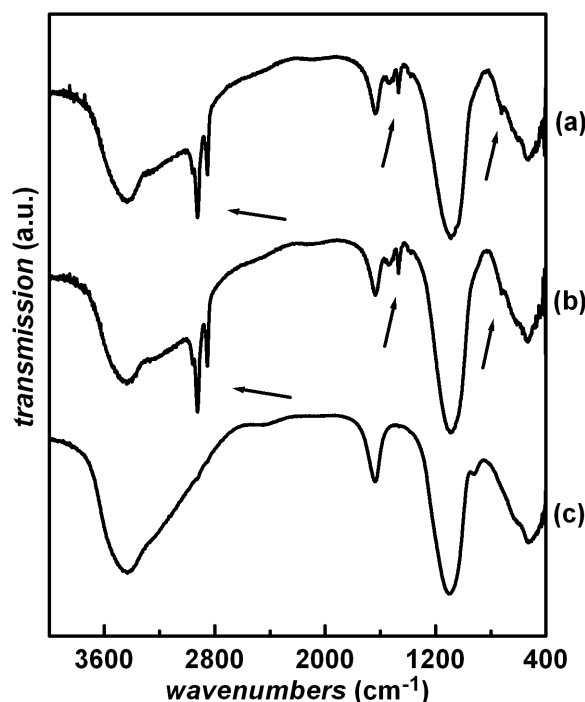


**Figure 5-3.** IR spectra of mesostructured aluminium phosphates prepared under alcoholic conditions with  $C_{16}$ -NH<sub>2</sub>; **(a)** as synthesised, **(b)** after thermal treatment, **(c)** after extraction of the surfactant. The arrows indicate characteristic C-H bands in the surfactant hydrocarbon chain, which disappear after its removal.

The extraction of the surfactant with methanol under acidic conditions is a very mild and convenient method for the complete removal of the organic structure-directing species from the samples. Moreover, the surfactant can be rescued and re-used after the extraction, which offers an economic advantage.

### 5.3. Nitrogen Physisorption

The porosity of the materials after the extraction of the surfactant was investigated by physisorption measurements. **Figure 5-4** shows the nitrogen adsorption/desorption isotherm of the sample prepared with  $C_{16}$ -NH<sub>2</sub>. At a relative pressure between 0.35 and 0.45 a well-defined step occurs, indicating capillary condensation. The isotherm is of type IV [110], as typical of mesoporous materials. The specific surface area (as calculated by the BET equation) is 580 m<sup>2</sup>/g. The pore size distribution (diameter, calculated by the BJH method [111]) has its maximum at 3.60 nm (**Figure 5-5**).

Corresponding results are found for products prepared with  $C_{12}-NH_2$  or  $C_{14}-NH_2$ , respectively (see Table 5-1, page 71).

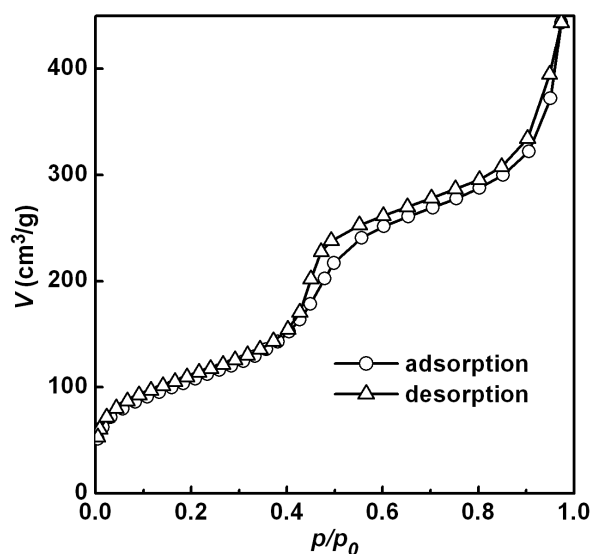


**Figure 5-4.** Nitrogen adsorption/desorption isotherm of a mesoporous aluminium phosphate prepared under alcoholic conditions from  $Al(O^iPr)_3$  and  $H_3PO_4$  with  $C_{16}-NH_2$ ; the specific BET surface area is  $580\text{ m}^2/\text{g}$ . An increase in the slope of both isotherm branches at *ca.*  $p/p_0 = 0.35 - 0.45$  indicates mesoporosity.

The sorption isotherms show a hysteresis, particularly above the relative pressure at which capillary condensation occurs; this may be explained by physisorption in the interparticle pore system: During the desorption, nitrogen in the supercritical state remains adsorbed on the interparticle surface; the (supposedly) small and uniform particle sizes lead to small distances between adjacent particles that are roughly in the same order of magnitude as the diameter of the tubular mesopores. This is consistent with the occurrence of a weak shoulder in the pore size distribution calculated from the desorption isotherm (BJH) at *ca.* 4 nm (diameter); the shoulder is absent if the pore size distribution is calculated from the adsorption branch. This hysteresis effect has been observed before [132,133]. (Apart from that, a hysteresis only in the  $p/p_0$  region of capillary condensation is frequently observed among mesoporous materials; it can be explained by differences in the mechanisms for the desorption the adsorption process.)

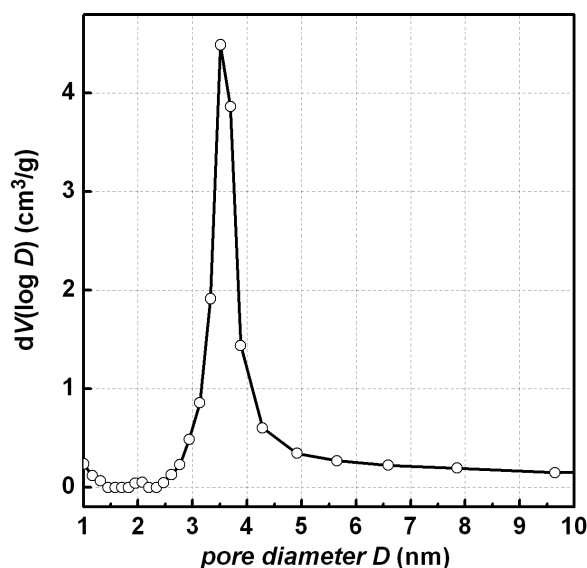


**Figure 5-5.** Pore size distribution (diameter) as calculated by the BJH method from the desorption branch in Figure 5-4.

#### 5.4. *In-situ* SAXS

The ethanolic synthesis with *n*-alkyl amines as structure-directors proceeds relatively slowly. **Figure 5-6** shows the temporal evolution of the SAXS diagrams of a typical reaction mixture with  $Al(iOPr)_3$ ,  $H_3PO_4$ , and *n*-hexadecylamine at 80 °C ( $Al/P/surfactant/ethanol/water = 1 / 1 / 0.5 / 32 / 3$ ). A single reflection with a *d* value of *ca.* 4.1 nm emerges approximately 30 minutes after the start of the reaction and slowly increases in intensity in the course of several hours. Due to limited synchrotron beamline time the measurement shown in the Figure was terminated after six hours, although *ex-situ* investigations have revealed that the evolution of the mesostructure continues for 24 – 48 hours. The SAXS data presented here are supposed to briefly illustrate the slow kinetics rather than give a complete, *i.e.* quantitative, study of the reaction.

The SAXS reflection is much broader and appears at a lower diffraction angle as compared to that in the powder diffraction (PXR) pattern of the respective final solid product (cf. Figure 5-1); this is attributable to a quite low degree of condensation of the inorganic units and relatively high amounts of solvent within the mesostructure at this early stage of the reaction.

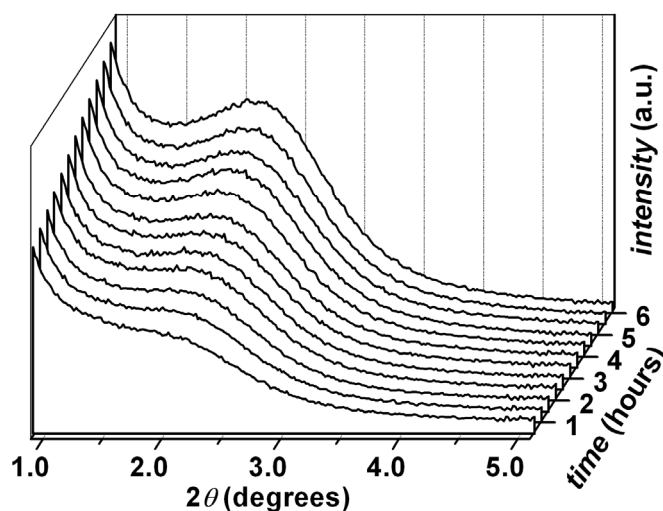


**Figure 5-6.** Temporal evolution of the SAXS diagrams of the alcoholic synthesis mixture:  $\text{Al}(\text{O}^i\text{Pr})_3 / \text{H}_3\text{PO}_4 / \text{C}_{16}\text{-NH}_2 / \text{ethanol} / \text{water} = 1 / 1 / 0.5 / 32 / 3$ .

The SAXS data reveal that the synthesis reaction proceeds much slower when *n*-alkyl amines are used as structure-directors than in case of *n*-dodecyl phosphate (cf. chapter 4.3); under the same synthesis conditions, the latter leads to the evolution of a well-defined (inverted hexagonal) mesostructure within less than one hour, even if this phase transforms into another (lamellar) structure afterwards.

As in case of *n*-dodecyl phosphate surfactant (cf. chapter 4) the pure *n*-alkyl amine surfactant / alcohol solutions are completely soluble in ethanol under the conditions used in the syntheses. The pure surfactant solutions are optically isotropic at room temperature as well as at 90 °C, as was verified by polarised-light optical microscopy (POM) and SAXS. This is another example of a highly co-operative synthesis of mesostructured materials.

## 5.5. NMR Spectroscopy

The  $^{27}\text{Al}$  and  $^{31}\text{P}$  MAS NMR spectra of all samples prepared with primary alkyl amines under alcoholic conditions are qualitatively comparable to those of the samples synthesised with  $\text{C}_{12}\text{-PO}_4$  in the same alcoholic media (see chapter 4.5). **Figure 5-7** shows the spectra of a sample prepared with  $\text{C}_{16}\text{-NH}_2$  before and after thermal treatment as well as after surfactant extraction.

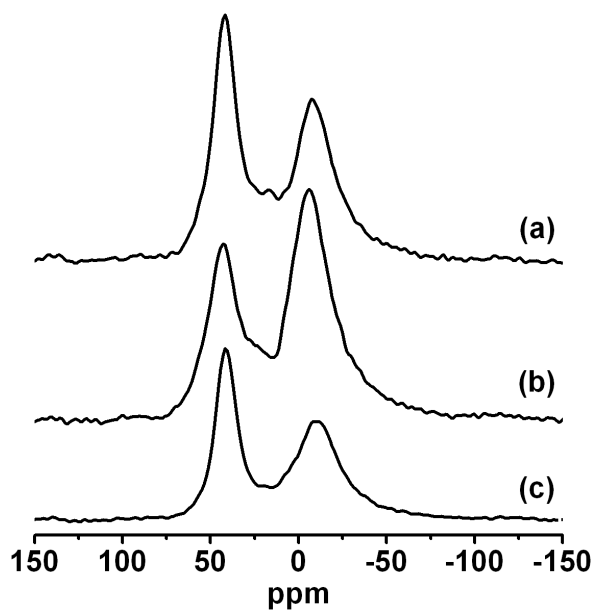


**Figure 5-7.** Solid-state  $^{27}\text{Al}$  MAS NMR spectra of mesostructured aluminium phosphates prepared under alcoholic conditions from  $\text{Al}(\text{O}^i\text{Pr})_3$  and  $\text{H}_3\text{PO}_4$  with  $\text{C}_{16}\text{-NH}_2$ ; (a) as synthesised, (b) after thermal treatment, (c) after surfactant extraction. The spectra show two resonances at *ca.* 42 and -7 ppm corresponding to  $\text{Al}(\text{OP})_4$  and  $\text{Al}(\text{OP})_x(\text{H}_2\text{O})_{6-x}$ , respectively; a weakly resolved third resonance at *ca.* 20 ppm can be suspected (cf. Figure 5-8).

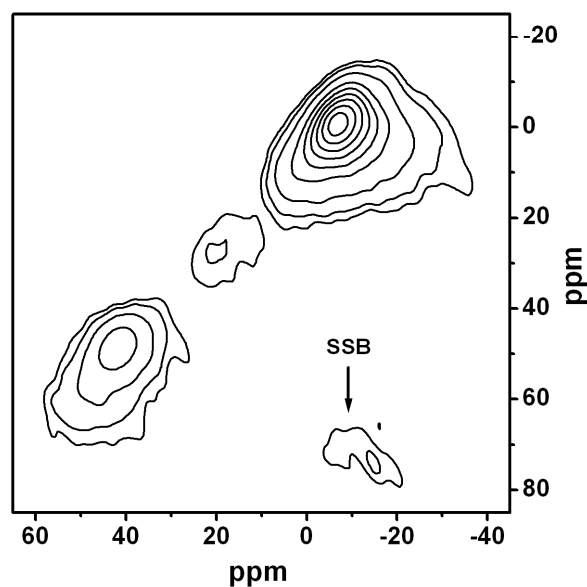


**Figure 5-8.** Sheared  $^{27}\text{Al}$  MQMAS spectrum of a mesostructured aluminium phosphate (as synthesised) prepared from  $\text{Al}(\text{O}^i\text{Pr})_3$  and  $\text{H}_3\text{PO}_4$  under alcoholic conditions with  $\text{C}_{16}\text{-NH}_2$ . Apart from the two signals at *ca.* 42 and -7 ppm, the spectrum reveals a third resonance at *ca.* 20 ppm, which cannot be identified unambiguously in the MAS spectrum (cf. Figure 5-7); it may be attributed to coordinated  $\text{Al}(\text{OP})_x(\text{H}_2\text{O})_{5-x}$ . (SSB : Spinning side band.)

All three spectra exhibit a resonance at *ca.* 42 ppm, which corresponds to tetrahedral Al(OP)<sub>4</sub> groups, and another resonance at *ca.* -7 ppm, which is attributable to six-fold coordinated Al with P in the second coordination shell and, presumably, additional H<sub>2</sub>O or OH groups, *i.e.* Al(OP)<sub>*x*</sub>(H<sub>2</sub>O)<sub>6-*x*</sub> (*x* ≤ 4). Additionally, there is a weakly resolved resonance around 20 ppm which can be identified unambiguously only in the MQMAS spectrum shown in **Figure 5-8**; This signal can be attributed to five-fold coordinated Al, again with P in the second shell, *i.e.* Al(OP)<sub>*x*</sub>(H<sub>2</sub>O)<sub>5-*x*</sub>.

The NMR spectra do not indicate the presence of any significant amounts of aluminium oxide and/or oxyhydroxide species in the samples. An interesting observation is that in the MAS spectra the relative intensity of the resonance at -7 ppm (*i.e.* the relative amount of octahedrally coordinated Al) considerably increases after the thermal treatment, which indicates that during this treatment (which proceeds under water atmosphere) additional water molecules coordinate to previously tetrahedral Al sites. This process seems to be reversible, since after the extraction of the surfactant the relative amount of tetrahedral Al returns to approximately its original value. In summary, the NMR data strongly suggest that the inorganic part of the samples consists of an aluminium phosphate network with Al-O-P linkages.

The origin of the water molecules that are coordinated to Al is an interesting issue. As mentioned before, certain quantities of water are present during the synthesis, which may serve as one possible explanation. More significantly, however, the products (which were not stored under vacuum or inert gas) take up significant amounts of water from ambient atmosphere. This 'ageing' was observed by comparison of samples a few days after their synthesis and some weeks later. After a longer time period <sup>27</sup>Al MAS NMR data reveal a higher relative amount of octahedral Al (*i.e.* Al(OP)<sub>*x*</sub>(H<sub>2</sub>O)<sub>6-*x*</sub>); larger quantities of water within the samples are also found by thermal analysis.

The <sup>31</sup>P MAS NMR spectra of the same samples prepared with C<sub>16</sub>-NH<sub>2</sub> (before and after thermal treatment as well as after surfactant extraction) are shown in **Figure 5-9**. Like the spectra of the samples prepared with C<sub>12</sub>-PO<sub>4</sub> under alcoholic conditions they exhibit relatively broad signals between 0 and -30 ppm.

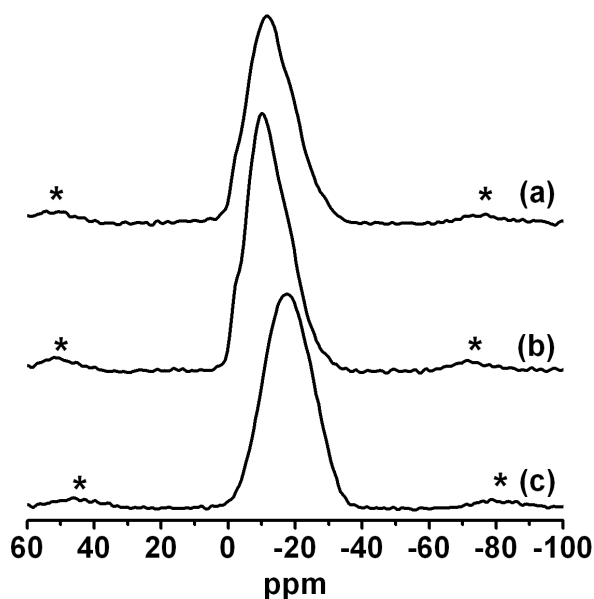


**Figure 5-9.** Solid-state  $^{31}\text{P}$  MAS NMR spectra of mesostructured aluminium phosphates prepared from  $\text{Al}(\text{O}^i\text{Pr})_3$  and  $\text{H}_3\text{PO}_4$  under alcoholic conditions with  $\text{C}_{16}\text{-NH}_2$ ; **(a)** as synthesised, **(b)** after thermal treatment, **(c)** after surfactant extraction. The spectra show broad lines which may consist of several resonances corresponding to  $\text{P}(\text{OAl})_x(\text{H}_2\text{O})_{4-x}$ . (\*: Spinning side bands).

In case of the samples before the surfactant extraction (**a** and **b**) the signals may consist of several resonances which are badly resolved from each other. These resonances may be attributed to four-fold coordinated P with O-Al (tetrahedral and/or octahedral Al) and various amounts of  $\text{H}_2\text{O}$  or OH groups, *i.e.*  $\text{P}(\text{OAl})_x(\text{H}_2\text{O})_{4-x}$ . Very similar  $^{31}\text{P}$  MAS NMR spectra were reported by SAYARI *et al.* for lamellar mesostructured aluminium phosphates synthesised under aqueous conditions with the utilization of the same primary amine surfactants [77,78]. However, the bad resolution of these resonances does not allow for more specific assignments to the diverse P environments. Particularly, it is not possible to distinguish between the P environment in the *as-synthesised* sample (**a**) and in the thermally treated sample (**b**). Finally, the spectrum of the extracted sample (**c**) shows a similarly broad signal which exhibits a more symmetric shape than that of the samples before extraction; it is not possible to distinguish whether it consists of one or more than one resonances. The signals are slightly shifted to lower fields as long as the surfactant molecules are still present (*i.e.* before the extraction); this may be explained by the influence of acidic protons of the surfactant head groups ( $\text{R-NH}_3^+$ ).

### 5.6. XANES Spectroscopy

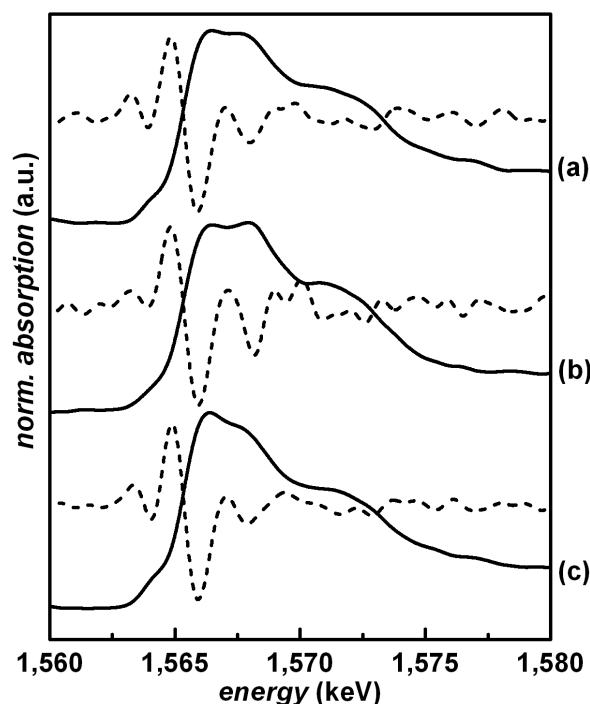


**Figure 5-10.** Al K-edge XANES spectra of mesostructured aluminium phosphates prepared with  $C_{16}-NH_2$ ; (a) as synthesised, (b) after thermal treatment, (c) after surfactant extraction. Solid lines: original spectra; dashed lines: second derivatives.

**Figure 5-10** shows the Al K-edge XANES spectra (and second derivatives) of a sample prepared with  $C_{16}-NH_2$  before and after thermal treatment as well as after extraction of the surfactant; the spectra qualitatively confirm the NMR data. However, a lower relative amount of octahedral Al, especially in the thermally treated sample, is found. Quantitative results derived from the XANES spectra may be less reliable than those from NMR data. On the other hand, it should be mentioned that different quantitative results were found by both NMR and XANES, depending on the age of the samples; as mentioned above, an irreversible uptake of water from air (*i.e.* a higher relative amount of octahedral Al) was observed by both methods after several months. Furthermore, dissimilar experimental conditions are used in XANES spectroscopy as compared to MAS NMR spectroscopy; for a XANES spectrum the sample is exposed to a high-intensity X-ray beam under vacuum, which may diminish the amount of water coordinated to Al.

### 5.7. Thermal Analysis

Figure 5-11 shows the thermal analysis of an *as-synthesised* sample prepared with C<sub>16</sub>-NH<sub>2</sub>. The thermogravimetric (TG) plot reveals a continuous mass loss of *ca.* 47 % between room temperature and *ca.* 650 °C.

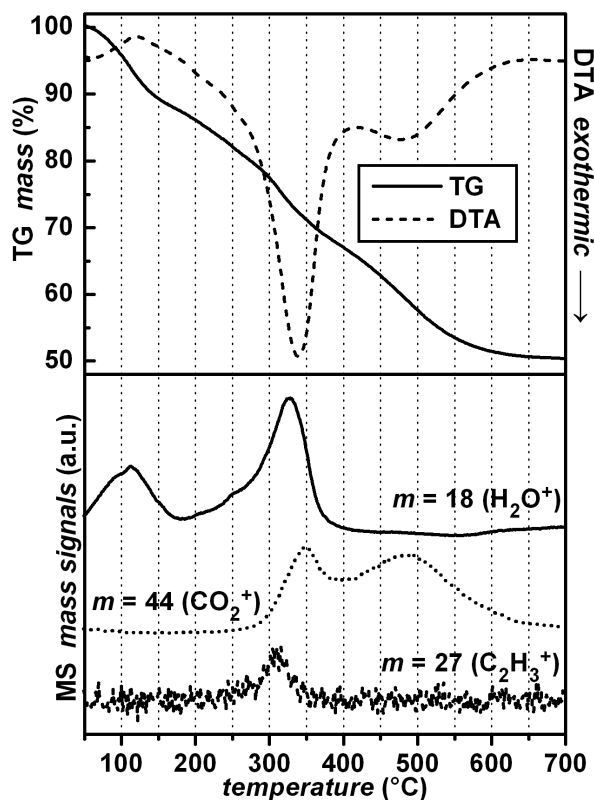


**Figure 5-11.** TG/DTA/MS diagram of a mesostructured aluminium phosphate prepared from Al(O<sup>i</sup>Pr)<sub>3</sub> and H<sub>3</sub>PO<sub>4</sub> under alcoholic conditions with C<sub>16</sub>-NH<sub>2</sub> (*ca.* 15 % w/w). The exothermic decomposition of the surfactant is completed at *ca.* 100 °C.

Taking into account the combination of differential thermal analysis (DTA) and mass spectrometry (MS) the mass loss can be divided up into three steps: Below *ca.* 200 °C there is an endothermic loss of water (*ca.* 10 %), which may be physisorbed on the inter-particle surface of the sample and/or reside within the channels, *i.e.* at the intra-particle surface. In a second step, between *ca.* 200 and 400 °C, a mass loss of *ca.* 18 % is observed, during which both water and several organic fragments (C<sub>2</sub>H<sub>3</sub><sup>+</sup> shown as an example) as well as carbon dioxide are detected. This exothermic step is attributable to the beginning decomposition of the surfactant. Finally, in a third step (*ca.* 400 – 650 °C) another exothermic mass loss of *ca.* 19 % occurs which is

accompanied by the detection of carbon dioxide, corresponding to a further decomposition of the organic part. These results are representative of all *as-synthesised* samples; likewise, all materials show the same thermal behaviour after the post-synthetic thermal treatment. After surfactant removal the samples show an endothermic mass loss (*ca.* 10 %) below 150 °C, attributable to physisorbed water, with no further mass change.

## 5.8. Conclusions

For the first time mesoporous aluminium phosphates were synthesised under basically non-aqueous conditions, although low quantities of water turn out to play a vital role in these syntheses. Also, a post-synthetic thermal treatment of the samples, in which water is involved as a necessary factor, leads to a significant improvement of the quality of the materials. The alcoholic preparation offers new perspectives for future syntheses. It has also led to the first successful utilisation of long-chain alkyl amines for the preparation of non-lamellar mesoporous aluminium phosphates.

## 6. Synthesis from a Single-source Precursor

### 6.1. Motivation and Scope

In the synthesis of mesostructured aluminium phosphates the exact stoichiometric composition and short-range order is a general problem. In contrast to their microporous analogues, which have well-defined crystalline structures and ideal  $\text{AlPO}_4$  stoichiometry, mesoporous materials lack crystallinity and vary in their relative Al/P ratios (cf. Table 1-1, page 18). Controlling the precise product composition and short-range order has turned out very difficult to achieve by means of varying the relative amounts of reactants (usually  $\text{H}_3\text{PO}_4$  and  $\text{Al}[\text{iOPr}]_3$ ) or other synthesis parameters.

The concept of using single-source molecular precursors (cf. chapter 1.1.4) offers a promising way to solve the above-mentioned synthesis problems. In order to serve as a potential precursor for a mesostructured aluminium phosphate with an ideal  $\text{AlPO}_4$  stoichiometry, a molecular unit must exhibit several crucial properties: (i) The building block, *i.e.* the core unit of the precursor, must contain equal amounts of alternating Al and P atoms connected with each other via bridging O atoms. (ii) During the synthesis of the mesostructured material it must be possible to hydrolytically remove the additional ligands from the building block. (iii) The building block itself must be stable enough to maintain its structure during the reaction. (iv) The precursor must be soluble in the (polar) medium in which the structure-directed synthesis carried out.

The literature offers a number of organic-soluble molecular compounds with  $\text{Al}_4\text{P}_4\text{O}_{12}$  core units analogous to that of the aluminosilicate discussed in chapter 1.1.4 (cf. Figure 1-3) [134-139]: The Al and P atoms are in a cube-like arrangement (in alternating order) and connected with each other by oxygen atoms. In most of these complexes the additional ligands coordinated to the Al and P atoms are alkyl groups (such as tert-butyl, iso-butyl, or methyl). Unfortunately, complexes with these kinds of ligands turn out not suitable for the utilisation as single-source precursors in the synthesis of mesostructured aluminium phosphates, since they are not sufficiently

soluble in the polar solvents necessary for these syntheses (*e.g.* water, short-chain alcohols, formamide).

## 6.2. The Single-source Precursor $[\text{Al}(\text{PO}_4)(\text{HCl})(\text{C}_2\text{H}_5\text{OH})_4]_4$

### *Structure and Properties*

A more promising 'candidate' for the utilisation as a single-source precursor in the synthesis of mesostructured aluminium phosphates has been introduced as early as 1975 by CASSIDY *et al.* [109]. This complex has the same  $\text{Al}_4\text{P}_4\text{O}_{12}$  core unit as the above-mentioned compounds, but different ligands: Each P atom carries one OH group whereas each Al atom is coordinated by three ethanol ligands, resulting in an overall six-fold coordination. A fourth ethanol ligand per Al atom is present in the coordination sphere, but not directly bound to any of the corner atoms of the core. Finally, a total of four chlorine atoms are also part of the tetrameric complex; the empirical formula is  $[\text{Al}(\text{PO}_4)(\text{HCl})(\text{C}_2\text{H}_5\text{OH})_4]_4$  (**Figure 6-1**).

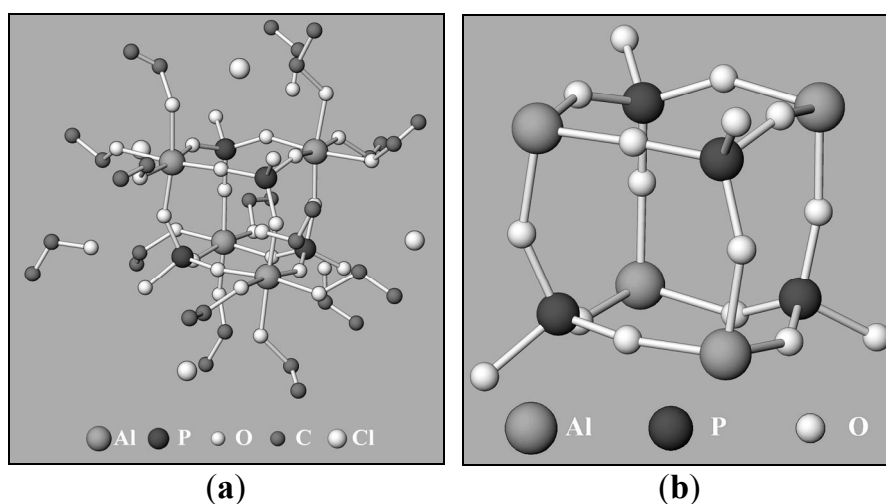


**Figure 6-1.** (a) Schematic representation of the molecular structure of  $[\text{Al}(\text{PO}_4)(\text{HCl})(\text{C}_2\text{H}_5\text{OH})_4]_4$ : P is coordinated by 4 O atoms, three of which are bridging towards Al; the fourth is terminal. Al is coordinated by 6 O atoms, with three of them bridging towards P and the other three belonging to ethanol ligands. Additional ethanol ligands as well as Cl atoms are found in the outer coordination shell. (b) The same view without the ethanol and Cl ligands clarifies the cube-like structure of the core unit. (Pictures were generated with *Atoms for Windows 3.2*; structural data were taken from reference [109]; H atom positions are not known.)

This precursor is soluble and stable in ethanol as well as in methanol. At room temperature the ligands serve as 'protective groups' that prevent the tetrameric units from linking together into a long-range  $\text{AlPO}_4$  structure; at elevated temperature ( $> 50\text{ }^\circ\text{C}$ ) the ligands are removed from the core, which leads to the precipitation of amorphous aluminium phosphate. The complex is not stable under aqueous conditions; hydrolysis not only of the ligands but also of the Al-O-P linkages in the core is observed when water is added to the alcoholic solution.

Owing to these solution properties and hydrolytic behaviour the complex is suitable for the structure-directed synthesis of mesostructured aluminium phosphates. Such a synthesis must be carried out under strictly non-aqueous conditions.

#### *Synthesis and Brief Characterisation*

Based on the vague synthesis information provided by CASSIDY *et al.* [109], the precursor was prepared from  $\text{H}_3\text{PO}_4$  and  $\text{AlCl}_3$  as described in chapter 2.1.4. The product is formed as a crystalline solid from the ethanolic mother liquor. When exposed to air, it decomposes within *ca.* 1 hour; instead of storing it under inert gas atmosphere it may also be conveniently kept in low amounts of dry ethanol. If the concentration of  $\text{AlCl}_3$  in the mother liquor is higher than approx. 0.5 mol/l, the product will rapidly precipitate during the addition of  $\text{H}_3\text{PO}_4$ . Otherwise it is possible to transfer the flask which contains the over-saturated solution of  $\text{Al}^{3+}$  and  $\text{PO}_4^{3-}$  (and  $\text{Cl}^-$ ) to a refrigerator; the product will then crystallise overnight, forming large crystals of up to 4 mm size. The latter procedure is to be favoured; the precipitation of the product as a fine powder should be avoided, since large crystals can more easily be dried in vacuum. This is a significant aspect, since a partial decomposition is observed when the product is exposed to vacuum for more than a few minutes. In order to improve the purity of the product and to avoid rapid precipitation it is advantageous to filter off any impurities from the  $\text{AlCl}_3$  solution before the addition of the  $\text{H}_3\text{PO}_4$  solution. Best yields (*ca.* 90 % with respect to  $\text{AlCl}_3$ ) are achieved when dry ethanol (99.8 %) is used.

**Figure 6-2** shows the experimental as well as the theoretical powder X-ray diffraction data of  $[\text{Al}(\text{PO}_4)(\text{HCl})(\text{C}_2\text{H}_5\text{OH})_4]_4$ . The diffraction pattern of the product

(a) was measured under air atmosphere within *ca.* 15 minutes; partial decomposition of the sample may have occurred during the measurement\*. The theoretical diffraction pattern (b) was calculated from the crystal data [109]\*\*. All reflections in the measured pattern are also present in the calculated one and vice versa; the differences in the relative intensities may possibly be attributed to preferred orientation effects in the sample.

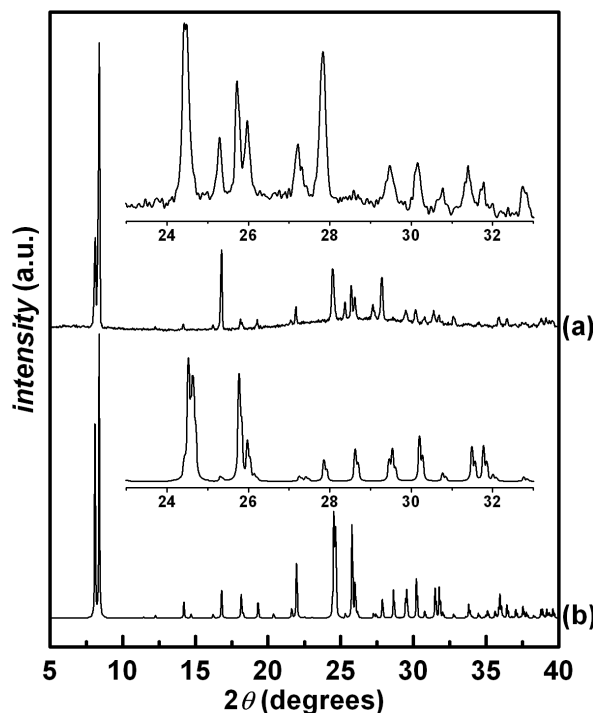


**Figure 6-2.** Powder XRD patterns of  $\text{Al}(\text{PO}_4)(\text{HCl})(\text{C}_2\text{H}_5\text{OH})_4$ ; (a) measured (see text); (b) simulated from single-crystal structure data [109].

The TG/DTA/MS diagram of the thermal decomposition of the product under flowing air atmosphere is shown in **Figure 6-3**. A mass loss of 58 % occurs in one single broad endothermic step between *ca.* 50 and 150 °C, which is accompanied by the detection of  $\text{H}_2\text{O}^+$ ,  $\text{C}_2\text{H}_3^+$ ,  $\text{CO}_2^+$ , and  $\text{HCl}^+$  mass fragments. For a quantitative thermal conversion of the molecular compound into an amorphous aluminium

\* Due to the instability of the sample under air atmosphere, a very short measuring time was chosen (0.25 seconds per data point; steps of  $0.01^\circ/2\theta$ ). For reasons of noise reduction, the diffraction pattern shown is the (smoothed) superposition of four individual measurements.

\*\* The simulation was carried out using *PowderCell for Windows 2.3*. Parameters were chosen in accordance with those in the measurement; the full-width-at-half-maximum of the profile function (Pseudo-Voigt 2) was adjusted to the experimental value.

phosphate the expected mass loss is 65 %. The fact that the observed value is lower can be attributed to a partial decomposition of the sample (removal of ethanol) before the measurement.

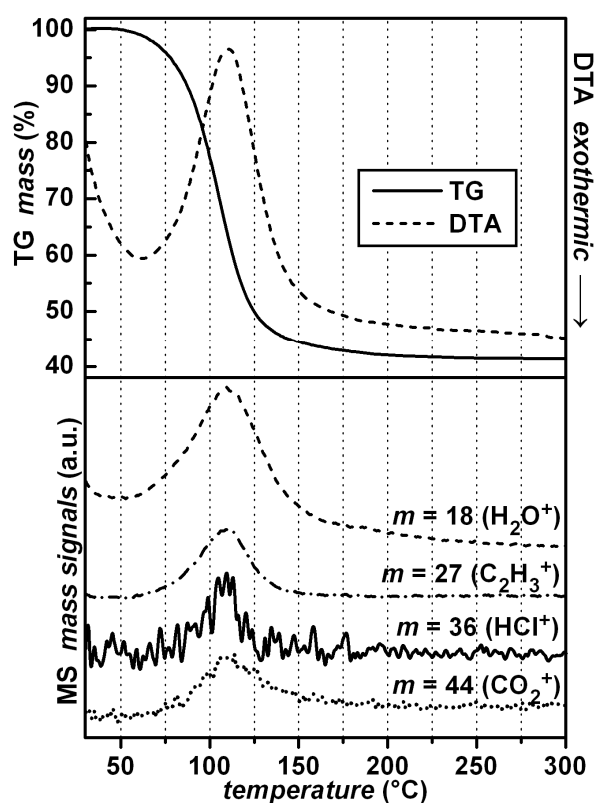


**Figure 6-3.** TG/DTA/MS diagram of  $\text{Al}(\text{PO}_4)(\text{HCl})(\text{C}_2\text{H}_5\text{OH})_4]_4$ ; a 58 % mass loss occurs in a single broad endothermic step between *ca.* 50 and 150 °C.

### 6.3. Basic Characterisation

The single-source molecular precursor  $[\text{Al}(\text{PO}_4)(\text{HCl})(\text{C}_2\text{H}_5\text{OH})_4]_4$  can be successfully used as a reactant in the alcoholic synthesis of ordered mesoporous aluminium phosphates. The powder X-ray diffraction patterns of the products (**Figure 6-4a**) indicate the same kind of randomly ordered arrangement of tubular  $\text{C}_n\text{-NH}_2$  surfactant arrays within the inorganic matrix as in case of the samples prepared from  $\text{Al}(\text{iOPr})_3$  and  $\text{H}_3\text{PO}_4$  under otherwise similar conditions (see chapter 5.1). Owing to the presence of HCl ligands in the coordination sphere of the precursor, the reaction mixture has a higher acidity than the corresponding  $\text{Al}(\text{iOPr})_3/\text{H}_3\text{PO}_4$  system. (When the same acidity is established in the latter system by

addition of HCl, the products exhibit only weak and broad reflections in the powder X-ray patterns.) It should be pointed out, however, that in this case the synthesis is purely non-aqueous; not even low quantities of water are present during the reaction.

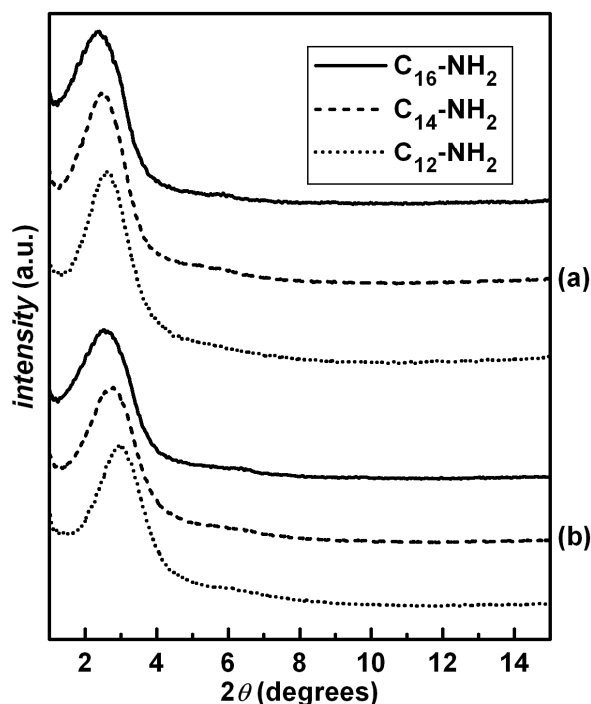


**Figure 6-4.** Powder XRD patterns of mesostructured aluminium phosphates prepared under alcoholic conditions from  $[\text{Al}(\text{PO}_4)(\text{HCl})(\text{C}_2\text{H}_5\text{OH})_4]_4$  with  $\text{C}_{12}\text{-NH}_2$ ,  $\text{C}_{14}\text{-NH}_2$ , and  $\text{C}_{16}\text{-NH}_2$  (ca. 15 % w/w); **(a)** as synthesised, **(b)** after extraction of the surfactant. The patterns are similar to those in Figure 5-1. The structural order remains intact after surfactant removal. For  $d$  spacings see Table 6-1.

The  $d$  values (**Table 6-1**) are slightly higher than those of the samples from the conventional synthesis (from  $\text{Al}(\text{iOPr})_3$  and  $\text{H}_3\text{PO}_4$ , cf. Table 5-1), whereas the pore diameters are smaller; this indicates that the inorganic walls are thicker, which is consistent with the fact that lower specific surface areas are found (see chapter 6.5).

The important difference between the products from the conventional synthesis (from  $\text{Al}(\text{iOPr})_3$  and  $\text{H}_3\text{PO}_4$ ) and the those from synthesis from the molecular precursor is the stoichiometry. Elemental analysis shows that in the samples prepared from  $[\text{Al}(\text{PO}_4)(\text{HCl})(\text{C}_2\text{H}_5\text{OH})_4]_4$  the Al/P ratio is always unity (**Table 6-2**) whereas a slight excess of Al was found in the samples prepared from  $\text{Al}(\text{iOPr})_3$  and  $\text{H}_3\text{PO}_4$  (cf. Table 5-2). This is a very strong indication that, as intended, the  $\text{Al}_4\text{P}_4\text{O}_{12}$  core unit

of the precursor remains intact during the synthesis of the mesostructured products, thus serving as a building unit for the inorganic network (**Figure 6-5**). If the core unit was hydrolysed during the reaction, such a highly reproducible ratio of Al/P = 1 would be unlikely.

**Table 6-1.** *d* Spacings and pore diameters of mesostructured aluminium phosphates as prepared under alcoholic conditions from  $[\text{Al}(\text{PO}_4)(\text{HCl})(\text{C}_2\text{H}_5\text{OH})_4]_4$  with  $\text{C}_{12}\text{-NH}_2$ ,  $\text{C}_{14}\text{-NH}_2$ , and  $\text{C}_{16}\text{-NH}_2$ , as well as after extraction of the surfactant.

surfactant	<i>d</i> spacing (nm)		pore diameter (nm)
	as synthesised	after surfactant extraction	
$\text{C}_{12}\text{-NH}_2$	3.39	2.98	2.6
$\text{C}_{14}\text{-NH}_2$	3.57	3.21	3.0
$\text{C}_{16}\text{-NH}_2$	3.74	3.42	3.2

**Table 6-2.** Relative molar ratios of Al, P, C, and N in three representative mesostructured aluminium phosphate samples as synthesised under alcoholic conditions from  $[\text{Al}(\text{PO}_4)(\text{HCl})(\text{C}_2\text{H}_5\text{OH})_4]_4$  according to elemental analysis.

surfactant	elemental analysis (relative molar amounts)				Al/P	$\text{C}_n\text{-NH}_2/\text{P}$
	Al	P	C	N		
$\text{C}_{12}\text{-NH}_2$	0.117	0.118	0.710	0.057	0.99	0.50
$\text{C}_{14}\text{-NH}_2$	0.100	0.101	0.752	0.052	1.00	0.53
$\text{C}_{16}\text{-NH}_2$	0.099	0.099	0.754	0.048	1.00	0.48

Lowering the acidity of the synthesis system, *e.g.* by addition of sodium hydroxide or tetramethylammonium hydroxide (one equivalent per HCl ligand of the precursor), leads to products with an Al/P ratio greater than one (comparable to the syntheses from  $\text{Al}(\text{iOPr})_3$  and  $\text{H}_3\text{PO}_4$ ); apparently, the  $\text{Al}_4\text{P}_4\text{O}_{12}$  core unit of the precursor is hydrolysed under these conditions. However, this effect may also be attributable to the fact, that the utilisation of the above-mentioned basic agents involves the addition of more or less significant amounts of water. (Tetramethylammonium hydroxide is used as the pentahydrate salt.)

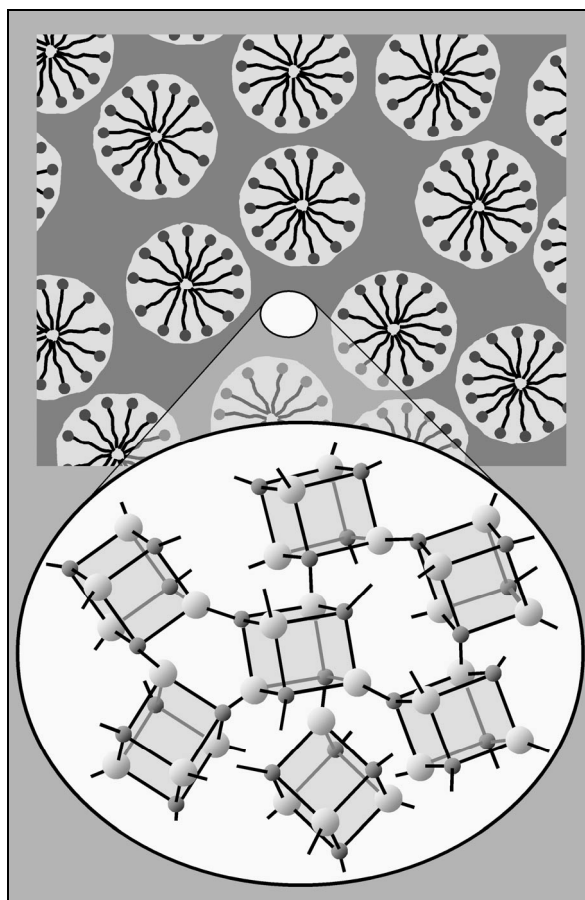


**Figure 6-5.** Schematic representation of a mesostructured aluminium phosphate prepared from the single-source molecular precursor  $[\text{Al}(\text{PO}_4)(\text{HCl})(\text{C}_2\text{H}_5\text{OH})_4]_4$ . The inorganic matrix consists of cube-like  $\text{Al}_4\text{P}_4\text{O}_{12}$  core units connected with each other by oxygen bridges; for clarity, oxygen atoms (cf. Figure 6-1) are not shown.

#### 6.4. Surfactant Removal

The products from the single-source synthesis are more stable than those prepared in the conventional synthesis (from  $\text{Al}(\text{O}^i\text{Pr})_3$  and  $\text{H}_3\text{PO}_4$ ); in particular, they do not need to be thermally treated in order to maintain their mesostructure upon the surfactant extraction with methanol/hydrochloric acid. Such a treatment does not have any impact on the X-ray diffraction patterns. The fact that thermal treatment is not required indicates that the condensation of the inorganic units is more complete after the initial preparation than in case of the conventional synthesis from  $\text{Al}(\text{O}^i\text{Pr})_3$  and  $\text{H}_3\text{PO}_4$ . The X-ray diffraction patterns of the samples after surfactant extraction

are shown in **Figure 6-4b**; as in case of the samples from the conventional synthesis, a slight decrease of the  $d$  spacings is observed as a result of the surfactant removal (see Table 6-1).

### 6.5. Nitrogen Physisorption

The nitrogen sorption isotherms of the products prepared from the single-source precursor are qualitatively similar to those of the products from the conventional syntheses. However, the specific (BET) surface areas are generally slightly lower. **Figure 6-6** shows the isotherms of a sample prepared with  $C_{16}$ - $NH_2$ ; the surface area is approximately  $410 \text{ m}^2/\text{g}$ .

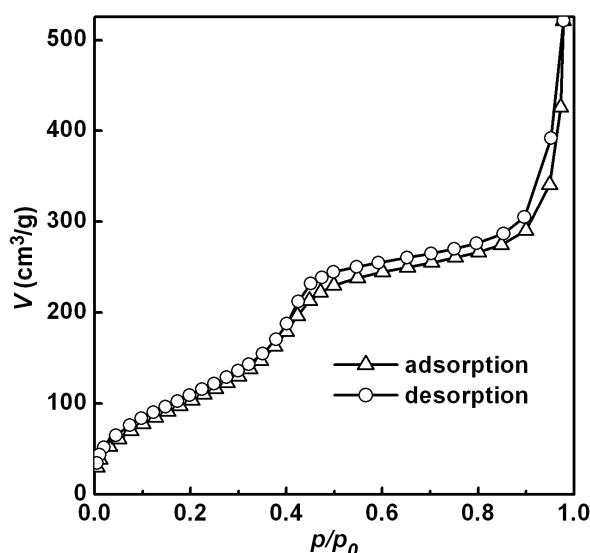


**Figure 6-6.** Nitrogen adsorption/desorption isotherm of a mesoporous aluminium phosphate prepared under alcoholic conditions from  $[Al(PO_4)(HCl)(C_2H_5OH)_4]_4$  with  $C_{16}$ - $NH_2$ ; the specific BET surface area is  $410 \text{ m}^2/\text{g}$ .

The hysteresis parallel to the pressure axis above the relative pressure at which capillary condensation occurs is weaker than in case of the sample from the conventional synthesis; this may indicate that the particle size is not as small as in the former sample (see chapter 5.3, page 74). The corresponding (BJH) pore size (diameter) distribution has its maximum at  $3.33 \text{ nm}$  (**Figure 6-7**; see Table 6-1)

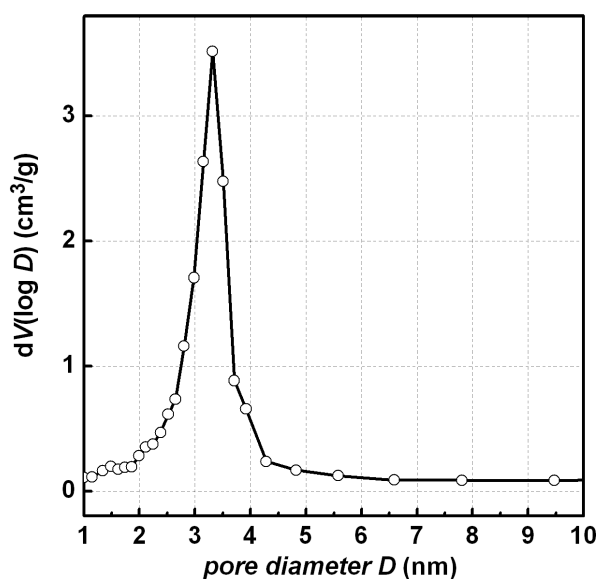


**Figure 6-7.** Pore size distribution (diameter) as calculated by the BJH method from the desorption branch in Figure 6-6.

## 6.6. NMR Spectroscopy

No significant differences in the solid-state NMR spectra are observed between samples from the conventional synthesis ( $\text{Al}(\text{O}^i\text{Pr})_3$  and  $\text{H}_3\text{PO}_4$ ) and those from the single-source synthesis ( $[\text{Al}(\text{PO}_4)(\text{HCl})(\text{C}_2\text{H}_5\text{OH})_4]_4$ ). **Figure 6-8** shows the  $^{27}\text{Al}$  MAS NMR spectra of a sample prepared with  $\text{C}_{16}\text{-NH}_2$  before and after removal of the surfactant. Both spectra exhibit resonances at *ca.* 42 ppm and -8 ppm, attributable to tetrahedral  $\text{Al}(\text{OP})_4$  groups, and  $\text{Al}(\text{OP})_x(\text{H}_2\text{O})_{6-x}$  ( $x \leq 4$ ), respectively. The presence of water in the Al coordination sphere of the sample before the removal of the surfactant is obviously attributable to the uptake of water from ambient atmosphere. After the surfactant extraction, an increase in the intensity of the octahedral resonance is observed, which indicates that additional water has been taken up by the sample.

**Figure 6-9** shows the  $^{31}\text{P}$  MAS NMR spectra of the same samples; as in case of the samples prepared from  $\text{Al}(\text{O}^i\text{Pr})_3$  and  $\text{H}_3\text{PO}_4$  one broad line between 0 and -30 ppm is observed, attributable to four-fold coordinated P with O-Al (tetrahedral and/or octahedral Al) and various amounts of  $\text{H}_2\text{O}$  or OH groups, *i.e.*  $\text{P}(\text{OAl})_x(\text{H}_2\text{O})_{4-x}$ .

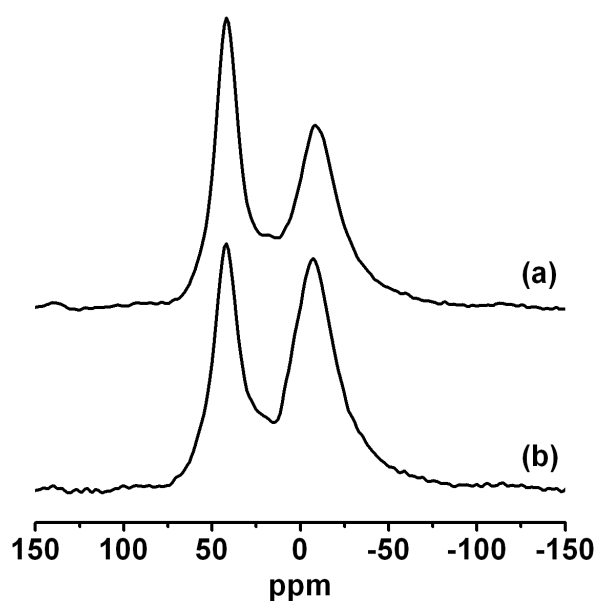


**Figure 6-8.**  $^{27}\text{Al}$  MAS NMR spectra of mesostructured aluminium phosphates prepared from  $[\text{Al}(\text{PO}_4)(\text{HCl})(\text{C}_2\text{H}_5\text{OH})_4]_4$  with  $\text{C}_{16}\text{-NH}_2$ ; **(a)** as synthesised and **(b)** after surfactant extraction. The two resonances at *ca.* 42 and -7 ppm correspond to  $\text{Al}(\text{OP})_4$  and  $\text{Al}(\text{OP})_x(\text{H}_2\text{O})_{6-x}$ , respectively.

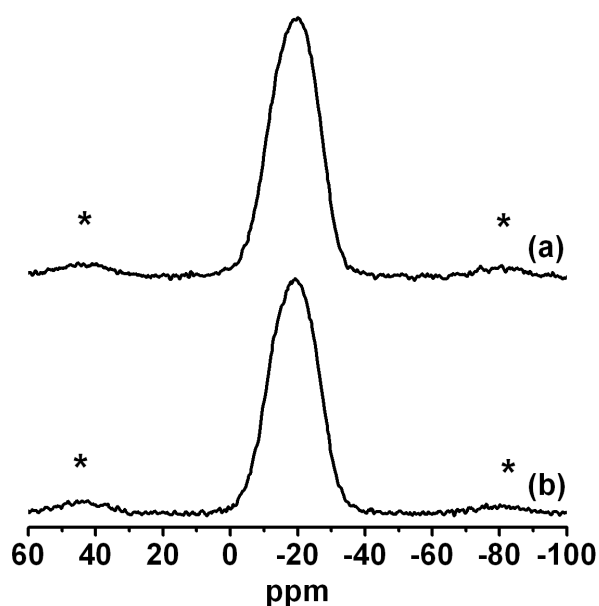


**Figure 6-9.**  $^{31}\text{P}$  MAS NMR spectra of mesostructured aluminium phosphates prepared from  $[\text{Al}(\text{PO}_4)(\text{HCl})(\text{C}_2\text{H}_5\text{OH})_4]_4$  with  $\text{C}_{16}\text{-NH}_2$ ; **(a)** as synthesised, **(b)** after surfactant extraction. The spectra show broad lines which may consist of several resonances corresponding to  $\text{P}(\text{OAl})_x(\text{H}_2\text{O})_{4-x}$ . (\* spinning side bands)

## 6.7. Conclusions

The utilisation of the single-source molecular precursor  $[\text{Al}(\text{PO}_4)(\text{HCl})(\text{C}_2\text{H}_5\text{OH})_4]_4$  as the reactant in the synthesis of ordered mesoporous aluminium phosphates leads to products with randomly ordered tubular pores. In comparison with samples prepared from the conventional reactants ( $\text{Al}(\text{O}^i\text{Pr})_3$  and  $\text{H}_3\text{PO}_4$ ) under comparable conditions, the powder XRD diffraction patterns and solid-state NMR spectra are quite similar; pore sizes and specific surface areas are slightly smaller. The synthesis is carried out under complete exclusion of water, whereas low quantities of water are needed in the synthesis from  $\text{Al}(\text{O}^i\text{Pr})_3$  and  $\text{H}_3\text{PO}_4$ . The most important quality of the products from the single-source synthesis is the strict Al/P ratio of 1, which is a strong indication that the  $\text{Al}_4\text{P}_4\text{O}_{12}$  core unit of the precursor is preserved during the synthesis, thus serving as a building block of the final mesostructured product. The single-source approach bears a promising potential for future syntheses; modification of the precursors (*i.e.* by incorporation of transition metal atoms) may lead to the possibility to tailor mesoporous materials based on aluminium phosphate.

## 7. Studies on the Phase Behaviour of the System *n*-Dodecyl Phosphate / Water

### 7.1. Motivation and Scope

Organic amphiphiles in a great variety are used as structure-directing agents in the synthesis of ordered mesostructured materials, their hydrophilic head groups ranging from cationic over neutral to anionic. Numerous investigations have been made on the role of the surfactant head groups, their interactions with the inorganic species, and the effect of the surfactant on the properties of the products [2,4,14,16,44,45]. Quaternary alkyl ammonium salts, such as *n*-hexadecyltrimethylammonium bromide (CTABr), and primary alkyl amines are commonly used for the synthesis of mesoporous or mesostructured silica phases [2,4,44,45], metal oxides [16], or aluminium phosphates (cf. chapter 1.2). Among the non-ionic surfactants, polyethylene oxides have turned out to be promising structure-directors for mesoporous silica and silica-based materials [8,140].

*n*-Dodecyl phosphate has been utilised for the synthesis of aluminium- and zinc-based mesostructured materials [4], for titania mesophases [15,129,141], and for mesoporous niobium [129] and zirconium [22] oxides. It also served for the preparation of chemical composites of hydroxyapatite and lamellar calcium dodecyl phosphate [142].

As mentioned in chapter 1.1.2, the phase behaviour of a surfactant/solvent system may change to a significant degree when the inorganic reactants are added for the synthesis of mesostructured materials. This problem may be overcome by utilising the surfactant in very large concentrations, in which case the mesostructure of the resulting inorganic/surfactant composite material usually quite exactly corresponds to that of the lyotropic surfactant/solvent system (LTC method) [41,42]. At any rate, it is of major interest to know the phase behaviour of the system in absence of the inorganic species in order to at least estimate the potential symmetries of the mesostructured products and to obtain information on the reaction mechanisms.

For some of the surfactant/solvent systems, that are of interest in the synthesis of mesostructured materials, the phase behaviour is well known, especially from X-ray diffraction studies. Detailed phase diagrams are available, for example, for the aqueous systems of *n*-hexadecyltrimethylammonium bromide (CTABr, *cf.* Figure 1-1, page 2) [12,13], *n*-dodecyltrimethylammonium bromide [143], or numerous non-ionic surfactants [144-147]. However, no information is found in the literature on the phase behaviour of *n*-dodecyl phosphate in any solvents so far.

## 7.2. Results and Discussion

The system *n*-dodecyl phosphate / water was investigated by temperature-resolved small angle X-ray scattering. Over the entire concentration and temperature range studied (20 - 90 % w/w and 20 - 110 °C) the diffraction patterns consist of peaks which may be explained as 00 $l$  reflections of one single lamellar phase. All samples exhibit at least three equidistant reflections corresponding to 00 $l$  indices. (For surfactant concentrations higher than 50 % w/w, the 003 reflection lies outside the detected region; in these cases its existence was verified by a different detector set-up.) The lamellar structure is confirmed by polarised light optical microscopy (POM); **Figure 7-1** shows the image of a sample with a concentration of 30 % w/w at 30 °C; the cross-shaped texture is typical of lamellar liquid-crystalline phases.

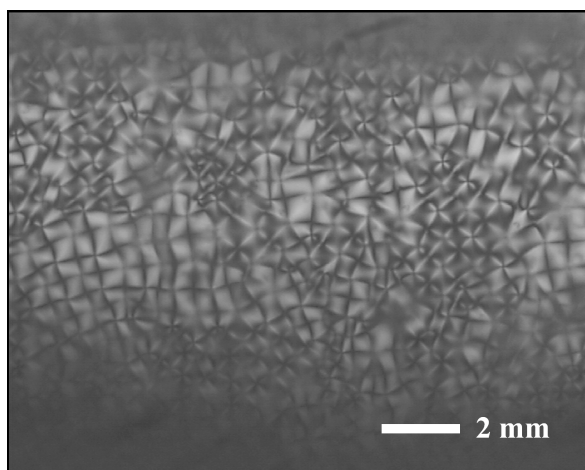


**Figure 7-1.** Polarised optical micrograph (POM) of the system  $C_{12}\text{-PO}_4$  / water (30/70 w/w) at 30 °C. The cross-shaped texture is typical of a lamellar lyotropic phase.

The repeat distance  $d$ , which is related to the reciprocal spacing  $s_{00l}$  by equation (1) (where  $l$  is the order of the  $00l$  reflection of the lamellar phase), changes considerably upon variation of the surfactant concentration.

$$d = \frac{l}{s_l} \quad (1)$$

At 20 °C the 90 % w/w sample has a repeat distance of  $d = 3.47$  nm. (According to the powder X-ray diffraction pattern, the pure surfactant in the solid-state at room temperature has a lamellar structure with a repeat distance of 2.87 nm.) A decrease of the relative amount of surfactant to 20 % w/w at a constant temperature of 20 °C leads to a considerable increase of the repeat distance to  $d = 15.0$  nm. At the same time the ordering of the lamellar structure decreases as the Bragg reflections become much broader and weaker. These two trends are visible in the example diffraction patterns in **Figure 7-2**, **Figure 7-3**, and **Figure 7-4**; the repeat distances as a function of both the surfactant concentration and the temperature are plotted in **Figure 7-5**.

The increase of the repeat distances as well as the loss of intensity and the broadening of the reflections can be explained by a subsequent increase of the amount of water between the surfactant bilayers; upon dilution, the distance between two adjacent bilayers grows, whereas the thickness of the bilayers themselves is not affected (see below). The significant loss of ordering in the structure is accounted for by fluctuations in the distance between the bilayers which becomes less well-defined as the amount of water between them is raised.

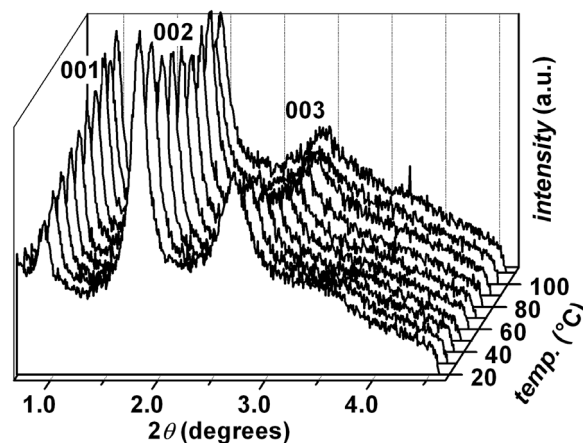


**Figure 7-2.** Thermal evolution of the diffraction patterns from a samples of *n*-dodecyl phosphate / water with a surfactant concentrations of 30 % w/w.

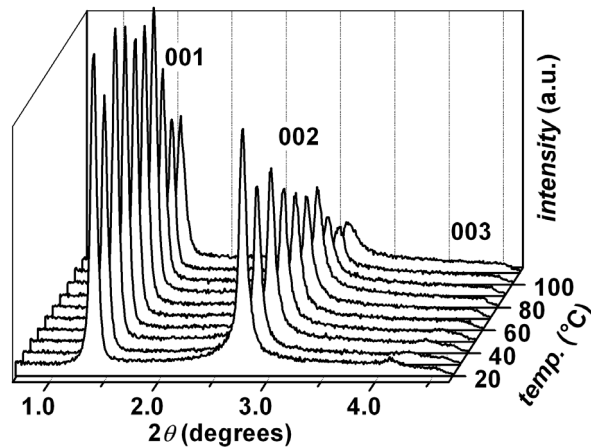


**Figure 7-3.** Thermal evolution of the diffraction patterns from a samples of *n*-dodecyl phosphate / water with a surfactant concentrations of 50 % w/w.

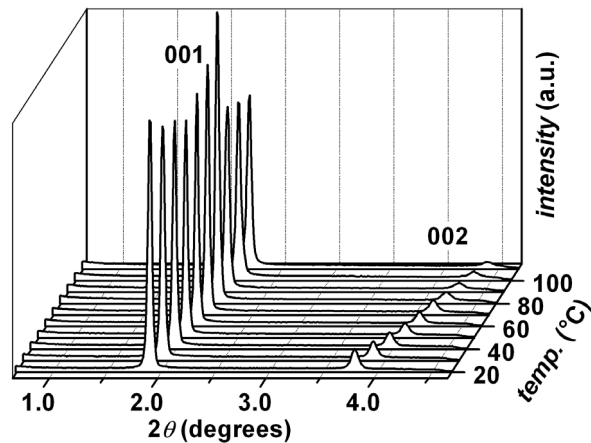


**Figure 7-4.** Thermal evolution of the diffraction patterns from a samples of *n*-dodecyl phosphate / water with a surfactant concentrations of 70 % w/w.

From the measured repeat distance  $d$  it is possible to determine the thickness  $d_L$  of the surfactant bilayers and the average area  $S$  available to one hydrophilic group on the surfactant-water interface if the density  $\rho_s$  of the surfactant at the respective temperature is known. According to LUZZATI [148]  $d_L$  may be calculated by equation 2, where  $c$  is the weight fraction of the surfactant (surfactant / surfactant+water) and  $\rho_w$  is the density of water.  $S$  ( $\text{nm}^2$ ) is obtained from equation 3, where  $M$  is the molecular weight of the surfactant and  $N_A$  is Avogadro's number.

$$d_L = d \cdot \left( 1 + \frac{\rho_s(1-c)}{\rho_w \cdot c} \right)^{-1} \quad (2)$$

$$S = \frac{2M}{d_L \cdot \rho_s \cdot 10^{-22} N_A} \quad (3)$$

Data on the density of *n*-dodecyl phosphate are available in the literature only for temperatures between 50 °C and 80 °C [149]; they are listed in **Table 7-1** (together with the respective values for water [150]).

**Table 7-1.** Densities of *n*-dodecyl phosphate ( $C_{12}$ - $PO_4$ ,  $\rho_s$ ) [149] and water ( $\rho_w$ ) [150] at various temperatures.

temperature (°C)	density $C_{12}$ - $PO_4$ $\rho_s$ (g/cm <sup>3</sup> )	density $H_2O$ $\rho_w$ (g/cm <sup>3</sup> )
50	1.011	0.988
60	1.003	0.983
70	0.988	0.977
80	0.977	0.972

The geometric parameters of the system within this temperature region are shown in **Figure 7-6** and **Figure 7-7**; the respective values for a temperature of 50 °C (as an example) are listed in **Table 7-2**. Samples with a surfactant concentration higher than 30 % w/w have relatively constant values of  $d_L$  and  $S$  at given temperatures.

**Table 7-2.** Repeat distance  $d$ , bilayer thickness  $d_L$ , and head group surface area  $S$  of lamellar *n*-dodecyl phosphate / water samples with variable surfactant concentrations at 50 °C.

surf. conc. (% w/w)	repeat distance $d$ (nm)	bilayer thickness $d_L$ (nm)	head group surface area $S$ (nm <sup>2</sup> )
40	7.52	2.97	0.295
50	6.03	2.98	0.294
60	5.10	3.03	0.288
70	4.37	3.04	0.288
80	3.89	3.10	0.282
90	3.40	3.05	0.286

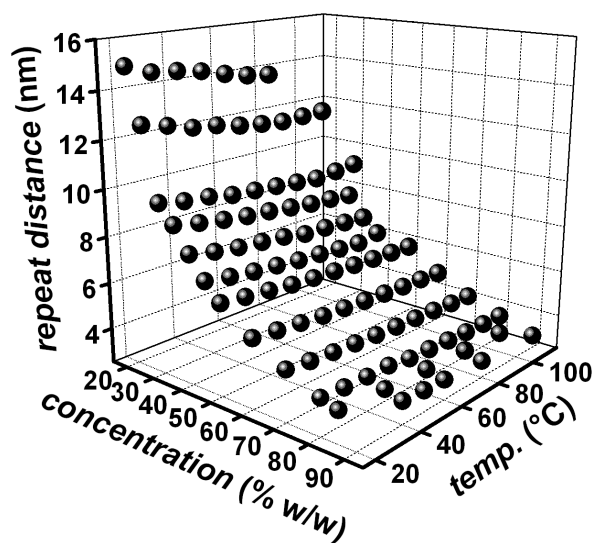


**Figure 7-5.** Repeat distances of the lamellar phase in the system  $C_{12}PO_4/water$  at variable surfactant concentrations and temperatures.

The repeat distance and, accordingly, the values of  $d_L$  and  $S$  also depend on the temperature. In general, there is a slight decrease of the repeat distance if the temperature is raised. This is explained by a shrinkage of the bilayer thickness due to the increase of thermal movement of the surfactant molecules within the bilayers; the lateral distance between the molecules grows as the hydrophobic chains are less rigidly in position. Since the bilayers may be presumed to remain free of water molecules, the greater lateral distance of the surfactant molecules must be compensated for by a decrease of the bilayer thickness. This explanation is consistent with the fact that  $d_L$  slightly shrinks upon increase of the temperature (cf. Figure 7-6); at the same time  $S$  becomes larger (cf. Figure 7-7).

In the temperature region above 50 °C, samples with surfactant concentrations of less than 35 % w/w show an irregular behaviour. The respective values of  $d_L$  and  $S$  seem to fluctuate temporally; this behaviour could not be systematically controlled during the experiments and the data from this temperature/concentration region are therefore not reproducible. In some of these samples phase separations were observed macroscopically as well as by polarised light optical microscopy.

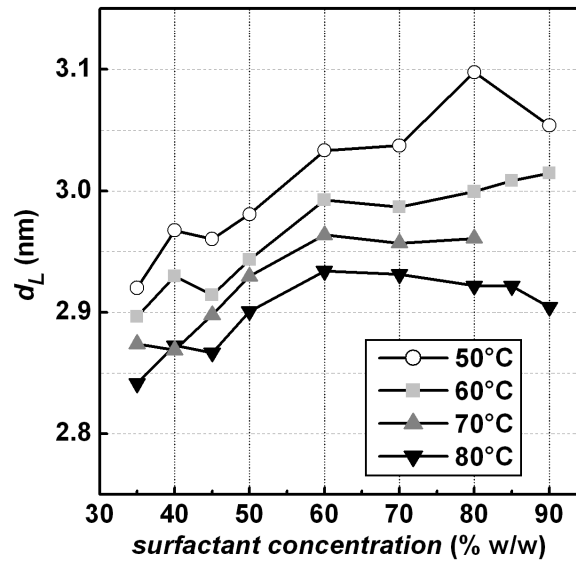


**Figure 7-6.** Thickness  $d_L$  of the surfactant bilayers in the system  $C_{12}\text{PO}_4/\text{water}$  at variable concentrations and temperatures.

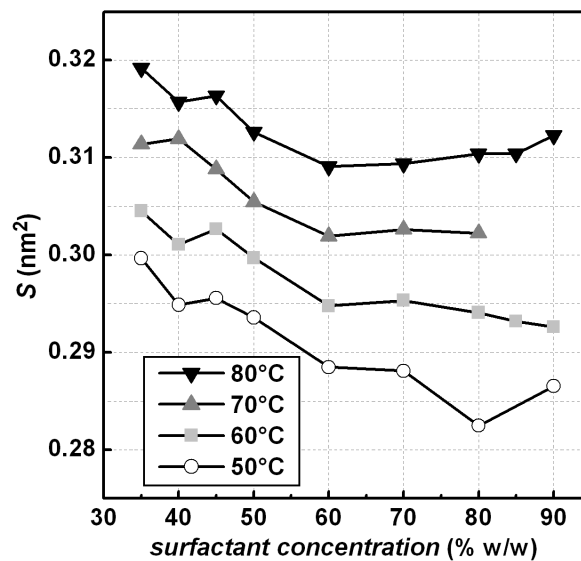


**Figure 7-7.** Average surface area  $S$  of the hydrophilic head groups of the surfactant in the system  $C_{12}\text{PO}_4/\text{water}$  at variable concentrations and temperatures.

### 7.3. Conclusions

The system *n*-dodecyl phosphate / water shows a lyotropic behaviour over the entire range of surfactant concentration studied. No lyotropic phase other than of lamellar

symmetry was found. The geometric parameters of the lamellar phase (surfactant bilayer thickness, hydrophilic head group surface area) are correlated with the surfactant concentration. Some irregularities in the behaviour were detected for surfactant concentrations below 35 % w/w; in these cases de-mixing of the components was observed.

## 8. Summary

The utilisation of self-assembled supramolecular arrays of organic amphiphiles as structure-directing species has become a widely explored synthesis method for nanoscopically structured materials, among them mesoporous (or mesostructured) aluminium phosphates. In the light of the significance of their microporous analogues (crystalline 'AlPO<sub>4</sub>-*n*', and related materials, with uniform pore diameters below 1 nm), particularly in the field of size-selective heterogeneous catalysis, there is an obvious demand for larger pores with an equally regular arrangement. Mesoporous aluminium phosphates exhibit uniform pore diameters between 2 and 4 nm; they are structured on the nanometer scale, but not crystalline. Their synthesis is generally quite complex; mutual interactions between the reactants and the (self-assembling) structure-directing species characterise a system which is rather difficult to control. This becomes apparent from the fact that the stoichiometric composition of the products often quite dramatically differs from the desired Al/P = 1 ratio. In a conventional synthesis phosphoric acid, H<sub>3</sub>PO<sub>4</sub>, and aluminium triisopropylate, Al(O<sup>*i*</sup>Pr)<sub>3</sub>, (or an aluminium oxide species) are used as the reactants. Porous, *i.e.* non-lamellar, aluminium phosphates have so far been prepared only by utilisation of cationic ammonium surfactants.

In this work several new preparations of mesostructured and mesoporous aluminium phosphates are introduced; the main objective is to develop strategies to decrease the complexity of the synthesis systems in order to gain a better control over the reactions. For this purpose various distinct concepts are pursued and, where possible, combined with each other. These include the choice of a new surfactant (anionic *n*-dodecyl phosphate), alcoholic (in stead of aqueous) conditions, and the utilisation of a single-source molecular precursor.

*n*-Dodecyl phosphate is used as the structure-directing species in aqueous and alcoholic synthesis. Under the appropriate synthesis conditions the phosphate head group of this surfactant may serve as the phosphorous source for the inorganic network, replacing the free phosphate ion usually employed as a reactant. For the first

time the surfactant plays the role of both the structure-director and a reactant; the complexity of the synthesis system is diminished. The incorporation of the surfactant head group into the inorganic network (when no free phosphate ions are offered as a phosphorous source) is confirmed by powder X-ray diffraction, thermal analysis, solid-state  $^{27}\text{Al}$  and  $^{31}\text{P}$  MAS NMR, and X-ray absorption spectroscopy. (Chapter 3)

Another means to improve the controllability of the synthesis is the employment of alcoholic, instead of aqueous, reaction conditions. This leads to considerably slower kinetics, which allows for a better handling and understanding of the reactions. Alcoholic conditions also provide the opportunity to prepare non-lamellar mesostructured aluminium phosphates by utilisation of amphiphiles other than cationic ammonium surfactants for the first time.

Depending on the reaction temperature and duration, utilisation of *n*-dodecyl phosphate under alcoholic conditions leads to the (simultaneous) formation of two distinct mesostructured phases: A lamellar phase is favoured at high temperatures (above *ca.* 60 °C) and/or long synthesis times (approximately more than 12 hours), whereas a phase with a hexagonal symmetry is predominant for lower temperatures and/or shorter duration of the reaction. *In-situ* small angle X-ray diffraction studies reveal that the hexagonal phase can be regarded as an intermediate which transforms into the lamellar phase in the course of the reaction; this phase transformation is accelerated at higher temperatures. Characterisation of the hexagonal phase indicates that the surfactant molecules are arranged in an inverted fashion, *i.e.* they are ordered in hexagonally arranged rod-like assemblies with their head groups turned inwards, encapsulating the inorganic part in the centers of the rods. Such an inverted structure has not been observed before among mesostructured materials; in the usual hexagonal arrangement the head groups are always turned outwards. (Chapter 4)

Utilisation of primary long-chain alkyl amines as structure-directing species under alcoholic conditions yields mesostructured aluminium phosphates with randomly ordered tubular surfactant arrangement. After a post-synthetic treatment in vapour these materials are stable enough to maintain their structure upon removal of the surfactant by acidic solvent extraction; this leads to mesoporous materials with specific surface areas up to *ca.* 600 m<sup>2</sup>/g. The alcoholic synthesis systems are not completely free of water; low, controlled amounts of water turn out to be essential for

the reactions. All surfactants used do not show any lyotropic behaviour with alcohols; it is only after the addition of the inorganic reactants that the mesostructures are formed. Thus, the alcoholic syntheses follow a highly co-operative mechanism. (Chapter 5)

The combination of alcoholic conditions with the utilisation of primary long-chain alkyl amines as structure-directing species provides the opportunity to use a soluble single-source molecular precursor for the synthesis of mesoporous aluminium phosphates, replacing the separate sources of aluminium and phosphorous. The core unit of the precursor consists of a cube-like arrangement of alternating aluminium and phosphorous atoms connected with each other by oxygen bridges. This unit remains intact during the synthesis of the mesostructured aluminium phosphate material, thus serving as a building block for the inorganic matrix. A strict molar ratio of Al/P = 1/1 is found by elemental analysis in all products. This is the first rational synthesis of mesoporous aluminium phosphates with such a well-defined Al/P stoichiometry. (Chapter 6)

Finally, the phase behaviour of the lyotropic system *n*-dodecyl phosphate / water is studied by temperature-resolved small angle X-ray diffraction. The aim of this study is to predict possible symmetries of mesostructured materials prepared with this surfactant as a structure-director under aqueous conditions. However, over the entire concentration and temperature range studied no phases other than lamellar are observed. (Chapter 7)

## 9. Zusammenfassung (German Summary)

Die Verwendung selbstanordnender supramolekularer Aggregate organischer Amphiphile ist eine mittlerweile weit verbreitete Synthesemethode für nanoskopisch strukturierte Materialien. Hierzu zählen auch die mesoporösen (oder mesostrukturierten) Aluminiumphosphate. Angesichts der großen Bedeutung ihrer mikroporösen Analoga (der kristallinen "AlPO<sub>4</sub>-*n*" und verwandter Materialien mit Porendurchmessern unterhalb 1 nm), insbesondere im Bereich der heterogenen Katalyse, besteht ein offensichtliches Interesse an größeren Poren in vergleichbar regelmäßiger Anordnung. Mesoporöse Aluminiumphosphate weisen einheitliche Porendurchmesser zwischen 2 und 4 nm auf. Trotz ihrer periodischen Struktur auf der Skala einiger weniger Nanometer sind sie nicht kristallin. Ihre Synthese ist komplexer Natur und aufgrund der zahlreichen Wechselwirkungen zwischen den Reaktanden und der (selbstanordnenden) strukturdirigierenden Spezies verhältnismäßig schwer zu kontrollieren. Dies wird deutlich aus dem Umstand, daß die stöchiometrische Zusammensetzung der Produkte oftmals recht drastisch von dem gewünschten Verhältnis Al/P = 1 abweicht. In einer herkömmlichen Synthese werden Aluminiumtriisopropylat (Al[<sup>*i*</sup>OPr]<sub>3</sub>) oder eine Aluminiumoxid-Spezies mit Phosphorsäure (H<sub>3</sub>PO<sub>4</sub>) umgesetzt. Poröse (d.h. nichtlamellare) Aluminiumphosphate konnten bislang nur unter Verwendung kationischer Ammoniumtenside hergestellt werden.

In dieser Arbeit werden verschiedene neue Synthesen mesostrukturierter und mesoporöser Aluminiumphosphate vorgestellt; Hauptanliegen ist dabei die Entwicklung von Strategien, die Komplexität der Synthesysteme herabzusetzen, um eine bessere Kontrolle über die Reaktionen zu erlangen. Zu diesem Zweck werden unterschiedliche Konzepte verfolgt und, sofern möglich, miteinander kombiniert. Dazu gehören die Wahl eines neuen Tensids (anionisches *n*-Dodecylphosphat), alkoholische (anstelle von wäßrigen) Bedingungen, sowie die Verwendung einer molekularen sogenannten *single-source*-Vorstufe.

*n*-Dodecylphosphat wird als strukturdirigierende Spezies sowohl in wäßriger als auch in alkoholischer Synthese verwendet. Unter geeigneten Bedingungen kann die Phosphat-Kopfgruppe dieses Tensids als Phosphorquelle für das anorganische Netzwerk fungieren und somit das freie Phosphat-Ion ersetzen, welches normalerweise als Reaktand eingesetzt wird. Auf diese Weise spielt das Tensid erstmals die Rolle sowohl eines Strukturleiters als auch eines Reaktanden; die Komplexität des Systems wird dadurch herabgesetzt. Der Einbau der Tensid-Kopfgruppe in das anorganische Netzwerk (wenn keine freien Phosphat-Ionen als Phosphorquelle zu Verfügung stehen) wird bestätigt durch Pulver-Röntgenbeugung, thermische Analyse, Festkörper-MAS-NMR-Spektroskopie ( $^{27}\text{Al}$  und  $^{31}\text{P}$ ) und Röntgenabsorptionsspektroskopie. (Kapitel 3)

Eine andere Methode, die Kontrolle über die Synthese zu verbessern, ist die Verwendung alkoholischer anstelle von wäßrigen Reaktionsbedingungen. Dies führt zu einer erheblich langsameren Kinetik, was eine leichtere Handhabung sowie ein besseres Verständnis der Reaktionen ermöglicht. Außerdem bieten alkoholische Bedingungen erstmals die Möglichkeit, nichtlamellare mesostrukturierte Aluminiumphosphate unter Verwendung nichtkationischer Tenside herzustellen.

Abhängig von der Reaktionstemperatur und -zeit führt die Verwendung von *n*-Dodecylphosphat unter alkoholischen Bedingungen zur (gleichzeitigen) Ausbildung zweier verschiedener mesostrukturierter Phasen: Eine lamellare Phase wird bevorzugt bei hohen Temperaturen (oberhalb ca. 60 °C) und/oder langen Synthesenzeiten (über etwa 12 Stunden) gebildet, wogegen eine Phase mit hexagonaler Symmetrie bei tieferen Temperaturen und/oder kürzerer Reaktionsdauer dominiert. Wie in-situ-Untersuchungen durch Kleinwinkel-Röntgenbeugung zeigen, kann die hexagonale Phase als Intermediat betrachtet werden, welches sich im Laufe der Reaktion in die lamellare Phase umwandelt; diese Phasentransformation wird durch erhöhte Temperatur beschleunigt. Die Charakterisierung der hexagonalen Phase zeigt, daß die Tensidmoleküle in einer invertierten Form vorliegen, d.h. in hexagonal geordneten stäbchenförmigen Anordnungen, bei denen die Kopfgruppen nach innen gewandt sind, so daß der anorganische Teil in den Zentren der Stäbchen eingeschlossen ist. Solch eine invertierte Struktur ist bei mesostrukturierten Materialien zuvor noch nicht

beobachtet worden; in der normalen hexagonalen Anordnung zeigen die Kopfgruppen immer nach außen. (Kapitel 4)

Die Verwendung primärer langkettiger Alkylamine als Strukturdirigenten unter alkoholischen Bedingungen führt zu mesostrukturierten Aluminiumphosphaten mit ungleichmäßig geordneten tubulären Tensidanordnungen. Nach einer post-synthetischen Behandlung mit Wasserdampf weisen diese Materialien eine hinreichend große Stabilität auf, um ihre Struktur nach Entfernen des Tensids durch saure Extraktion beizubehalten; dies führt zu mesoporösen Materialien mit spezifischen Oberflächen bis zu ca.  $600 \text{ m}^2/\text{g}$ . Die alkoholischen Synthesen verlaufen nicht unter vollkommen wasserfreien Bedingungen; geringe, kontrollierte Mengen Wasser erweisen sich als erforderlich für die Reaktionen. Alle verwendeten Tenside zeigen kein lyotropes Verhalten mit Alkoholen; Mesostrukturen bilden sich erst nach Hinzufügen der anorganischen Reaktanden aus. Die alkoholischen Synthesen folgen also hoch kooperativen Mechanismen. (Kapitel 5)

Die Kombination alkoholischer Synthesebedingungen mit der Verwendung primärer langkettiger Alkylamine bietet die Möglichkeit, für die Synthese mesoporöser Aluminiumphosphate eine lösliche molekulare *single-source*-Vorstufe einzusetzen, welche die sonst üblichen separaten Quellen für Aluminium und Phosphor ersetzt. Die Grundeinheit der Vorstufe besteht aus einer würfelförmigen Anordnung alternierender Aluminium- und Phosphoratome, die über Sauerstoffbrücken verknüpft sind. Diese Einheit bleibt intakt bei der Synthese des mesostrukturierten Aluminiumphosphats und fungiert somit als ein Baustein für die anorganische Matrix. In allen Produkten findet sich ein striktes molares Verhältnis von  $\text{Al/P} = 1/1$ . Dies ist die erste systematische Synthese mesoporöser Aluminiumphosphate mit einer derart wohldefinierten Al/P-Stöchiometrie. (Kapitel 6)

Desweiteren wird das Phasenverhalten des lyotropen Systems *n*-Dodecylphosphat / Wasser durch temperaturlöste Kleinwinkel-Röntgenbeugung untersucht. Ziel dieser Studie ist eine Voraussage hinsichtlich möglicher Symmetrien mesostrukturierter Materialien, die mit diesem Tensid als Strukturdirektor unter wässrigen Bedingungen hergestellt werden. Über den gesamten untersuchten Konzentrations- und Temperaturbereich wird jedoch keine nichtlamellare Phase beobachtet. (Kapitel 7)

## 10. References

- [1] C. T. Kresge, M. E. Leonowicz, W. J. Roth, J. C. Vartuli, J. S. Beck, *Nature* **1992**, 359, 710-712.
- [2] J. S. Beck, J. C. Vartuli, W. J. Roth, M. E. Leonowicz, C. T. Kresge, K. D. Schmitt, C. T.-W. Chu, D. H. Olson, E. W. Sheppard, S. B. McCullen, J. B. Higgins, J. L. Schlenker, *J. Am. Chem. Soc.* **1992**, 114, 10834-10843.
- [3] K. S. W. Sing, D. H. Everett, R. A. W. Haul, L. Moscou, R. A. Pierotti, J. Rouquérol, T. Siemieniewska, *Pure Appl. Chem.* **1985**, 57, 603-619.
- [4] Q. Huo, D. I. Margolese, U. Ciesla, P. Feng, T. E. Gier, P. Sieger, R. Leon, P. M. Petroff, F. Schüth, G. Stucky, *Nature* **1994**, 368, 317-321.
- [5] Q. Huo, R. Leon, P. M. Petroff, G. D. Stucky, *Science* **1995**, 268, 1324-1327.
- [6] Q. Huo, D. I. Margolese, G. D. Stucky, *Chem. Mater.* **1996**, 8, 1147-1160.
- [7] D. Zhao, Q. Huo, J. Feng, J. Kim, Y. Han, G. D. Stucky, *Chem. Mater.* **1999**, 11, 2668-2672.
- [8] S. A. Bagshaw, E. Prouzet, T. J. Pinnavaia, *Science* **1995**, 269, 1242-1244.
- [9] P. T. Tanev, T. J. Pinnavaia, *Science* **1995**, 267, 865-867.
- [10] R. Ryoo, J. M. Kim, C. H. Ko, C. H. Shin, *J. Phys. Chem.* **1996**, 100, 17718-17721.
- [11] P. Behrens, A. Glaue, C. Haggemüller, G. Schechner, *Solid State Ionics* **1997**, 101-103, 255-260.
- [12] T. Wärnheim, A. Jönsson, *J. Colloid Interface Sci.* **1988**, 125, 627-633.
- [13] X. Auvray, C. Pepitas, R. Anthore, I. Rico, A. Lattes, *J. Phys. Chem.* **1989**, 93, 7458-7464.
- [14] Q. Huo, D. I. Margolese, U. Ciesla, D. G. Demuth, P. Feng, T. E. Gier, P. Sieger, A. Firouzi, B. F. Chmelka, F. Schüth, G. D. Stucky, *Chem. Mater.* **1994**, 6, 1176-1191.
- [15] D. M. Antonelli, J. Y. Ying, *Angew. Chem. Int. Ed.* **1995**, 34, 2014-2017.
- [16] P. Behrens, *Angew. Chem. Int. Ed.* **1996**, 35, 515-518.

- [17] U. Ciesla, S. Schacht, G. D. Stucky, K. K. Unger, F. Schüth, *Angew. Chem. Int. Ed.* **1996**, *35*, 541-543.
- [18] D. M. Antonelli, J. Y. Ying, *Angew. Chem. Int. Ed.* **1996**, *35*, 426-430.
- [19] D. M. Antonelli, A. Nakahira, J. Y. Ying, *Inorg. Chem.* **1996**, *35*, 3126-3136.
- [20] M. Fröba, O. Muth, A. Reller, *Solid State Ionics* **1997**, *101-103*, 249-253.
- [21] Z.-R. Tian, W. Tong, J.-Y. Wang, N.-G. Duan, V. V. Krishnan, S. L. Suib, *Science* **1997**, *276*, 926-930.
- [22] M. S. Wong, J. Y. Ying, *Chem. Mater.* **1998**, *10*, 2067-2077.
- [23] M. Fröba, O. Muth, *Adv. Mater.* **1999**, *11*, 564-567.
- [24] U. Ciesla, M. Fröba, G. Stucky, F. Schüth, *Chem. Mater.* **1999**, *11*, 227-234.
- [25] P. V. Braun, P. Osenar, S. I. Stupp, *Nature* **1996**, *380*, 325-328.
- [26] M. Fröba, N. Oberender, *Chem. Commun.* **1997**, 1729-1730.
- [27] S. Neeraj, C. N. R. Rao, *J. Mater. Chem.* **1998**, *8*, 279-280.
- [28] M. J. MacLachlan, N. Coombs, G. A. Ozin, *Nature* **1999**, *397*, 681-684.
- [29] M. J. MacLachlan, N. Coombs, R. L. Bedard, S. White, L. K. Thompson, G. A. Ozin, *J. Am. Chem. Soc.* **1999**, *121*, 12005-12017.
- [30] L. Chen, P. J. Klar, W. Heimbrod, N. Oberender, D. Kempe, M. Fröba, *Appl. Phys. Lett.* **2000**, *77*, 3965-3967.
- [31] M. Wachhold, K. K. Rangan, S. J. L. Billinge, V. Petkov, J. Heising, M. G. Kanatzidis, *Adv. Mater.* **2000**, *12*, 85-91.
- [32] M. Wachhold, K. K. Rangan, M. Lei, M. F. Thorpe, S. J. L. Billinge, V. Petkov, J. Heising, M. G. Kanatzidis, *J. Solid State Chem.* **2000**, *152*, 21-36.
- [33] A. Sayari, *Chem. Mater.* **1996**, *8*, 1840-1852.
- [34] P. Behrens, *Angew. Chem. Int. Ed.* **1996**, *35*, 515-518.
- [35] X. S. Zhao, G. Q. Lu, G. J. Millar, *Ind. Eng. Chem. Res.* **1996**, *35*, 2075-2090.
- [36] A. Sayari, P. Liu, *Microporous Mater.* **1997**, *12*, 149-177.
- [37] K. Moller, T. Bein, *Chem. Mater.* **1998**, *10*, 2950-2963.
- [38] M. Lindén, S. Schacht, F. Schüth, A. Steel, K. K. Unger, *J. Porous Mater.* **1998**, *5*, 177-193.
- [39] U. Ciesla, F. Schüth, *Microporous Mesoporous Mater.* **1999**, *27*, 131-149.
- [40] J. Y. Ying, C. P. Mehnert, M. S. Wong, *Angew. Chem. Int. Ed.* **1999**, *38*, 56-77.
- [41] G. S. Attard, J. C. Glyde, C. G. Göltner, *Nature* **1995**, *378*, 366-368.

- [42] C. G. Göltner, M. Antonietti, *Adv. Mater.* **1997**, *9*, 431-436.
- [43] A. Monnier, F. Schüth, Q. Huo, D. Kumar, D. Margolese, R. S. Maxwell, G. D. Stucky, M. Krishnamurty, P. Petroff, A. Firouzi, M. Janicke, B. F. Chmelka, *Science* **1993**, *261*, 1299-1303.
- [44] J. S. Beck, J. C. Vartuli, G. J. Kennedy, C. T. Kresge, W. J. Roth, S. E. Schramm, *Chem. Mater.* **1994**, *6*, 1816-1821.
- [45] P. T. Tanev, T. J. Pinnavaia, *Chem. Mater.* **1996**, *8*, 2068-2079.
- [46] C. J. Glinka, J. M. Nicol, G. D. Stucky, E. Ramli, D. Margolese, Q. Huo, J. B. Higgins, M. E. Leonowicz, *J. Porous Mater.* **1996**, *3*, 93-98.
- [47] A. Firouzi, D. Kumar, L. M. Bull, T. Besier, P. Sieger, Q. Huo, S. A. Walker, J. A. Zasadzinski, C. Glinka, J. Nicol, D. Margolese, G. D. Stucky, B. F. Chmelka, *Science* **1995**, *267*, 1138-1143.
- [48] A. Firouzi, F. Atef, A. G. Oertli, G. D. Stucky, B. F. Chmelka, *J. Am. Chem. Soc.* **1997**, *119*, 3596-3610.
- [49] J. Rathouský, G. Schulz-Ekloff, J. Had, A. Zukal, *Phys. Chem. Chem. Phys.* **1999**, *1*, 3053-3057.
- [50] S. O'Brien, R. J. Francis, S. J. Price, D. O'Hare, S. M. Clark, N. Okazaki, K. Kuroda, *J. Chem. Soc., Chem. Commun.* **1995**, 2423-2425.
- [51] S. O'Brien, R. J. Francis, A. Fogg, D. O'Hare, N. Okazaki, K. Kuroda, *Chem. Mater.* **1999**, *11*, 1822-1832.
- [52] D. C. Calabro, E. W. Valyocsik, F. X. Ryan, *Microporous Mater.* **1996**, *7*, 243-259.
- [53] O. Regev, *Langmuir* **1996**, *12*, 4940-4944.
- [54] S. Pevzner, O. Regev, *Microporous Mesoporous Mater.* **2000**, *38*, 413-421.
- [55] J. Zhang, Z. Luz, D. Goldfarb, *J. Phys. Chem. B* **1997**, *101*, 7087-7094.
- [56] A. Galarneau, F. Di Renzo, F. Fajula, L. Mollo, B. Fubini, M. F. Ottaviani, *J. Colloid Interface Sci.* **1998**, *201*, 105-117.
- [57] M. Lindén, S. A. Schunk, F. Schüth, *Angew. Chem. Int. Ed.* **1998**, *37*, 821-823.
- [58] P. Ågren, M. Lindén, J. B. Rosenholm, R. Schwarzenbacher, M. Kriechbaum, H. Amenitsch, P. Laggner, J. Blanchard, F. Schüth, *J. Phys. Chem. B* **1999**, *103*, 5943-5948.

- [59] M. Lindén, J. Blanchard, S. Schacht, S. A. Schunk, F. Schüth, *Chem. Mater.* **1999**, *11*, 3002-3008.
- [60] M. Lindén, P. Ågren, S. Karlsson, *Langmuir* **2000**, *16*, 5831-5836.
- [61] P. Ågren, M. Lindén, J. B. Rosenholm, *Langmuir* **2000**, *16*, 8809-8813.
- [62] M. Birot, J.-P. Pillot, J. Dunogues, *Chem. Rev.* **1995**, *95*, 1443-1471.
- [63] J. Bill, F. Aldinger, *Adv. Mater.* **1995**, *7*, 775-783.
- [64] H.-P. Baldus, M. Jansen, *Angew. Chem. Int. Ed.* **1997**, *36*, 328-338.
- [65] R. J. P. Corriu, *Eur. J. Inorg. Chem.* **2001**, 1109-1121.
- [66] C. A. Fyfe, G. Fu, *J. Am. Chem. Soc.* **1995**, *117*, 9709-9714.
- [67] G. Fu, C. A. Fyfe, W. Schwieger, G. T. Kokotailo, *Angew. Chem. Int. Ed.* **1995**, *34*, 1499-1502.
- [68] B. T. Holland, P. K. Isbester, C. F. Blanford, E. J. Munson, A. Stein, *J. Am. Chem. Soc.* **1997**, *119*, 6796-6803.
- [69] B. T. Holland, P. K. Isbester, E. J. Munson, A. Stein, *Mater. Res. Bull.* **1999**, *34*, 471-482.
- [70] S. T. Wilson, B. M. Lok, C. A. Messina, T. R. Cannan, E. M. Flanigen, *J. Am. Chem. Soc.* **1982**, *104*, 1146-1147.
- [71] B. M. Lok, C. A. Messina, R. L. Patton, R. T. Gajek, T. R. Cannan, E. M. Flanigen, *J. Am. Chem. Soc.* **1984**, *106*, 6092-6093.
- [72] M. Hartmann, L. Kevan, *Chem. Rev.* **1999**, *99*, 635-663.
- [73] S. Oliver, A. Kuperman, N. Coombs, A. Lough, G. A. Ozin, *Nature* **1995**, *378*, 47-50.
- [74] S. Oliver, N. Coombs, G. A. Ozin, *Adv. Mater.* **1995**, *7*, 931-935.
- [75] G. A. Ozin, S. Oliver, *Adv. Mater.* **1995**, *7*, 943-947.
- [76] G. A. Ozin, *Acc. Chem. Res.* **1997**, *30*, 17-27.
- [77] A. Sayari, V. R. Karra, J. S. Reddy, I. L. Moudrakovski, *Chem. Commun.* **1996**, 411-412.
- [78] A. Sayari, I. Moudrakovski, J. S. Reddy, C. I. Ratcliffe, J. A. Ripmeester, K. F. Preston, *Chem. Mater.* **1996**, *8*, 2080-2088.
- [79] A. Chenite; Y. Le Page, V. R. Karra, A. Sayari, *Chem. Commun.* **1996**, 413-414.
- [80] Q. Gao, R. Xu, J. Chen, R. Li, S. Li, S. Qui, Y. Yue, *J. Chem. Soc., Dalton Trans.* **1996**, 3303-3307.

- [81] Q. Gao, J. Chen, R. Xu, Y. Yue, *Chem. Mater.* **1997**, *9*, 457-462.
- [82] Y. Z. Khimiyak, J. Klinowski, *J. Chem. Soc., Faraday Trans.* **1998**, *94*, 2241-2247.
- [83] Y. Z. Khimiyak, J. Klinowski, *Chem. Mater.* **1998**, *19*, 2258-2265.
- [84] Y. Z. Khimiyak, J. Klinowski, *Phys. Chem. Chem. Phys.* **2000**, *2*, 5275-5285.
- [85] T. Kimura, Y. Sugahara, K. Kuroda, *Phosphorus Res. Bull.* **1996**, *6*, 205-208.
- [86] T. Kimura, Y. Sugahara, K. Kuroda, *Chem. Mater.* **1999**, *11*, 508-518.
- [87] C. Pophal, R. Schnell, H. Fuess, *Stud. Surf. Sci. Catal.* **1997**, *105*, 101-108.
- [88] J. O. Perez O., B. B. Borade, A. Clearfield, *J. Mol. Struct.* **1998**, *470*, 221-228.
- [89] M. Eswaramoorthy, S. Neeraj, C. N. R. Rao, *Microporous Mesoporous Mater.* **1999**, *28*, 205-210.
- [90] B. Kraushaar-Czarnetzki, W. H. J. Stork, R. J. Dogterom, *Inorg. Chem.* **1993**, *32*, 5029-5033.
- [91] P. Feng, X. Bu, G. D. Stucky, *Inorg. Chem.* **2000**, *39*, 2-3.
- [92] S. Cheng, J.-N. Tzeng, B.-Y. Hsu, *Chem. Mater.* **1997**, *9*, 1788-1796.
- [93] P. Feng, Y. Xia, J. Feng, X. Bu, G. D. Stucky, *Chem. Commun.* **1997**, 949-950.
- [94] D. Zhao, Z. Luan, L. Kevan, *Chem. Commun.* **1997**, 1009-1010.
- [95] Z. Luan, D. Zhao, H. He, J. Klinowski, L. Kevan, *J. Phys. Chem. B* **1998**, *102*, 1250-1259.
- [96] D. Zhao, Z. Luan, L. Kevan, *J. Phys. Chem. B* **1997**, *101*, 6943-6948.
- [97] Z. Luan, D. Zhao, L. Kevan, *Microporous Mesoporous Mater.* **1998**, *20*, 93-99.
- [98] Z. Luan, D. Zhao, H. He, J. Klinowski, L. Kevan, *Stud. Surf. Sci. Catal.* **1998**, *117*, 103-110.
- [99] T. Kimura, Y. Sugahara, K. Kuroda, *Chem. Lett.* **1997**, 983-984.
- [100] T. Kimura, Y. Sugahara, K. Kuroda, *Chem. Commun.* **1998**, 559-560.
- [101] T. Kimura, Y. Sugahara, K. Kuroda, *Microporous Mesoporous Mater.* **1998**, *22*, 115-126.
- [102] B. Chakraborty, A. C. Pulikottil, S. Das, B. Viswanathan, *Chem. Commun.* **1997**, 911-912.
- [103] B. Chakraborty, A. C. Pulikottil, B. Viswanathan, *Appl. Catal. A* **1998**, *167*, 173-181.

- [104] D. A. Kron, B. T. Holland, R. Wipson, C. Maleke, A. Stein, *Langmuir* **1999**, *15*, 8300-8308.
- [105] S. Cabrera, J. E. Haskouri, C. Guillem, A. Beltrán-Porter, D. Beltrán-Porter, S. Mendioroz, M. D. Marcos, P. Amorós, *Chem. Commun.* **1999**, 333-334.
- [106] M. P. Kapoor, A. Raj, *Appl. Catal. A* **2000**, *203*, 311-319.
- [107] H. Tanaka, M. Chikazawa, *J. Mater. Chem.* **1999**, *9*, 2923-2927.
- [108] H. Tanaka, M. Chikazawa, *Mater. Res. Bull.* **2000**, *35*, 75-84.
- [109] J. E. Cassidy, J. A. J. Jarvis, R. N. Rothon, *J. Chem. Soc., Dalton Trans.* **1975**, 1497-1499.
- [110] K. S. W. Sing, D. H. Everett, R. A. W. Haul, L. Moscou, R. A. Pierotti, J. Rouquérol, T. Siemieniowska, *Pure Appl. Chem.* **1985**, *57*, 603-619.
- [111] E. P. Barrett, L. G. Joyner, P. P. Halenda, *J. Am. Chem. Soc.* **1951**, *73*, 373-380.
- [112] J. Wong, G. Shimkaveg, W. Goldstein, M. Eckart, T. Tanaka, Z. U. Rek, H. Tompkins, *Nucl. Instr. and Meth. in Phys. Res. A* **1990**, *291*, 243-249.
- [113] J. Wong, T. Tanaka, M. Rowen, F. Schäfers, B. R. Müller, Z. U. Rek, *J. Synchrotron Rad.* **1999**, *6*, 1086-1095.
- [114] T. Ressler, *J. Synchrotron Rad.* **1998**, *5*, 118-122.
- [115] A. Gabriel, *Rev. Sci. Instrum.* **1977**, *48*, 1303-1305.
- [116] C. Boulin, R. Kempf, M. H. J. Koch, S. M. McLaughlin, *Nucl. Instr. and Meth. in Phys. Res. A* **1986**, *249*, 399-407.
- [117] T. C. Huang, H. Toraya, T. N. Blanton, Y. Wu, *J. Appl. Crystallogr.* **1993**, *26*, 180-184.
- [118] L. Frydman, J. S. Harwood, *J. Am. Chem. Soc.* **1995**, *117*, 5367-5368.
- [119] J. P. Amoureux, *Solid State NMR* **1996**, *6*, 73-83.
- [120] A.-R. Massiot, A. Kretschner, V. C. Cajipe, *Magn. Reson. Chem.* **1997**, *35*, 86.
- [121] C. S. Blackwell, R. L. Patton, *J. Phys. Chem.* **1984**, *88*, 6135-6239.
- [122] M. E. Davis, C. Montes, P. E. Hathaway, J. P. Arhancet, D. L. Hasha, J. M. Garces, *J. Am. Chem. Soc.* **1989**, *111*, 3919-3924.
- [123] J. J. Fitzgerald, G. Piedra, S. F. Dec, M. Seger, G. E. Maciel, *J. Am. Chem. Soc.* **1997**, *119*, 7832-7842.
- [124] M. Fröba, J. Wong, M. Rowen, G. E. Brown Jr., T. Tanaka, Z. Rek, *Physica B* **1995**, *208&209*, 555-556.

- [125] J. M. Bennet, J. W. Richardson, J. J. Pluth, J. V. Smith, *Zeolites* **1987**, 7, 160-162.
- [126] A. Savitzky, M. J. E. Golay, *Anal. Chem.* **1964**, 36, 1627-1639.
- [127] M. Yada, M. Machida, T. Kijima, *Chem. Commun.* **1996**, 769-770.
- [128] M. Yada, H. Takenaka, M. Machida, T. Kijima, *J. Chem. Soc., Dalton Trans.* **1998**, 1547-1550.
- [129] V. F. Stone, R. Davis, *J. Chem. Mater.* **1998**, 10, 1468-1474.
- [130] S. S. Funari, *Eur. Biophys. J.* **1998**, 27, 590-594.
- [131] S. Oliver, A. Kuperman, G. A. Ozin, *Angew. Chem. Int. Ed.* **1998**, 37, 46-62.
- [132] Y. Long, T. Xu, Y. Sun, W. Dong, *Langmuir* **1998**, 14, 6173-6178.
- [133] C. G. Sonwane, S. K. Bhatia, *Langmuir* **1999**, 15, 2809-2816.
- [134] Y. Yang, H.-G. Schmidt, M. Noltemeyer, J. Pinkas, H. W. Roesky, *J. Chem. Soc., Dalton Trans.* **1996**, 3609-3610.
- [135] Y. Yang, M. G. Walawalkar, J. Pinkas, H. W. Roesky, H.-G. Schmidt, *Angew. Chem. Int. Ed.* **1998**, 37, 96-98.
- [136] J. Pinkas, H. Wessel, Y. Yang, M. L. Montero, M. Noltemeyer, M. Fröba, H. W. Roesky, *Inorg. Chem.* **1998**, 37, 2450-2457.
- [137] J. Pinkas, D. Chakraborty, Y. Yang, R. Murugavel, M. Noltemeyer, H. W. Roesky, *Organometallics* **1999**, 18, 523-528.
- [138] M. G. Walawalkar, H. W. Roesky, R. Murugavel, *Acc. Chem. Res.* **1999**, 32, 117-126.
- [139] M. R. Mason, R. M. Matthews, M. S. Mashuta, J. F. Richardson, *Inorg. Chem.* **1996**, 35, 5756-5757.
- [140] E. Prouzet, T. J. Pinnavaia, *Angew. Chem. Int. Ed.* **1997**, 36, 516-518.
- [141] R. L. Putnam, N. Nakagawa, K. M. McGrath, N. Yao, I. A. Aksay, S. M. Gruner, A. Navrotsky, *Chem. Mater.* **1997**, 9, 2690-2693.
- [142] G. A. Ozin, N. Varaksa, N. Coombs, J. E. Davies, D. D. Perovic, M. Ziliox, *J. Mater. Chem.* **1997**, 7, 1601-1607.
- [143] K. M. McGrath, *Langmuir* 1995, 11, 1835-1840.
- [144] D. J. Mitchell, G. J. T. Tiddy, L. Waring, T. Bostock, M. P. McDonald, *J. Chem. Soc., Faraday Trans.* **1993**, 79, 975-1000.

- [145] S. S. Funari, M. C. Holmes, G. J. T. Tiddy, *J. Phys. Chem.* **1994**, *98*, 3015-3023.
- [146] S. S. Funari, M. C. Holmes, G. J. T. Tiddy, *J. Phys. Chem.* **1992**, *96*, 11029-11038.
- [147] S. S. Funari, G. Rapp, *J. Phys. Chem. B* **1997**, *101*, 732-739.
- [148] V. Luzzati, in *Biological Membranes* (D. Chapman, Ed.), p. 71, Academic Press, London, 1968.
- [149] P. E. Chaplanov, N. A. Toporkova, T. A. Moiseeva, *J. Appl. Chem. USSR, Engl. Trans.* **1988**, *61*, 169-171.
- [150] D. R. Lide (Ed.), *Handbook of Chemistry and Physics*, 78th Edition, CRC Press, Boca Raton, 1997.



## Thanks

I would like to thank:

- Prof. Dr. Michael Fröba for the opportunity to work on this thesis with great freedom of decision and for the continuous and excellent supervision
- Felix Brieler, Daniela Kempe, Ralf Köhn, Dr. Olaf Muth, Nadine Oberender, and Uta Sazama for making me feel at home in the lab
- Marcus Schulz and Prof. Dr. Christian Jäger at *Friedrich-Schiller-Universität Jena* for recording and helpful discussion of the NMR data
- Dr. Sérgio S. Funari and Dr. Gert Rapp at *Hamburger Synchrotronstrahlungslabor (HASYLAB)* for their help at the synchrotron (SAXS) beamlines and valuable discussion of the data
- Jeff Moore at *Stanford Synchrotron Radiation Laboratory (SSRL)* and Rogério J. Prado, Dr. Anne-Marie Flank, and Dr. Pierre Lagarde at *Laboratoire pour l'Utilisation du Rayonnement Électromagnétique (LURE)* for their help at the synchrotron (XAS) beamlines
- Dr. Stefan Ebbinghaus, Dr. Florian Ende, Heinz Graeske, Prof. Dr. Armin Reller, Berti Vogts, Dr. Joe Wong, Sigrid Zeckert
- My parents
- Elke

## List of Publications

### Peer-reviewed Papers

M. TIEMANN, M. FRÖBA, Mesoporous Aluminophosphates from a Single-source Precursor. **2001**, submitted.

M. TIEMANN, M. FRÖBA, *Short Review: Mesostructured Aluminophosphates Synthesised Utilizing Supramolecular Structure-Directors*, *Chem. Mater.* **2001**, in press.

M. TIEMANN, M. SCHULZ, C. JÄGER, M. FRÖBA, Mesoporous Aluminophosphate Molecular Sieves Synthesised under Non-aqueous Conditions. *Chem. Mater.* **2001**, in press.

M. SCHULZ, M. TIEMANN, M. FRÖBA, C. JÄGER, NMR Characterization of Mesostructured Aluminophosphates. *J. Phys. Chem. B* **2000**, *104*, 10473-10481.

M. TIEMANN, M. FRÖBA, G. RAPP, S. S. FUNARI, Non-aqueous Synthesis of Mesostructured Aluminophosphate / Surfactant Composites: Synthesis, Characterization, and *In-situ* SAXS Studies. *Chem. Mater.* **2000**, *12*, 1342-1348.

M. TIEMANN, M. FRÖBA, G. RAPP, S. S. FUNARI, *In-situ* small angle X-ray scattering (SAXS) studies on the formation of mesostructured aluminophosphate / surfactant composite materials. *Stud. Surf. Sci. Catal.* **2000**, *129*, 559-566.

M. FRÖBA, M. TIEMANN, A New Role of the Surfactant in the Synthesis of Mesostructured Phases: Dodecylphosphate as Template and Reactant for Aluminophosphates. *Chem. Mater.* **1998**, *10*, 3475-3483.

W. MEYER-KLAUCKE, T. GLASER, M. FRÖBA, M. TIEMANN, E. BILL, J. WONG, K. WIEGHARDT, A.X. TRAUTWEIN, Multiple K-edge XAS for the Structural Analysis of Thiophenolate Bridged Heteronuclear Complexes. *J. Synchrotron Rad.* **1998**, *6*, 397-399.

M. TIEMANN, M. FRÖBA, J. WONG, Synthesis and Al K-Edge XANES Investigation of Mesostructured Aluminophosphates. *Mat. Res. Soc. Symp. Proc.* **1998**, *547*, 87-92.

### Reports and Extended Abstracts

- M. TIEMANN, M. FRÖBA, Al K-edge XANES Investigation of Mesostructured Aluminophosphates. *Laboratoire pour l'Utilisation du Rayonnement Électromagnétique (LURE) Activity Report 2000*, in press.
- M. FRÖBA, G. SCHECHNER, M. TIEMANN, B. PILLEP, J. WONG, P. BEHRENS, Structural Order in Biomineralized Silica investigated by Si K XANES Spectroscopy. *Beih. z. Eur. J. Mineral.* **2000**, *12*, 52-53.
- M. TIEMANN, S. S. FUNARI, G. RAPP, M. FRÖBA, In-situ SAXS studies on the template-directed non-aqueous synthesis of mesostructured aluminophosphates. *Hamburger Synchrotronstrahlungslabor (HASYLAB) Annual Report 1999*, 703-704.
- M. TIEMANN, S. S. FUNARI, G. RAPP, M. FRÖBA, SAXS Studies on the System mono-Dodecyl Phosphate / Water. *Hamburger Synchrotronstrahlungslabor (HASYLAB) Annual Report 1998*, 173-174.
- M. TIEMANN, S. S. FUNARI, G. RAPP, M. FRÖBA, SAXS Studies on Aqueous Synthesis Mixtures for the Preparation of Mesostructured Aluminophosphates with Dodecyl Phosphate as Template. *Hamburger Synchrotronstrahlungslabor (HASYLAB) Annual Report 1998*, 175-176.
- M. TIEMANN, S. S. FUNARI, G. RAPP, M. FRÖBA, SAXS Studies on Alcoholic Synthesis Mixtures for the Preparation of Mesostructured Aluminophosphates with Dodecyl Phosphate as Template. *Hamburger Synchrotronstrahlungslabor (HASYLAB) Annual Report 1998*, 177-178.
- M. FRÖBA, M. TIEMANN, N. OBERENDER, R. KÖHN, O. MUTH, D. KEMPE, J. WONG, G. SCHECHNER, P. BEHRENS, B. PILLEP, I. GROHMANN, A. HESS, E. KEMNITZ, H. THOMS, M. EPPLE, A. RELLER, XANES Spectroscopy in the 1-2 keV Region: A Synchrotron Probe to Investigate Important low-Z Materials. *Stanford Synchrotron Radiation Laboratory (SSRL) Activity Report 1998*, 7/260.
- M. TIEMANN, M. FRÖBA, J. WONG, Quantitative Determination of the Coordination Numbers of Al in mesostructured Aluminophosphates by Al K-Edge XANES Spectroscopy. *Stanford Synchrotron Radiation Laboratory (SSRL) Activity Report 1997*, 7/241.

### Oral Presentations

- M. TIEMANN, M. FRÖBA, Mesoporöse Alumophosphate: Nichtwässrige Synthese und Charakterisierung. *GDCh-Vortragstagung: Anorganische Funktionsmaterialien*, Münster (Germany), Sep. 26.-29. 2000

M. TIEMANN, M. FRÖBA, Non-aqueous Synthesis of Mesoporous Aluminophosphates. *International Symposium on Mesoporous Molecular Sieves*, Quebec City (Canada), Aug. 27. - Sep. 2. 2000.

M. TIEMANN, M. FRÖBA, Nanostrukturierte Alumophosphate. *Zweites Norddeutsches Doktoranden-Kolloquium*, Hamburg (Germany), Oct. 8.-9. 1999.

#### Poster Presentations

M. TIEMANN, M. FRÖBA, Mesoporous Aluminophosphate Molecular sieves: Alcoholic Synthesis and Characterisation. *8th European Conference on Solid State Chemistry*, Oslo (Norway), July. 3.-7. 2001.

M. TIEMANN, M. FRÖBA, Non-aqueous Synthesis of Mesoporous Aluminophosphate Molecular Sieves. *13. Deutsche Zeolith-Konferenz*, Erlangen (Germany), Mar. 7.-9. 2001.

M. TIEMANN, M. FRÖBA, Mesostructured Aluminophosphates: Structural Studies and Perspectives for Improved Syntheses. *International Symposium on Mesoporous Molecular Sieves*, Quebec City (Canada), Aug. 27. – Sep. 2. 2000.

M. TIEMANN, M. FRÖBA, Mesostructured Aluminophosphates: Non-aqueous Synthesis, Characterisation, and In-situ Small Angle X-ray Scattering. *Symposium on Access in Nanoporous Materials II*, Banff (Canada), May 25.-28. 2000.

M. TIEMANN, S. S. FUNARI, G. RAPP, M. FRÖBA, In-Situ SAXS Studies on the Template-Directed Non-Aqueous Synthesis of Mesostructured Aluminophosphates. *HASYLAB Users' Meeting 2000*, HASYLAB at DESY, Hamburg (Germany), Jan. 28. 2000.

M. SCHULZ, M. TIEMANN, M. FRÖBA, C. JÄGER, NMR Investigations of Mesostructured Aluminophosphates with Dodecyl Phosphate. *11. Deutsche Zeolith-Konferenz*, Stuttgart (Germany), Mar. 3.-5. 1999.

M. TIEMANN, M. FRÖBA, SAXS Studies on Dodecyl Phosphate: Phase Behaviour in Water / Alcohols and Utilisation as Template for the Synthesis of Mesostructured Aluminophosphates. *11. Deutsche Zeolith-Konferenz*, Stuttgart (Germany), Mar. 3.-5. 1999.

M. TIEMANN, M. FRÖBA, Synthesis of Hexagonal Mesostructured Aluminophosphates from Alcoholic Systems. *11. Deutsche Zeolith-Konferenz*, Stuttgart (Germany), Mar. 3.-5. 1999.

M. TIEMANN, S. S. FUNARI, G. RAPP, M. FRÖBA, SAXS Studies on Dodecyl Phosphate: Phase Behaviour in Water / Alcohols and Utilisation as Template for the

Synthesis of Mesostructured Aluminophosphates. *HASYLAB Users' Meeting 1999*, HASYLAB at DESY, Hamburg (Germany), Jan. 29. 1999.

M. TIEMANN, M. FRÖBA, J. WONG, Synthesis and Al K-Edge XANES Investigation of Mesostructured Aluminophosphates. *Fall Meeting Materials Research Society*, Boston (USA), Nov. 30. - Dec. 12. 1998.

M. TIEMANN, M. FRÖBA, Synthese mesostrukturierter Alumophosphate: Dodecylphosphat als Templat und Reaktand. *GDCh-Vortragstagung: Syntheseprinzipien in der Festkörperchemie*, Saarbrücken (Germany), Sep. 23.-25. 1998.

M. TIEMANN, M. FRÖBA, Synthesis and Characterisation of Lamellar Mesostructured Aluminophosphates with Dodecylphosphate Surfactant. *Summer School on Applications of Synchrotron Radiation in Materials Science and Physics*, European Synchrotron Radiation Society (ESRS), Luso (Portugal), May 6.-14. 1998.

M. TIEMANN, M. FRÖBA, Mesostructured Aluminophosphates. *10. Deutsche Zeolith-Konferenz*, Bremen (Germany), Mar. 9.-11. 1998.

M. FRÖBA, O. MUTH, N. OBERENDER, R. KÖHN, M. TIEMANN, The Use of Supramolecular Templates as Structure-directing Agents in the Synthesis of Mesostructured Materials. *VI. European Conference on Solid State Chemistry*, Zurich (Switzerland), Sep. 17.-20. 1997.

## Curriculum Vitae

**Michael Tiemann, born September 30, 1969 in Hamburg, Germany.**

1976 – 1980	Elementary School <i>Grundschule Am Windmühlenweg</i> in Hamburg
1980 - 1989	Grammar School <i>Gymnasium Christianeum</i> in Hamburg
May 1989	<i>Abitur</i>
June 1989 - Sept. 1990	National Civil Service in Hamburg
Oct. 1990 - March 1991	Study of Engineering at <i>Technische Universität Hamburg-Harburg</i>
Oct. 1991 – Sept. 1997	Study of Chemistry at <i>Universität Hamburg</i>
Dec. 1993	<i>Diplomvorprüfung</i>
Jan. - March 1995	Guest study at <i>Exeter University</i> , Great Britain (inorganic chemistry research project in the group of Prof. Robert C. T. Slade)
Feb. - Sep. 1997	Work on Diploma Thesis " <i>Synthese und Charakterisierung mesostrukturierter Alumophosphate</i> " in the group of Dr. Michael Fröba
Sep. 1997	<i>Diplomhauptprüfung</i>
Oct. 1997 - July 2001	Work on Dissertation (PhD Thesis) " <i>Mesostructured Aluminium Phosphates Synthesised by Supramolecular Structure-Direction</i> " in the group of Prof. Dr. Michael Fröba
Apr. - Aug. 1997	Fellowship of <i>Werner-Ranz-Stiftung</i>
Apr. 1998 - March 1999	Fellowship of <i>Freie und Hansestadt Hamburg</i>
Apr. 1999 - Sep. 2001	employed as Scientific Assistant at <i>Universität Hamburg</i>

## Hazardous Chemicals

The following table provides information on potential hazards caused by the chemicals in this work according to European Union classification.

compound name	hazard category <sup>a</sup>	R phrase <sup>b</sup>	S phrase <sup>c</sup>
aluminium triisopropylate	F	R11	S8-16
aluminium chloride	C	R34	S7/8-28.1-45
phosphoric acid	C	R34	S26-36/37/39-45
tetramethylammonium hydroxide	C	R22-34	S26-36/37/39-45
<i>n</i> -dodecyl phosphate	C	R34	S26-36/37/39-45
<i>n</i> -dodecylamine	C	R22-35	S26-28.1-36/37/39-45
<i>n</i> -tetradecylamine	Xi	R36/37/38	S26-36
<i>n</i> -hexadecylamine	C	R34	S26-36/37/39-45
ethanol	F	R11	S7-16
methanol	F, T	R11-23/24/25-39/23/24/25	S7-16-36/37-45

<sup>a</sup> F - highly flammable; C - corrosive; Xi – irritant; T – toxic

<sup>b</sup> R11 - highly flammable; R22 - harmful if swallowed; R23 - toxic by inhalation; R24 - toxic in contact with skin; R25 - toxic if swallowed; R34 - causes burns; R35 - causes severe burns; R36 - irritating to the eyes; R37 - irritating to the respiratory system; R38 - irritating to the skin; R39 - danger of very serious irreversible effects

<sup>c</sup> S7 - keep container tightly closed; S8 - keep container dry; S16 - keep away from sources of ignition - no smoking; S26 - in case of contact with eyes, rinse immediately with plenty of water and seek medical advice; S28.1 - after contact with skin, wash immediately with plenty of water; S36 - wear suitable protective clothing; S37 - wear suitable gloves; S39 - wear eye/face protection; S45 - in case of accident or if you feel unwell, seek medical advice immediately (show label where possible)



